



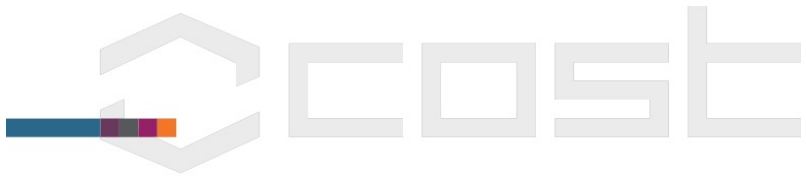
Short-Term Scientific Missions: Years 4 & 5

Editors:

L. Pajewski, I. Rodriguez-Abad & M. Marciniak

January 2018

www.GPRadar.eu



COST ACTION TU1208

CIVIL ENGINEERING APPLICATIONS OF GROUND PENETRATING RADAR

Short-Term Scientific Missions: Years 4 & 5

Editors:

Lara Pajewski, Isabel Rodriguez-Abad & Marian Marciniak

Publisher: TU1208 GPR Association

Rome, Italy, January 2018;

ISBN 9788888173085; DOI (ISBN-A): 10.978.8888173/085.

PREFACE

SHORT-TERM SCIENTIFIC MISSIONS: YEARS 4 & 5

COST ACTION TU1208

“CIVIL ENGINEERING APPLICATIONS OF GROUND PENETRATING RADAR”

Short-Term Scientific Missions (STSMs) are among the most interesting networking tools of COST (European COoperation in Science and Technology) Actions. They are aimed at supporting individual mobility of European researchers; they significantly strengthen scientific networks and foster collaborations.

In a STSM, a scientist from a COST Country or from an approved Institution in a Near Neighbour Country (NNC) has the opportunity to visit an institution or laboratory in a COST Country participating in the Action, or an approved NNC institution, or else an approved International Partner Country (IPC) institution. A STSM shall specifically contribute to the scientific objectives of the Action offering the grant, at the same time allowing the visiting scientist to learn new techniques or gain access to specific instruments and/or methods not available in the home institution.

STSM proposals are submitted by using the online application form, at <https://e-services.cost.eu/stsm>. When an Action receives a proposal, the Management Committee (MC) performs their evaluation. The MC of Action TU1208 formally delegated the evaluation of STSM applications to the Action Chair and STSM Manager. The selection is based on the scientific scope of the STSM application, which must be in line with the Action



objectives, and on the applicant curriculum vitae. Geographical issues and gender balance are taken into consideration, as well. A STSM applicant must be engaged in a research programme as a postgraduate student or postdoctoral fellow, or be employed by or officially affiliated to a public/private institution or legal entity.

Standard STSMs may have a minimum duration of 5 days and a maximum duration of 90 days. They have to be carried out in their entirety within a single grant period and within the Action's lifetime. Early-Career Investigators (ECIs) may extend the duration of the STSM beyond the 90 days in well-justified cases (the maximum allowed duration is 180 days).

The participation of ECIs in STSMs is strongly encouraged. For COST, the definition of ECI is based on the time that elapses between the date of the PhD (or equivalent experience) and the date of involvement in a COST Action. If this time span is less than eight years, a person fits the definition; periods of career's leave have to be added to the mentioned time span. Supporting ECIs to develop independent careers and to establish their first research group under their own responsibility is a strategic priority for COST.

A STSM grant is a fixed financial contribution, based on the budget requested by the applicant and on the evaluation of the application by the MC. The aim of the grant is to support the costs associated with the exchange visit. It does not necessarily cover all expenses and has to be intended as a contribution to the travel and subsistence costs of the scientist performing the mission.



During Grant Periods 4 and 5 of COST Action TU1208, eleven STSMs were funded and fruitfully carried out (note that Grant Period 4 had a standard duration of twelve months, whereas the additional Grant Period 5 had a shorter duration of six months). This book is a collection of scientific reports prepared by the scientists who performed the missions, in cooperation with the host scientists.

We are deeply grateful to COST, for funding and supporting COST Action TU1208 “Civil Engineering Applications of Ground Penetrating Radar” and the research activities presented in this volume. We also thank TU1208 GPR Association for funding the publication of this volume.

Lara Pajewski, Chair of COST Action TU1208
Isabel Rodriguez-Abad, WG Member of COST Action TU1208
Marian Marciniak, STSM Manager of COST Action TU1208



STSM 1

ENHANCEMENT OF GPR-GROUND MATCHING BY A CHIRPED MULTILAYER STRUCTURE: NUMERICAL MODELLING BY THE METHOD OF SINGLE EXPRESSION

VISITING SCIENTIST: TAMARA KNYAZYAN, NATIONAL POLYTECHNIC
UNIVERSITY OF ARMENIA, YEREVAN, ARMENIA
KTAMARA@SEUA.AM

HOST SCIENTIST: MARIAN MARCINIAK, NATIONAL INSTITUTE OF
TELECOMMUNICATION, WARSAW, POLAND
M.MARCINIAK@ITL.WAW.PL

STSM DATES: 1ST AUGUST – 19TH AUGUST 2016

1. PURPOSE OF THE STSM

The purpose of the STSM was to analyse the possibility of enhancing the electromagnetic matching of ground penetrating radar (GPR) signal with the ground, by means of a chirped multilayer structure. The scenario was modelled by using the method of single expression (MSE). Achieving a better matching with the ground increases the signal penetration depth, minimizes back reflection into the transmitter and enhances the signal/noise ratio at the receiving end.

2. DESCRIPTION OF THE WORK CARRIED OUT DURING THE STSM AND MAIN RESULTS

In the preliminary study carried out during the STSM, the interaction of an electromagnetic plane wave with the ground was considered. The plane wave impinges normally on the ground. We found that the use of a suitable chirped multilayer structure, positioned at the interface between air and ground, allows



reducing the reflectance from the ground. Such structure was designed after investigating the behaviour of various chirped multilayer structures: in particular, the number and thicknesses of layers was varied, while we aimed at minimizing the back reflection into the transmitting antenna. The distribution of the electric field components and the power flow density within the multilayer structure were calculated.

The modelling of the scenario was performed by using MSE, which is a convenient tool for wavelength-scale analysis of multilayer and modulated structures comprising loss, gainy and nonlinear (Kerr-type) dielectric, semiconductor and metallic layers [1-5].

Here, the backbone of the MSE is presented. From Maxwell's equations in the one-dimensional (1D) case, the following Helmholtz equation can be obtained for a linearly polarized complex electric field component $\dot{E}_x(z)$:

$$\frac{d^2 \dot{E}_x(z)}{dz^2} + k_0^2 \tilde{\varepsilon}(z) \dot{E}_x(z) = 0 \quad (1)$$

where $k_0 = \omega/c$ is the free space propagation constant and $\tilde{\varepsilon}(z) = \varepsilon'(z) + j\varepsilon''(z)$ is the complex permittivity of a medium. The essence of the MSE is to obtain a general solution of Helmholtz equation for the electric field component $\dot{E}_x(z)$ in a special form, i.e., with a single expression, instead of using the traditional presentation of the solution as a sum of counter-propagating waves. The single-expression solution has the form:

$$\dot{E}_x(z) = U(z) \cdot \exp(-jS(z)) \quad (2)$$

where $U(z)$ and $S(z)$ are real quantities describing the resulting electric field amplitude and phase respectively. Time dependence $\exp(j\omega t)$ is assumed, but suppressed throughout the analysis. A solution as in Eq. 2 prevails upon the traditional approach of counter-propagating waves. Besides, it is more general because it



is not relied on the superposition principle. This form of solution describes all possible distributions in space of electric field amplitude, corresponding to propagating, standing or evanescent waves in a medium of negative permittivity. It means that no preliminary assumptions concerning the Helmholtz equation's solution in different media are needed in the MSE. This gives advantages when investigating wave interactions with any longitudinally non-uniform linear and intensity dependent non-linear media with the same ease and exactness.

Based on Eq. 2, it is possible to reformulate Eq. 1 as a set of first order differential equations, regarding the electric field amplitude $U(z)$, its spatial derivative $Y(z)$ and a quantity $P(z)$ - proportional to the power flow density (Poynting vector) in a medium:

$$\begin{cases} \frac{dU(z)}{d(k_0z)} = Y(z) \\ \frac{dY(z)}{d(k_0z)} = \frac{P^2(z)}{U^3(z)} - \varepsilon'(z) \cdot U(z) \\ \frac{dP(z)}{d(k_0z)} = \varepsilon''(z) \cdot U^2(z) \end{cases} \quad (3)$$

Here, $P(z) = U^2(z) \frac{dS(z)}{d(k_0z)}$.

The sign of $\varepsilon'(z)$ can be positive or negative, describing relevant electromagnetic features of dielectric media or metal (plasma) respectively. The sign of $\varepsilon''(z)$ indicates loss or gain in a medium.

The set of differential equations in Eq. 3 can be integrated numerically, starting from the non-illuminated side of a multilayer structure, where only one outgoing travelling wave is supposed to be present. Initial values for the integration are obtained from the boundary conditions of electrodynamics at the non-illuminated side of the structure. Numerical integration of the set in Eq. 3 goes step by step towards the illuminated side of the structure taking into account an actual value of structure's permittivity for the



given coordinate at each step of integration. In the process of integration, any variable of the set can be stored, in order to have, at the end of the calculation, full information regarding the spatial distribution of electric-field components, their derivatives and the power flow densities inside and outside of a structure. At the borders between the layers of a multilayer structure, the application of ordinary boundary conditions of electrodynamics brings to the continuity of $U(z)$, $Y(z)$ and $P(z)$. From the boundary conditions of electrodynamics at the illuminated side of the structure, the amplitude of incident field E_{inc} and power reflection coefficient R are retrieved at the end of calculation. The power transmission coefficient is obtained as the ratio of transmitted power to the incident one.

In this work, as already said, we looked for advantageous configurations that would allow the enhancement of matching between GPR signal and ground. To this aim, different chirped multilayer structures contacted with the ground were studied.

The time-schedule of the STSM was:

1. Literature review and data collection and analysis (3 days).
2. Choosing a proper electrodynamical model for the considered scenario. Implementing the chosen approach, to simulate the interaction of a plane wave with a chirped multilayer structure contacted with the ground (4 days).
3. Detailed numerical analysis of a series of chirped multilayer structures contacted with the ground, looking for the structure that provided best results in terms of the enhancement of GPR antenna – ground matching (5 days).
4. Discussion of the obtained results (2 days).
5. Future work planning (1 day).

As is well known, GPR is an electromagnetic technique used to detect and image buried objects, with resolution ranging from a couple of centimetres to a few meters [6-11]. GPR uses the same



fundamental physical principles as conventional radars and it customarily works in a frequency range from 10 MHz to 5 GHz. Within this range, the operational range depends on the measurement requirements (resolution and penetration). Examples of sought targets are buried pipes, cables, reinforcements, caverns, flaws and cracks, as well as ground water, moisture, etc. [11-16]. GPR finds application in archaeology, military, civil, hydrogeological, geophysical and geotechnical engineering [11-16].

GPR is based on the principle of detecting back-scattered energy from a target: the radar transmitting antenna illuminates the ground and the receiving antenna captures reflections from the target; the radar system is moved along a line or a grid and an image of the target is generated. Depth and shape of the target can be calculated from the return time of the reflected signals.

GPR resolution is a function of the operation frequency and the dielectric constant of the studied medium, as well as of the antenna properties [7]. High resolution is reached at the cost of penetration depth; the attenuation of electromagnetic waves in common materials is rather high and increases with frequency [17, 18]. Gravel, sand, dry rock and fresh water are relatively easy to be inspected by GPR. Salt water, clay soils and conductive ores or minerals are inspected with worse resolution or shallower penetration depth.

Antennas are essential components of GPR systems. Different types of antennas are used, but dipole and bowtie antennas are the most common. Most systems are equipped with two antennas: one for transmitting and the other for receiving, although they can be packaged together. Shielded antennas are used to avoid reflections from objects in the air. The antenna gain is very important to emit and receive electromagnetic energy efficiently. Antennas with a high gain improve the signal/noise ratio. A low operating frequency requires larger antennas. Small antennas



make the system compact, but they have a low gain at high frequencies [17, 18].

Though the GPR technique is mature enough and a large variety of GPR systems are in use, some problems are still waiting for their solution [11]. One of them is to achieve a better matching of GPR signal with the ground.

The scenario considered in this work is schematized in Figure 1. Preliminary results were presented in the EGU General Assembly 2016 [19].

In our MSE models, we assumed normal incidence of the plane wave, the wavelength was $\lambda_0 = 10\text{ cm}$ and the ground had complex permittivity $\hat{\epsilon} = \epsilon' + j\epsilon'' = 10 - j0.3$ [20].

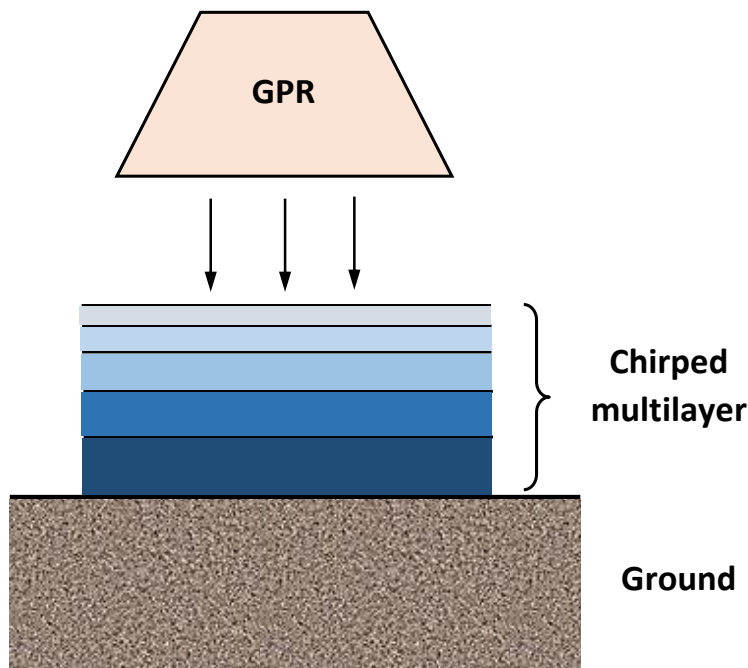


FIG. 1 – Plane wave interaction with the ground through chirped multilayer structure contacted with the ground.



Here we show results obtained for a chirped multilayer structure consisting of two slabs of low $\epsilon'_{low} = 2.25$ and high $\epsilon'_{high} = 6.0$ permittivity, creating bilayers of increasing thickness towards the ground. The bilayers have a normalized thickness NT :

$$NT_i = 0.3471; 0.4471; 0.5471$$

where $NT_i = L_i / \lambda$ ($i=1,2,3$ is a number of bilayers) and $\lambda = \lambda_0 / \sqrt{\epsilon}$ is the wavelength in the slab with ϵ'_{low} and ϵ'_{high} permittivity. Two cases are presented, as depicted in Figure 2:

Structure a) The material with low permittivity ϵ'_{low} is contacted with the ground, and:

$$NT_1 = 0.3471 (\epsilon'_{high} / \epsilon'_{low})$$

$$NT_2 = 0.4471 (\epsilon'_{high} / \epsilon'_{low})$$

$$NT_3 = 0.5471 (\epsilon'_{high} / \epsilon'_{low})$$

Structure b) The material with high permittivity ϵ'_{high} is contacted with the ground, and:

$$NT_1 = 0.3471 (\epsilon'_{low} / \epsilon'_{high})$$

$$NT_2 = 0.4471 (\epsilon'_{low} / \epsilon'_{high})$$

$$NT_3 = 0.5471 (\epsilon'_{low} / \epsilon'_{high})$$

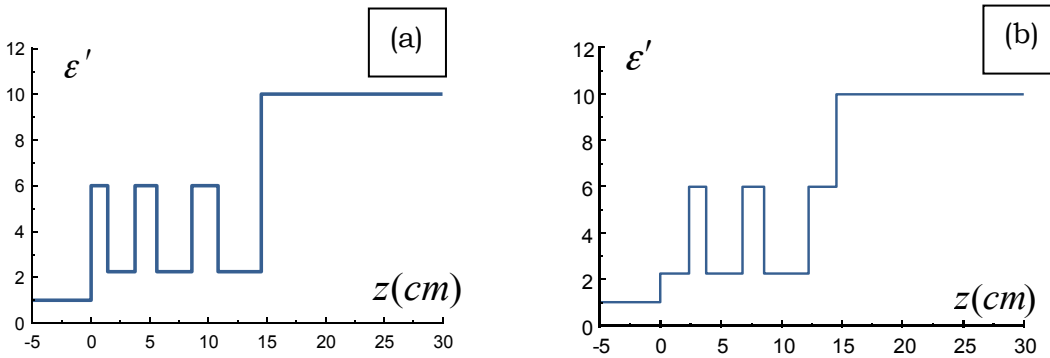


FIG. 2 – Permittivity profiles of two chirped multilayer structures contacted with the ground. Wave incidence from the left is considered.



The structure (b) described in Figure 2(b), where the layer of high permittivity is contacted with the ground, allowed to obtain an antenna-ground matching with a reflectance of $R \approx 0.0019$; the structure depicted in Figure 2a, gave a reflectance $R \approx 0.25$, which is close to the critical value of reflectance ($R \approx 0.27$) for an air-ground interface (in the absence of the multilayer structure). Here, the reflectance was defined as $R = P_{ref}/P_{inc}$: P_{inc} was the power flow density (Poynting vector) of the electromagnetic wave emitted from the GPR and impinging on the chirped multilayer structure contacted with the ground (or on the air-ground interface, in the absence of the multilayer structure); P_{ref} was the power flow density (Poynting vector) of the electromagnetic wave reflected by the structure (or by the air-ground interface, in the absence of the multilayer structure).

In general, R depends on permittivities and thicknesses of all layers composing the structure, as well as on the permittivities of surrounding media. The MSE reflectance is defined as:

$$R = \left| \frac{E_{ref}}{E_{inc}} \right|^2 = \left| \frac{U^2(0) \cdot \sqrt{\varepsilon_l} - P(0) - jU(0) \cdot Y(0)}{U^2(0) \cdot \sqrt{\varepsilon_l} + P(0) + jU(0) \cdot Y(0)} \right|^2 \quad (4)$$

where ε_l is the permittivity of the medium in front of the structure at $z < 0$, which in the case considered here is air, E_{ref} is the amplitude of reflected wave and E_{inc} is the amplitude of the incident wave:

$$E_{inc} = \left| \frac{U^2(0) \cdot \sqrt{\varepsilon_l} + P(0) + jU(0) \cdot Y(0)}{2U(0) \cdot \sqrt{\varepsilon_l}} \right| \quad (5)$$

In Eq. 5, $U(0)$ is the resultant amplitude of electromagnetic wave, $Y(0)$ is its derivative and $P(0)$ is the power flow density at the illuminated interface of the structure at $z = 0$.

The variables of the MSE are found through direct numerical integration of the system of differential equations in Eq. 3, which



is equivalent to the Helmholtz’s Eq. 1, by applying boundary conditions of electrodynamics. The calculations start from the non-illuminated side of the structure.

In the absence of a chirped multilayer structure (air-ground interface) the reflectance R is defined as:

$$R = \left| \frac{\sqrt{\varepsilon_l} - \sqrt{\hat{\varepsilon}}}{\sqrt{\varepsilon_l} + \sqrt{\hat{\varepsilon}}} \right|^2 \quad (6)$$

that is the reflectance of the air-ground interface, so called Fresnel reflection coefficient, and equals to $R \approx 0.27$ in the case that we are treating here.

Our calculations suggest that for a better antenna-ground matching a chirped multilayer structure with a layer of high permittivity contacted with the ground should be chosen (which gave us a reflectance of $R \approx 0.0019$). To study more in depth the physics of operation of the two chirped multilayer structures, as well as of the air-ground interface without multilayer structure, the distributions of electric field amplitude and Poynting vector within and outside the structures were obtained via numerical simulation by the MSE. The results are presented in Figure 3 and Figure 4. The plotted quantities strongly depend on the layers alternation. Due to the absence of losses in the chirped multilayer structures, P is constant in them and \hat{E} presents oscillating behaviour, following the permittivity profiles of the multilayer structures.

In front of the structures at $z < 0$, the Poynting vector P was defined as $P = P_{inc} - P_{ref} = P_{inc}(1 - R)$. A partially standing wave amplitude of electric field was formed (a), indicating higher reflectance R and lower value of $P \approx 11.93$. Approximately (quasi) travelling wave pattern was created in the front of the structure (b), indicating lower reflectance R and higher value of $P \approx 15.97$.



The power flow penetrating into the ground increased of a factor 1.34 with the antenna-ground matching, and correspondingly, the penetration depth will be increased by the same value.

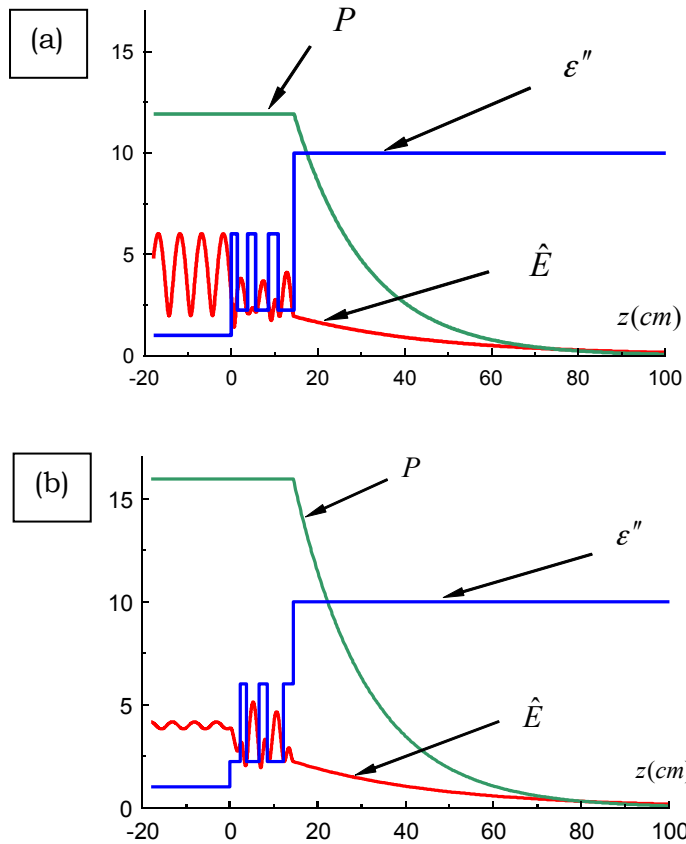


FIG. 3 – Permittivity profile, distributions of electric field amplitude \hat{E} and Poynting vector P , within and outside of the chirped multilayer structures. In both cases, the amplitude of incident wave (from the left) was the same $E_{inc} = 4a.u.$ In the absence of multilayer structures, standing wave amplitude of electric field was formed at the air-ground interface at $z < 0$, which indicated high reflectance from the interface and exponentially decreased in the ground (Figure 4).



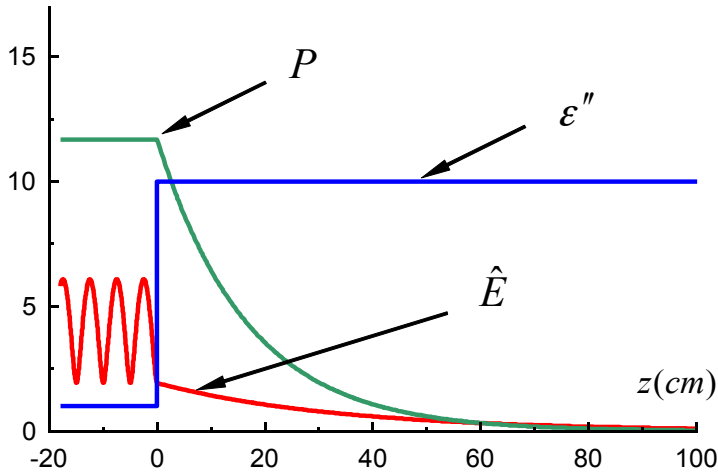


FIG. 4 – Permittivity profile, distributions of electric field amplitude \hat{E} and Poynting vector P within the air and the ground. The amplitude of incident wave (from the left) is $E_{inc} = 4a.u.$

P is constant in the air and exponentially decreases in the ground. Consequently, because of high reflectance from the air-ground interface and the small value of $P \approx 11.68$, the penetration depth into the ground was small.

To obtain better antenna matching with the ground, three bilayers of high and low permittivity are proposed, where the highest value of permittivity doesn't exceed the permittivity of the ground. Bilayers should have increasing thickness towards the ground and – as already mentioned – for a better matching the layer closer to the ground should be of higher permittivity.

3. FUTURE COLLABORATION WITH THE HOST INSTITUTION

This STSM, carried out in the framework of the Action TU1208, strengthened the long-term scientific cooperation between the Armenian research team and Prof. Marian Marciniak. The collaboration will certainly continue in the future.



4. FORESEEN PUBLICATIONS/ARTICLES RESULTING FROM THE STSM

The scientific outcomes of this STSM were published on a paper included in the Special Issue “Recent Progress in Electromagnetic Theory and its Applications,” organized by the COST Action TU1208 on the Journal of Telecommunications and Information Technology (JTIT).

5. ACKNOWLEDGEMENTS

The Authors thank COST, European Cooperation in Science and Technology, for funding the Action TU1208 and this STSM.

6. REFERENCES

- [1] H.V. Baghdasaryan. Photonic Devices for Telecommunications: how to model and measure. Publisher: Springer-Verlag, pp.56-65 (1999).
- [2] H.V. Baghdasaryan, T.M. Knyazyan. Problem of plane EM wave self-action in multilayer structure: An exact solution. Optical and Quantum Electronics, vol. 31, pp. 1059 – 1072 (1999).
- [3] H.V. Baghdasaryan, T.M. Knyazyan. Modelling of strongly nonlinear sinusoidal Bragg gratings by the Method of Single Expression. Optical and Quantum Electronics, 32 (6/8), pp. 869-883 (2000).
- [4] H.V. Baghdasaryan, T.M. Knyazyan. Method of single expression – an exact solution for wavelength scale 1D photonic structures’ computer modeling. Proceedings of SPIE 5260, pp. 141-148 (2003).
- [5] H.V. Baghdasaryan. Basics of the Method of Single Expression: New Approach for Solving Boundary Problems in Classical Electrodynamics. Yerevan, Chartaraget, (2013).
- [6] L.B. Conyers, D. Goodman. Ground Penetrating Radar: An Introduction for Archaeologists. Publisher: Alta Mira Press, Walnut Creek, London and New Delhi (1997).
- [7] D.J. Daniels. Ground Penetrating Radar. Publisher: The Institution of Engineering and Technology (2004).



- [8] H.M. Jol. Ground Penetrating Radar: Theory and Applications. Publisher: Elsevier, 509 pp. (2009).
- [9] D.J. Daniels. GPR Design Challenges. COST Action TU1208, First General meeting – Proceedings, Rome, Italy, July 22-24, (2013).
- [10] R. Persico. Introduction to Ground Penetrating Radar. Publisher: IEEE Press, Wiley, 368 pp. (2014).
- [11] A. Benedetto, L. Pajewski. Civil Engineering Applications of Ground Penetrating Radar. Publisher: Springer, 371 pp. (2015).
- [12] F. Finck. Introduction of a ground penetrating radar system for investigations on concrete structures. Otto-Graf-Journal vol. 14, pp. 35-44 (2003).
- [13] R. J. Yelf. Application of Ground Penetrating Radar to Civil and Geotechnical Engineering. Electromagnetic Phenomena, vol. 7, n° 1 (18), pp. 102-117 (2007).
- [14] D. Goodman, S. Piro. GPR Remote Sensing in Archaeology. Geotechnologies and the Environment, vol. 9 (2013).
- [15] L. Pajewski, A. Benedetto. Proceedings of COST Action TU1208: Civil Engineering Applications of Ground Penetrating Radar, First General Meeting (2013).
- [16] L. Pajewski, X. Derobert. Proceedings of COST Action TU1208: Civil Engineering Applications of Ground Penetrating Radar, 2014 Working Group Progress Meeting. (2014).
- [17] K. Takahashi, J. Igel, H. Preetz, S. Kuroda. Basics and Application of Ground-Penetrating Radar as a Tool for Monitoring Irrigation Process, Problems, Perspectives and Challenges of Agricultural Water Management. InTech, pp. 155-180 (2012).
- [18] A. P. Annan. Ground Penetrating Radar Principles, Procedures & Applications. Publisher: Sensors & Software Inc. (2003).
- [19] H. V. Baghdasaryan, T. M. Knyazyan, T. T. Hovhannisyan, M. Marciniak, L. Pajewski. Numerical modelling of GPR ground-matching enhancement by a chirped multilayer structure - output of cooperation within COST Action TU1208. EGU General Assembly 2016, Geophysical Research Abstracts, vol. 18, EGU2016-18507 (2016).



- [20] L. Yang-yang , Z. Kai, R. Jian-hua, D. Yan-ling, W. Li-li. Analysis of the dielectric constant of saline-alkali soils and the effect on radar backscattering coefficient: A case study of soda alkaline saline soils in western Jilin province using RADARSAT-2 Data. The Scientific World Journal (2014).



STSM 2

TESTING OF A NEW LIGHTWEIGHT RADAR SYSTEM FOR TOMOGRAPHICAL RECONSTRUCTION OF CIRCULAR STRUCTURES

VISITING SCIENTIST: ALESSANDRO FEDELI, UNIVERSITY OF GENOA,
GENOA, ITALY
ALESSANDRO.FEDELI@EDU.UNIGE.IT

HOST SCIENTISTS: JANA JEZOVÁ & SÉBASTIEN LAMBOT,
UNIVERSITÉ CATHOLIQUE DE LOUVAIN, LOUVAIN-LA-NEUVE, BELGIUM
JANA.JEZOVA@UCLOUVAIN.BE & SEBASTIEN.LAMBOT@UCLOUVAIN.BE

STSM DATES: 12ND SEPTEMBER – 23RD SEPTEMBER 2016

1. PURPOSE OF THE STSM

Ground penetrating radar (GPR) is becoming one of the most effective tools for geophysical inspection and evaluation. Many different areas of application exist: from the conventional task of buried object detection in subsurface regions to the recent developments related to the assessment of tree trunks [1, 2] or other civil engineering structures [3].

On one hand, the need of devising new and more efficient GPR measurement systems has a key importance, because the emerging applications often require portable and lightweight – but powerful – systems. In particular, an accurate modelling of the physical effects that occur between the antenna structure and the soil interface is fundamental for a correct acquisition and interpretation of GPR measurements.

On the other hand, there is an ever-growing interest in the development of advanced data processing techniques for GPR, since the raw data are usually very difficult to interpret and skilled



professionals are often required for deducing the actual configuration of the buried objects. In particular, both qualitative and quantitative imaging algorithms developed in the area of electromagnetic inverse scattering theory [4] may be successfully applicable to the processing of GPR data. The benefits of applying such techniques reside in the possibility of retrieving not only the shape and location of the hidden objects or inclusions, but also the distribution of their electromagnetic properties.

At the intersection point between these two emerging research trends, the main goal of the present STSM was the combination of the experimental and modelling skills of the Georadar Research Centre at the Université Catholique de Louvain (UCL), Belgium, with the data processing techniques developed at the Applied Electromagnetics Laboratory of the DITEN Department of the University of Genoa (UNIGE), Italy.

Therefore, the STSM has been focused on both: the acquisition and the inversion of experimental measurements. Such experimental data were obtained by using a novel radar prototype. Circular structures in free space and buried in a sandy soil were considered. The new system was tested in several different configurations and with different antennas. The acquired experimental data were pre-processed with a state-of-the-art calibration technique developed at UCL. Furthermore, the possibility of applying advanced inversion methods aimed at reconstructing the characteristics of the inspected targets both qualitatively and quantitatively was explored with promising results.

2. DESCRIPTION OF THE WORK CARRIED OUT DURING THE STSM

In this STSM, two different kinds of work were done: experimental measurements and data processing. The experimental activities were carried out at the laboratory of the Georadar Research Centre of the Université Catholique de Louvain in Louvain-la-Neuve,



Belgium. The experimental test site includes a 3D high-precision positioning system, two sand boxes of different size, a circular cylinder filled with sand, a large copper sheet for antenna calibration, and a vector network analyser, which is used for acquiring measurements. After the GPR data acquisition, MATLAB and C++ codes were utilized for the processing steps.

2.1. TEST OF THE RADAR PROTOTYPE WITH DIFFERENT ANTENNAS

Several types of GPR custom antennas were tested during the STSM for being used with the new radar prototype. All the antennas were calibrated by fitting the accurate far-field model developed by Lambot et al. [5].

In particular, the calibration was performed by measuring the complex reflection coefficient of the antennas at different distances from a large square copper sheet with 3 m side length (Figure 1). Both air- and dielectric-coupled antennas were calibrated, as reported in Table 1.



FIG. 1 – Antenna placed at some distance from a large copper sheet for the calibration phase.



TABLE 1– Antennas tested and calibrated during the STSM.

ANTENNA	TYPE	CALIBRATED FREQUENCY RANGE
#1	Aluminum air coupled	800 MHz – 4 GHz
#2	Copper air coupled	800 MHz – 4 GHz
#3	Dielectric coupled	800 MHz – 4 GHz

2.2. ANTENNA COUPLING WITH SAND OF DIFFERENT VOLUMETRIC WATER CONTENT

Some experiments aimed at verifying the coupling of different kinds of antennas in front of a sand box with different levels of sand moisture were done (Figure 2).



FIG. 2 – Measurements in small sand box with different volumetric water contents.

Antennas #1, #2 and #3 were used for this task, acquiring for each antenna four A-scans at different distances from the interface with the sand layer. As sketched in Figure 3, the sand box has a square



section with side length $s = 0.96$ m, its height is $h = 0.1$ m and it is contained in a wood structure made of four laths $t = 0.02$ m thick. At the bottom, a conducting square metal plate of $l = 1$ m side length is positioned.

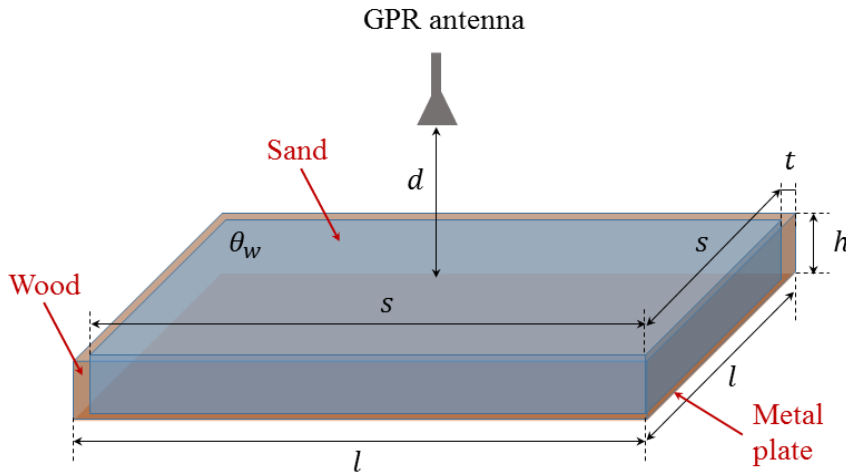


FIG. 3 – Geometrical configuration of the sand box used for the A-scan measurements with different levels of volumetric water content and different antennas.

The antennas under test were placed, in turn, at the center of the sand box at a distance d from the air-sand interface. The considered distances are $d = \{0, 1, 10, 20\}$ cm. Specific quantities of water were added to the sand and accurately mixed with it in order to obtain values of soil percentage volumetric water content $\theta_w = \{0, 3, 6, 9, 12, 16, 20, 24\}$ %. After having moistened and carefully mixed the sand, A-scans with the three custom antennas were measured for each considered value of distance d .

2.3 MEASUREMENTS IN SAND BOX WITH BURIED OBJECTS

The second experimental work carried out during this STSM concerns the acquisition of B-scans in a sand box (Figure 4) with different antennas and several values of distance between the



antenna and the soil interface. The box is a parallelepiped with horizontal sides of length $s = 3$ m and height $h = 1$ m, and it is filled with dry sand. At the bottom, a $3\text{ m} \times 3\text{ m}$ metal plate is placed. Two different test sets were prepared.



FIG. 4 - An empty PVC circular cylinder is being buried during the preparation of the test sets for the B-scans in the sand container.

In the first one, whose cross section is schematized in Figure 5, a circular metallic rebar of length $l_1 = 2.5$ m and diameter $d_1 = 0.03$ m is located at the centre of the box, $z_1 = 0.1$ m deep. In addition, an empty PVC tube with length $l_2 = 0.9$ m, outer diameter $d_2 = 0.08$ m and thickness $t_2 = 0.0018$ m was positioned at a depth $z_2 = 0.085$ m. The surface of the sand was levelled by using a tool mounted on the arm of the 3D positioning system. It is worth noting that three other water-filled pipes are present in the sand box from a previous experiment.

However, we have positioned the new targets such as their scattering contributions in the B-scan remained separate. By using antenna #1, B-scans of length $L = 2.4$ m were taken, at distances $d = \{0.01, 0.1, 0.15, 0.2, 0.3\}$ m above the soil. With antenna #3, we have acquired B-scans of length $L = 2.1$ m at distances $d = \{0.01, 0.12, 0.2\}$ m. In all cases, a constant spacing step of 1 cm between measurements was used.



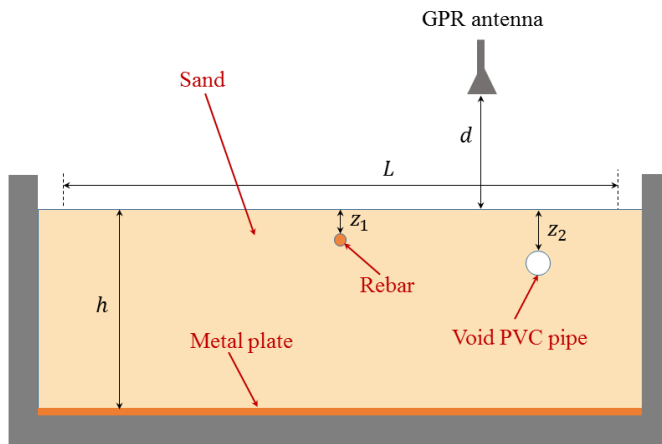


FIG. 5 – First test set. Configuration of the sand box with one buried void PVC pipe and a metallic rebar.

The second test set that was prepared in the sand box (Figure 6) includes three pipes of different sizes and filling materials. Two of them (cylinder #1 and cylinder #3) were filled with air.

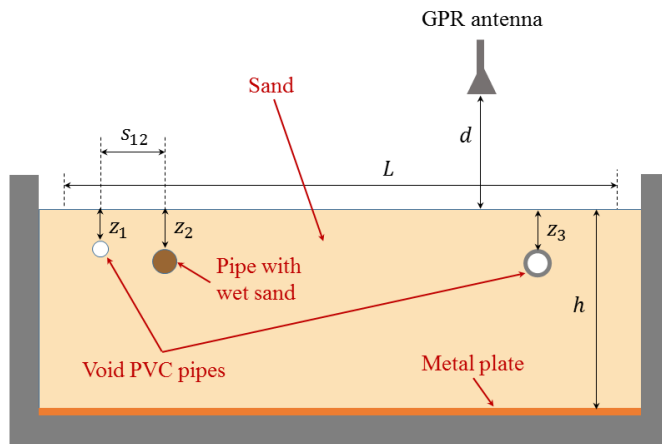


FIG. 6 – Second test set. Configuration of the sand box with two buried void PVC pipes of different sizes and one PVC tube filled with wet sand of 24% volumetric water content.



The other cylinder (cylinder #2) was completely filled with wet sand characterized by $\theta_w = 24\%$ volumetric water content (see Figures 7 and 8).

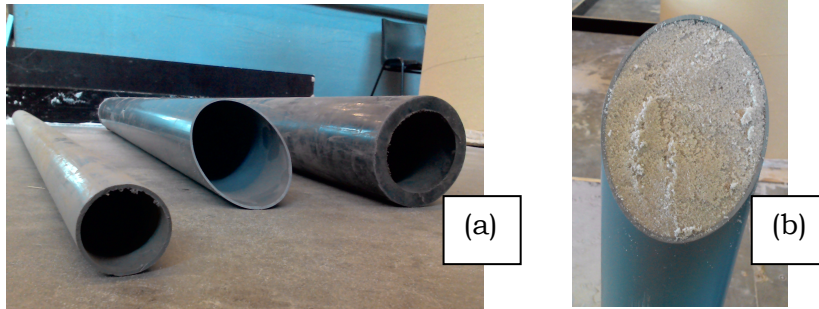


FIG. 7 – Second test set. PVC circular cylinders before being buried in the sand box: (a) all the cylinders empty; (b) cylinder #2 filled with wet sand with 24% volumetric water content.



FIG. 8 – Second test set. PVC circular cylinders during burial: (a) cylinders #1 and #2; (b) cylinder #3.

The main parameters of the buried targets involved in this experiment are summarized in Table 2. The reported values of depth are referred to the top of the cylinders, and were measured after the sand levelling. The horizontal spacing between cylinder #1 and cylinder #2 is $s_{12} = 0.185$ m (referred to the centre of the pipes). B-scans of length $L = 2.4$ m (subdivided into 241 equally spaced steps with 1 cm distance between each other) were taken,



with antenna #1 located at a distances $d = \{0.01, 0.1, 0.2\}$ m above the soil.

TABLE 2 – Properties of the tubes buried in the sand box for the second test set.

CYLINDER	FILLING MATERIAL	LENGTH	OUTER DIAMETER	THICKNESS	TOP DEPTH
#1	Air	1.16 m	0.04 m	0.0018 m	0.125 m
#2	Wet sand	0.90 m	0.08 m	0.0018 m	0.155 m
#3	Air	1.03 m	0.09 m	0.0120 m	0.130 m

2.4 MEASUREMENTS AROUND CIRCULAR CYLINDER WITH VOID INCLUSION

The last set of measurements was taken around a circular cylinder with one void inclusion (Figure 9).



FIG. 9 – Measurements around the circular cylinder with void inclusion.



The geometrical configuration of the analysed structure is shown in Figure 10. The outer structure is a paper cylinder with outer diameter $d_o = 0.82$ m. Inside, there is a void PVC tube with diameter $d_i = 0.4$ m. The internal space between the two cylinders is filled by dry sand. The GPR measurements were acquired starting from the initial position indicated in Figure 10 and with counter clockwise rotation direction. The angular spacing between two subsequent measurement points was chosen equal to $\Delta\phi = 5.6^\circ$. Antennas #1 and #2 were used for inspecting this structure, with distances $d = \{0, 0.01, 0.1, 0.2\}$ m between the antenna aperture and the outer paper cylinder. The angular spacing was kept the same in all cases.

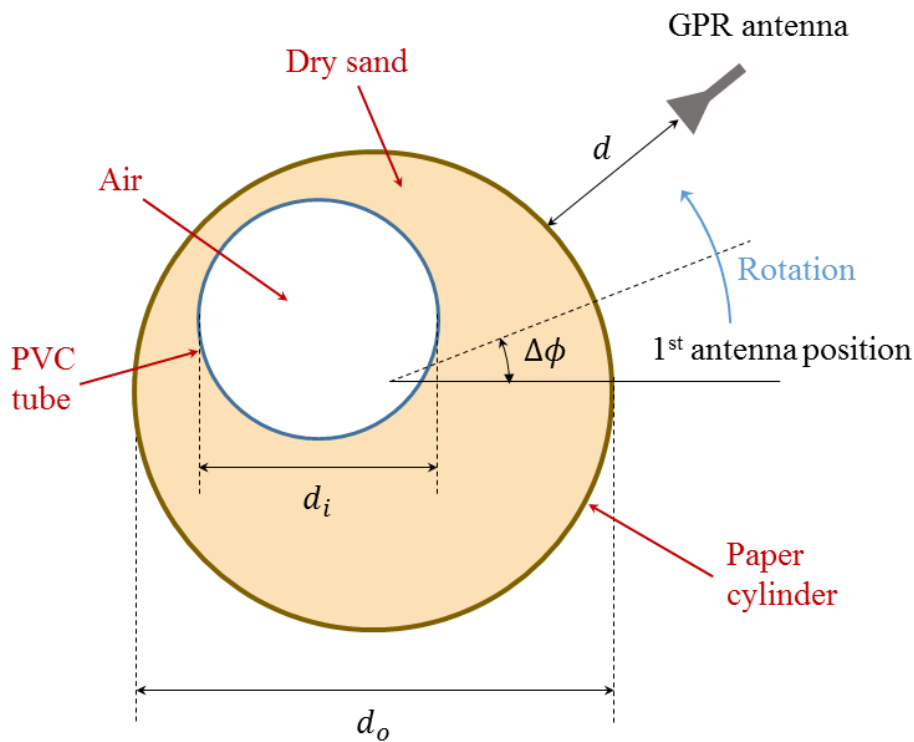


FIG. 10 – Geometrical configuration of the experiments concerning one circular cylinder with void inclusion.



2.5 RECONSTRUCTION METHODS APPLIED TO GPR DATA

After the acquisition of GPR measurements, the pre-processing method proposed in [5] was applied for filtering out antenna effects. To this end, the calibration described above was employed for each antenna. Subsequently, some of the measured GPR data were further processed with two reconstruction methods developed at the Applied Electromagnetics Laboratory of the University of Genoa and modified during the STSM in order to be applied to the present cases.

The first method that was used with experimental data is the qualitative reconstruction procedure outlined in [6]. Essentially, it is based on a filtering step combined with a Delay-and-Sum beamforming. First of all, the field scattered by the buried objects is estimated and separated from the scattering contributions of the soil. After that, a qualitative image of the subsurface domain is obtained by properly combining all the measured data through a time-shift and an integral operator. From the resulting image, the location of the buried targets can be estimated, and rough information about their shape is provided.

The second technique used for processing the experimental data is a quantitative inexact-Newton inverse scattering method [7]. The goal of this procedure is to retrieve the spatial distribution of the dielectric properties (i.e., dielectric permittivity and electric conductivity) in the investigation region. The algorithm, which is able to simultaneously process data acquired at different frequencies, is composed by two nested iterative loops. Since the electromagnetic inverse scattering problem without approximations is nonlinear [8], the outer loop performs a linearization of the scattering equation around the current estimated dielectric properties by means of a Gauss-Newton algorithm. Furthermore, an inner Landweber method solves the obtained linear problem in a regularized way. This method has been extensively tested in presence of simulated data. During the



STSM, the experimental validation of the method has been initiated.

3. DESCRIPTION OF THE MAIN RESULTS OBTAINED DURING THE STSM

In this section, the most significant results obtained in the framework of the present STSM are presented. It is worth remarking that the results shown here are still preliminary, but really promising. The joint work started with this STSM is currently in progress. In particular, the implementation of some modifications in the processing method is being studied, in order to improve the obtained results.

3.1 EXPERIMENTS WITH SAND OF DIFFERENT VOLUMETRIC MOISTURE CONTENT

For an effective application of data processing algorithms and models, the performance of the GPR antenna used for acquiring measurements represents a crucial point. In particular, on one hand the antenna should be well-coupled with the material that surrounds the targets to be inspected. On the other hand, the bandwidth should be sufficiently large in order to collect information about the target in a wide range of frequencies. Both these important parameters have been analyzed for several antennas with different structures during the STSM.

As described in Section 2, A-scans were recorded with the antennas placed on a sand box with different volumetric water contents. Antennas #1, #2, and #3 were used, in the frequency range between 800 MHz and 3 GHz. The results are shown in Figures 11, 12, 13.

Antenna #1 gives the best results. When the volumetric water content is low, a lighter reflection arises from the air-sand interface, and the reflection from the bottom conducting plate is more evident. An opposite trend occurs in presence of high levels



of volumetric water content. The results obtained with antenna #2 are still good, but less stable. Because of the restricted bandwidth, the calibration is more critical, and the signal-to-noise ratio is reduced. Worse results were obtained with antenna #3. Even when the antenna is in contact with the inspected structure, it is difficult to see the reflections from the bottom metal plate. A-scans appear to be significantly corrupted by noise at greater distances from the soil level, too.

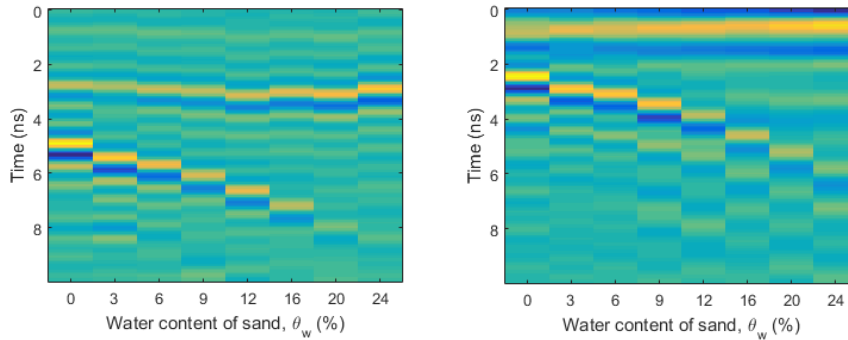


FIG. 11 – A-scans acquired on the sand box with antenna #1, versus the volumetric water content of sand, for different distances from the soil d : $d = 0$ m in the left panel; $d = 0.2$ m in the right panel.

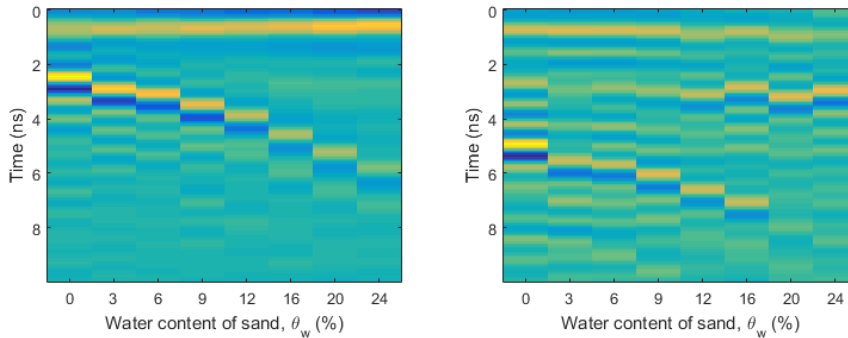


FIG. 12 – Same as in Fig. 11, with Antenna #2.



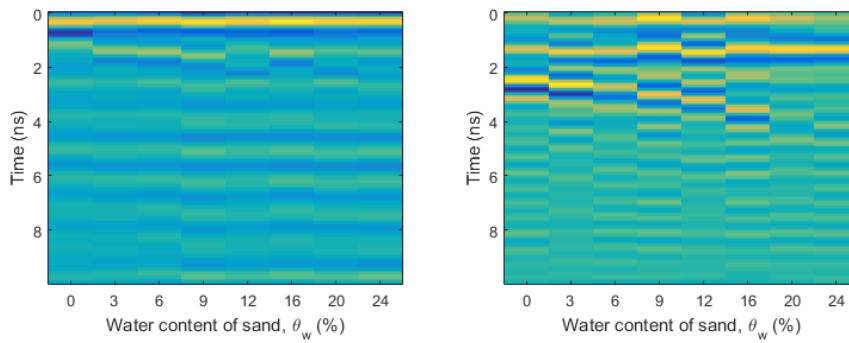


FIG. 13 – Same as in Fig. 11, with Antenna #3.

3.2 SAND BOX WITH BURIED OBJECTS

Some B-scan measurements acquired during the STSM are reported in this section. Let us consider the first test set. In Figure 14, the raw data of the B-scan with antenna #1 at distance $d = 0.01$ m above the soil is depicted. Frequencies between 800 MHz and 3 GHz were considered.

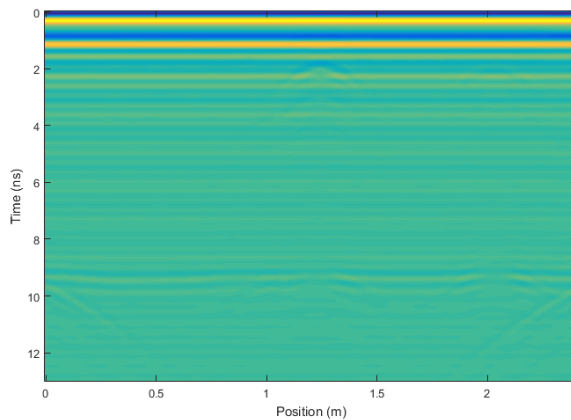


FIG. 14 – First test set in sand box. B-scan acquired with antenna #1 at a distance $d = 0.01$ m from the soil level. No filters to remove antenna effects are applied.



The pre-processed data, obtained after the application of the filter to remove antenna effects are reported in Figure 15. Clearly, this step is fundamental in order to see the reflection hyperbolas arising from the buried objects, that otherwise are hidden behind the internal reflections inside the antenna structure. Since this pre-processing step utilizes the far field model, a better filtering can be made when the antenna is more distant from the soil level. Close to the soil, the near field model described in [9] should be used.

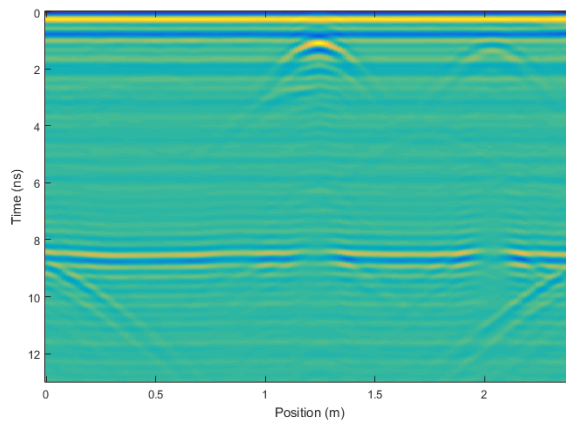


FIG. 15 – First test set in sand box. B-scan acquired with antenna #1 at a distance $d = 0.01$ m from the soil level. Antenna filters are applied.

As an example, in Figures 16 and 17 the raw and the pre-processed B-scans with the same antenna at a distance $d = 0.15$ m from the soil interface are shown. It is easy to see that the filtering step based on the far field model is performing better in this case.

Similar remarks still hold for the results obtained with antenna #3. However, this antenna has a restricted bandwidth. Therefore, only frequencies in the range between 800 MHz and 1.7 GHz were considered.



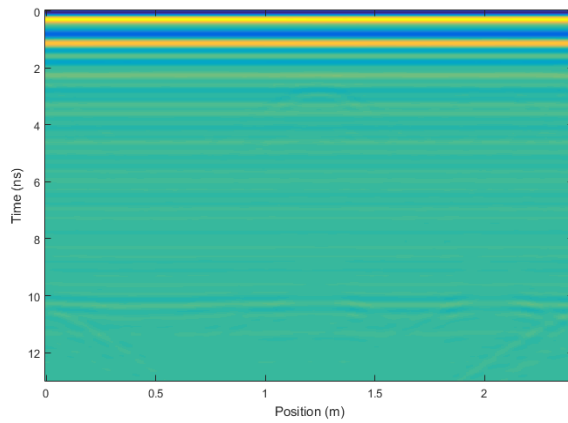


FIG. 16 – First test set in sand box. B-scan acquired with antenna #1 at a distance $d = 0.15$ m from the soil level. No filters to remove antenna effects are applied.

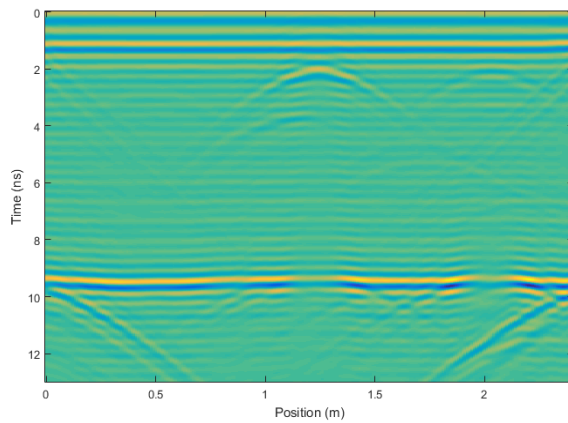


FIG. 17 – First test set in sand box. B-scan acquired with antenna #1 at a distance $d = 0.15$ m from the soil level. Antenna filters are applied.

In Figures 18 and 19 the raw and pre-processed results with antenna #3 placed $d = 0.01$ m far from the soil are presented. Not all the antenna effects are removed in this case, and buried objects are barely visible.

With an increased distance from the soil (e.g. when $d = 0.12$ m, as reported in Figures 20 and 21) results are better and antenna effects are removed. However, the limited bandwidth influences the resolution of the B-scan image significantly.

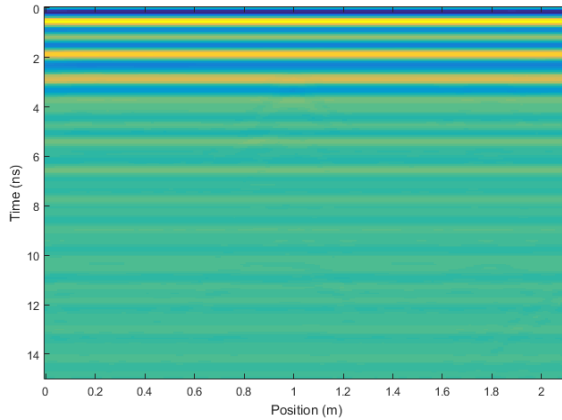


FIG. 18 – First test set in sand box. B-scan acquired with antenna #3 at a distance $d = 0.01$ m from the soil level. No filters to remove antenna effects are applied.

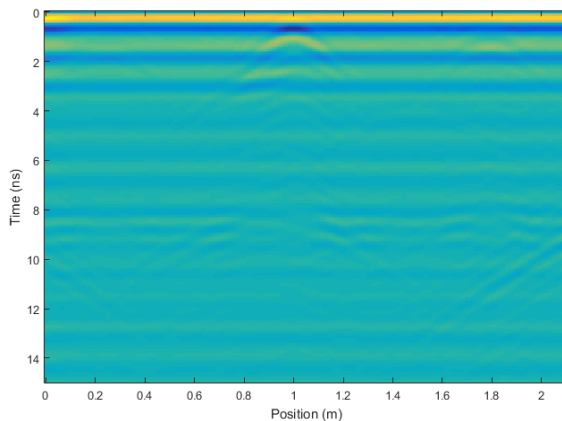


FIG. 19 – First test set in sand box. B-scan acquired with antenna #3 at a distance $d = 0.01$ m from the soil level. Antenna filters are applied.



For the second test set, B-scans collected at heights $d = 0.01$ m and $d = 0.1$ m by using Antenna #1 are shown in Figures 22 – 25. Raw data are in Figures 22 and 24, the processed ones are in Figures 23 and 25. The filtering step appears to be very important and it works better when the far field condition is fulfilled.

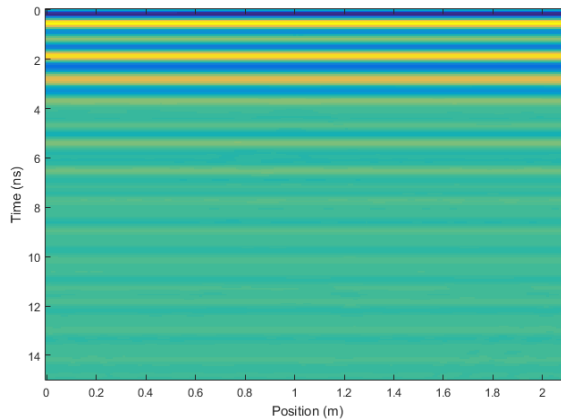


FIG. 20 – First test set in sand box. B-scan acquired with antenna #3 at a distance $d = 0.12$ m from the soil level. No filters to remove antenna effects are applied.

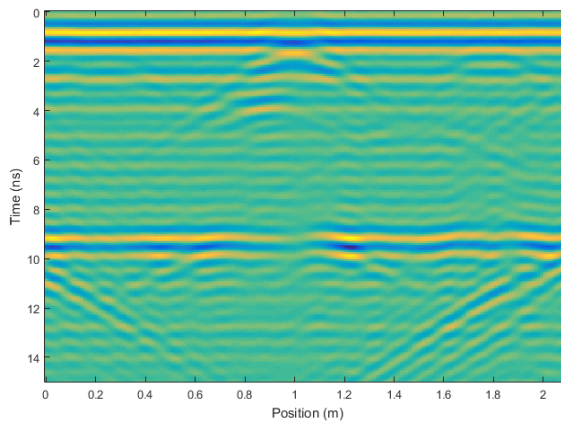


FIG. 21 – First test set in sand box. B-scan acquired with antenna #3 at a distance $d = 0.12$ m from the soil level. Antenna filters are applied.



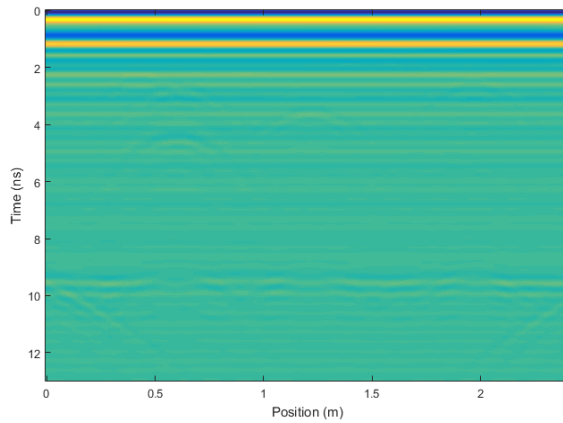


FIG. 22 – Second test set in sand box. B-scan acquired with antenna #1 at a distance $d = 0.01$ m from the soil level. No filters to remove antenna effects are applied.

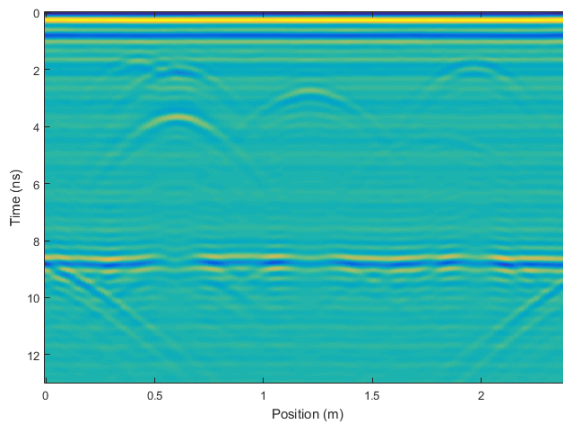


FIG. 23 – Second test set in sand box. B-scan acquired with antenna #1 at a distance $d = 0.01$ m from the soil level. Antenna filters are applied.

Reconstructions results of the targets belonging to the first test set in sand box are shown in Figure 26. Here, the qualitative imaging algorithm presented above was applied to the B-scan at $d = 0.01$ m. As it can be seen, the targets were detected in all cases.



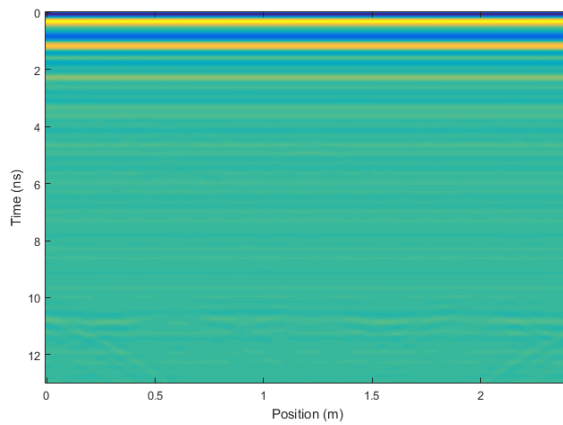


FIG. 24 – Second test set in sand box. B-scan acquired with antenna #1 at a distance $d = 0.1$ m from the soil level. No filters to remove antenna effects are applied.

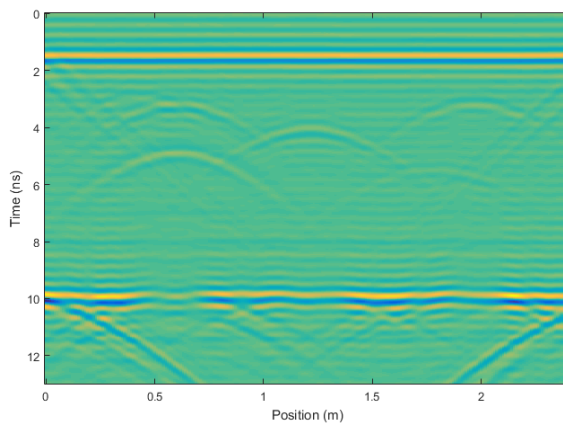


FIG. 25 – Second test set in sand box. B-scan acquired with antenna #1 at a distance $d = 0.1$ m from the soil level. Antenna filters are applied.

A preliminary quantitative reconstruction of the buried void PVC tube is shown in Figure 27. The tube is correctly identified as filled by air (relative dielectric permittivity $\epsilon_r = 1$). Further developments

will be devoted to the detailed analysis of the quantitative imaging results.

Qualitative reconstructions of the second test set are reported in Figure 28, by using the B-Scan at a distance $d = 0.01$ m from the soil. All the three buried cylinders were detected. However, the reconstruction of cylinder #1 is partially obscured by the very close cylinder #2, which has a significantly stronger contrast with respect to the background dielectric properties.

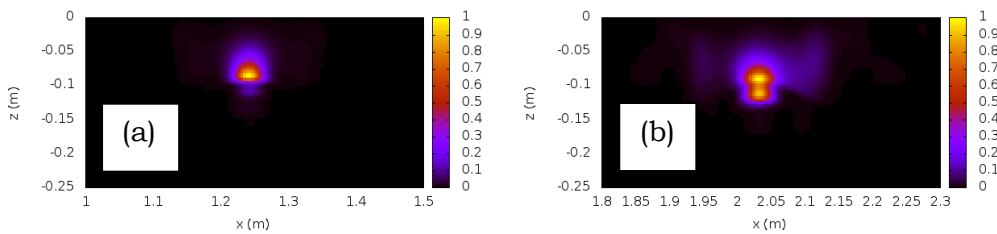


FIG. 26 – First test set in sand box. Qualitative reconstruction results obtained with antenna #1 at a distance $d = 0.01$ m from the soil level: (a) metallic rebar; (b) void PVC tube.

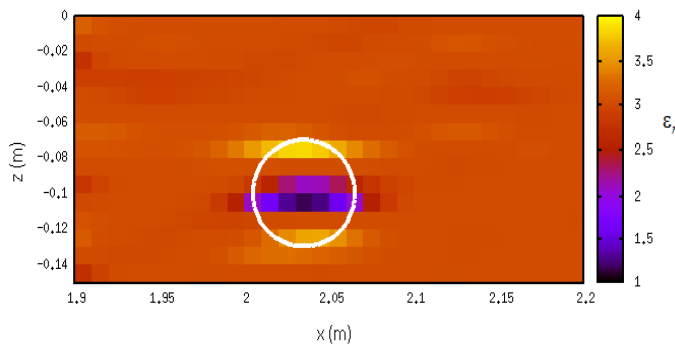


FIG. 27 – Reconstructed distribution of the relative dielectric permittivity obtained with antenna #1 at a distance $d = 0.20$ m from the soil level.



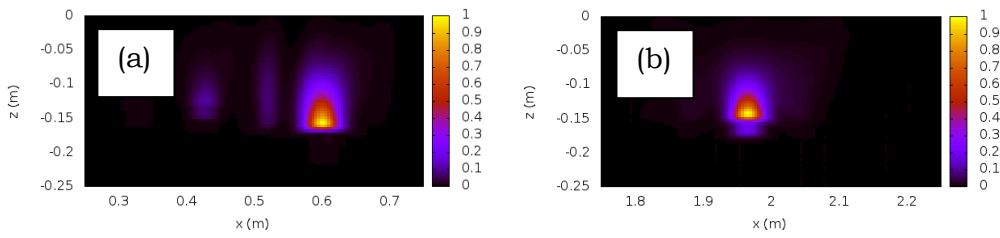


FIG. 28 – Second test set in sand box. Qualitative reconstruction results obtained with antenna #1 at a distance $d = 0.01$ m from the soil level: (a) cylinder #1 and cylinder #2; (b) cylinder #3.

3.3 CIRCULAR CYLINDER WITH VOID INCLUSION

The filtered B-scans acquired with antenna #1 and antenna #2 at two different distances from the circular structure described above are reported in Figures 29 – 32. Results with antenna #1 (Figure 29 and 31) are more stable. The sinusoidal feature due to the inner void cylinder is clearly visible in all cases.

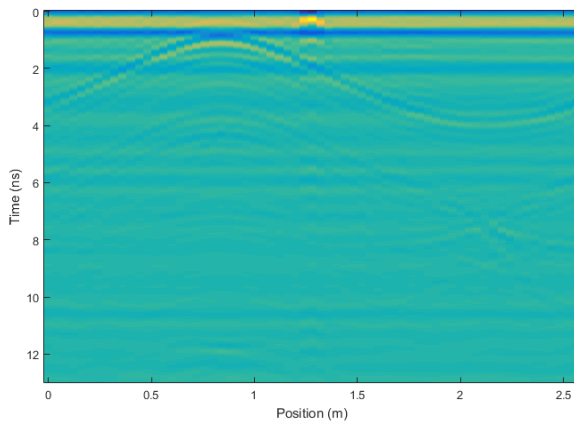


FIG. 29 – Circular cylinder with void inclusion. B-scan acquired with antenna #1 at a distance $d = 0$ m from the sample. Antenna filters are applied.



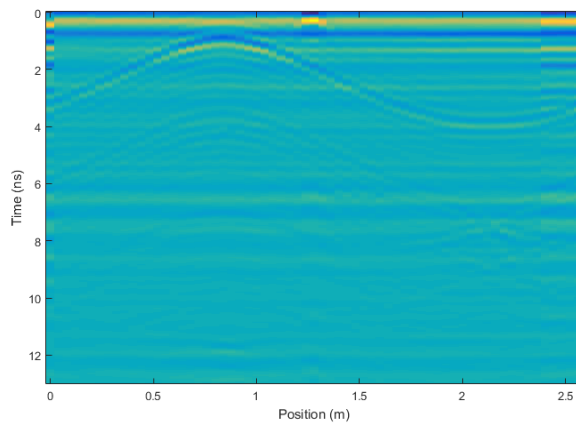


FIG. 30 – Circular cylinder with void inclusion. B-scan acquired with antenna #2 at a distance $d = 0$ m from the sample. Antenna filters are applied.

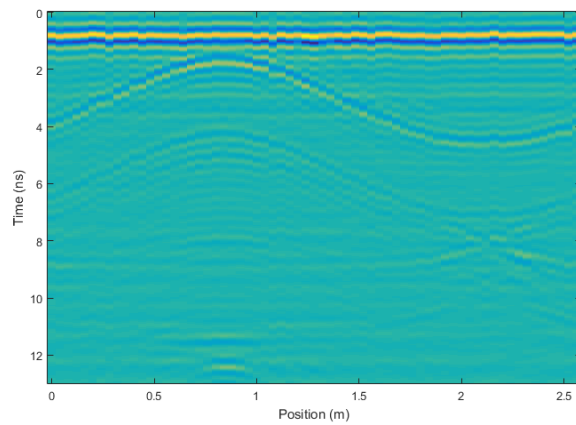


FIG. 31 – Circular cylinder with void inclusion. B-scan acquired with antenna #1 at a distance $d = 0.1$ m from the sample. Antenna filters are applied.



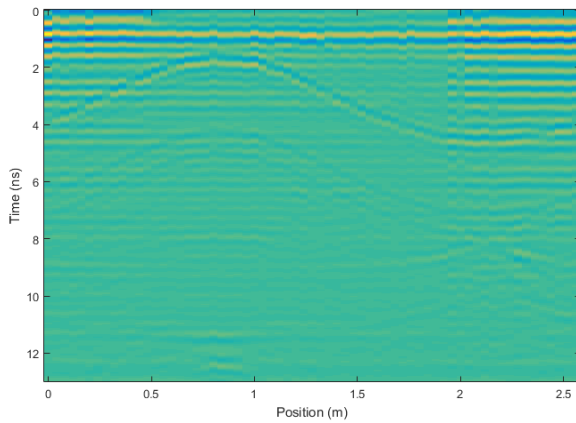


FIG. 32 – Circular cylinder with void inclusion. B-scan acquired with antenna #2 at a distance $d = 0.1$ m from the sample. Antenna filters are applied.

In Figures 33 and 34, the results obtained by means of the qualitative reconstruction method applied to the circular cylinder configuration are shown.

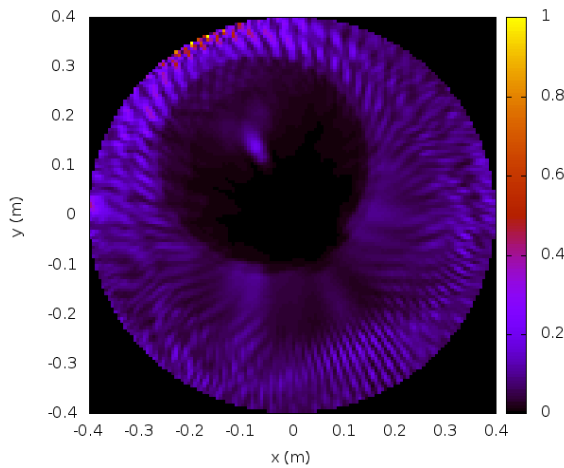


FIG. 33 – Circular cylinder with void inclusion. Qualitative reconstruction result obtained with antenna #1 at a distance $d = 0$ m from the sample.



In particular, Figure 33 is the result with antenna #1, Figure 34 is the corresponding one with antenna #2, both in contact with the outer cylinder. The inner void inclusion was detected, located and correctly shaped in all these tomographic images. Its detected diameter corresponds to the actual value. An artifact appears near the center of the void PVC tube, and this is supposed to be due to the incorrect wave speed used for back-propagating the signals inside the void inclusion (propagation speed value in sand has been always used). As it happened in other cases, the better results are those obtained with antenna #1.

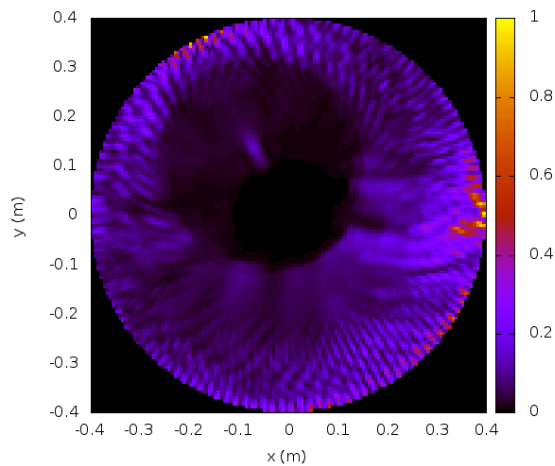


FIG. 34 - Circular cylinder with void inclusion. Qualitative reconstruction result obtained with antenna #2 at a distance $d = 0$ m from the sample.

4. FUTURE COLLABORATION WITH THE HOST INSTITUTION

The present STSM has been very useful not only to face the problem of the tomographical reconstruction of circular structures from an experimental point of view, but also for starting a cooperation between the University of Genoa and the Université Catholique de Louvain in the framework of the development and testing of new systems and reconstruction techniques applied to GPR measurements. This collaboration will be hopefully kept



active with the publication of joint works. Moreover, the processing and the inversion of the all data acquired during the present STSM is not yet completed, since it requires a significant effort from both a mathematical and a computational point of view. Therefore, the possibility of new scientific missions will be considered.

5. FORESEEN PUBLICATIONS/ARTICLES RESULTING FROM THE STSM

The joint activities carried out during this STSM, expanded and integrated with further GPR data processing results that are currently in progress, are expected to be included in a scientific paper to be submitted to an IEEE peer-reviewed international journal, such as the IEEE Transactions on Geoscience and Remote Sensing.

6. ACKNOWLEDGEMENTS

The Authors thank COST, European Cooperation in Science and Technology, for funding COST Action TU1208 and this STSM.

7. REFERENCES

- [1] J. Jeřáková, L. Mertens, and S. Lambot, “Ground-penetrating radar for observing tree trunks and other cylindrical objects,” *Constr. Build. Mater.*, vol. 123, pp. 214–225, Oct. 2016.
- [2] M. Pastorino et al., “A microwave tomographic system for wood characterization in the forest products industry,” *Wood Mater. Sci. Eng.*, vol. 10, no. 1, pp. 75–85, 2015.
- [3] A. Benedetto and L. Pajewski, *Civil Engineering Applications of Ground Penetrating Radar*. Cham: Springer International Publishing, 2015.
- [4] I. Catapano, A. Randazzo, E. Slob, and R. Solimene, “GPR imaging via qualitative and quantitative approaches,” in *Civil Engineering Applications of Ground Penetrating Radar*, A. Benedetto and L. Pajewski, Eds. Springer International Publishing, 2015, pp. 239–280.



- [5] S. Lambot, E. C. Slob, I. van den Bosch, B. Stockbroeckx, and M. Vanclooster, "Modeling of ground-penetrating Radar for accurate characterization of subsurface electric properties," *IEEE Trans. Geosci. Remote Sens.*, vol. 42, no. 11, pp. 2555–2568, Nov. 2004.
- [6] A. Fedeli, M. Pastorino, and A. Randazzo, "A two-step multifrequency imaging technique for ground penetrating radar," in *2016 10th European Conference on Antennas and Propagation (EuCAP)*, 2016.
- [7] C. Estatico, A. Fedeli, M. Pastorino, and A. Randazzo, "A multifrequency inexact-Newton method in L_p Banach spaces for buried objects detection," *IEEE Trans. Antennas Propag.*, vol. 63, no. 9, pp. 4198–4204, Sep. 2015.
- [8] M. Pastorino, *Microwave imaging*. John Wiley & Sons, 2010.
- [9] S. Lambot and F. André, "Full-Wave Modeling of Near-Field Radar Data for Planar Layered Media Reconstruction," *IEEE Trans. Geosci. Remote Sens.*, vol. 52, no. 5, pp. 2295–2303, May 2014.



STSM 3 & STSM 4

DEVELOPMENT OF GUIDELINES FOR FLEXIBLE PAVEMENT EVALUATION AND FOR THE DETECTION OF BURIED UTILITIES AND VOIDS IN URBAN AREAS, BY USING GROUND PENETRATING RADAR

VISITING SCIENTISTS: XAVIER DÉROBERT, IFSTTAR, BOUGUENAI, FRANCE; SIMONA FONTUL, LNEC, LISBOA, PORTUGAL
XAVIER.DEROBERT@IFSTTAR.FR, SIMONA@LNEC.PT

HOST SCIENTIST: LARA PAJEWSKI, SAPIENZA UNIVERSITY OF ROME, DEPARTMENT OF INFORMATION ENGINEERING ELECTRONICS AND TELECOMMUNICATIONS, ROME, ITALY
LARA.PAJEWSKI@UNIROMA1.IT

STSM DATES: 17TH OCTOBER – 21ST OCTOBER 2016

1. PURPOSE OF THE JOINT STSM

Technical guidelines for the use of Ground Penetrating Radar in civil engineering represent one of the main deliverables of Working Group 2 of COST Action TU1208.

The development of three guidelines was planned:

1. Guidelines for the detection and mapping of underground utilities and voids, in urban areas
2. Guidelines for investigating flexible pavements
3. Guidelines for investigating concrete structures

Additionally, recommendations for a safe use of GPR were already developed and published by a team of Action Members and external experts [1]. Recommendations for the use of GPR in buildings were prepared and will be published as a report.



The main objective of this joint STSM was to work at the guidelines for the investigation of flexible pavement. The STSM represented also an opportunity for making corrections and improvements in the draft guidelines for the detection and mapping of underground utilities and voids.

2. DESCRIPTION OF THE WORK CARRIED OUT DURING THE STSM

The STSM was carried out according to the timeline provided below.

Day 1

- Discussion concerning the most appropriate format and table of contents of the guidelines.
- Planning of the week and interaction with colleagues working remotely, who expressed their availability to contribute and cooperate with us.

Day 2

- Review of severable available reference documents, useful for the development of guidelines.
- Review of draft TU1208 guidelines.

Days 3-4

- Writing of guideline sections, in cooperation with colleagues in remote connection.

Day 5

- Finalization of the updated drafts.
- Discussion of system performance compliance tests to be proposed in the guidelines.
- Definition of tasks for the visiting scientists, the host scientist and the remote contributors, to be fulfilled during the upcoming weeks.



The updated drafts of TU1208 guidelines, produced during this STSM, were subsequently presented and discussed during the Sixth General Meeting in Split, Croatia, November 7-9, 2016.

The updated drafts represent the main deliverable of this STSM and were submitted as an annex, along with this short report. For obvious reasons, the drafts are not included here. The final version of the guidelines will be soon available on the website of COST Action TU1208.

3. FUTURE COLLABORATION WITH THE HOST INSTITUTION

Near-future collaboration will be focused on the finalization of the guidelines.

The STSM strengthened the professional and personal relationship between the visiting and host scientists, we will surely continue our collaboration beyond the Action lifetime.

In the framework of the Action, we experienced that STSMs and small WG meetings are amazing networking tools, which allow achieving significant results in a limited amount of time.

4. ACKNOWLEDGEMENT

The visiting scientists and the host scientist would like to thank COST for funding COST Action TU1208 and this joint STSM.

5. REFERENCES

- [1] R. Persico, A. Provenzano, C. Trela, M. Sato, K. Takahashi, S. Arcone, S. Koppenjan, L. G. Stolarczyk, E. C. Utsi, S. Ebihara, K. Wada, E. Pettinelli, L. Pajewski. Recommendations for the safety of people and instruments in Ground-Penetrating Radar and near-surface geophysical prospecting. Authors: Publishing House: European Association of Geoscientists and Engineers (EAGE) June 2015. ISBN 978-94-628-2162-0.



STSM 5

FINALIZATION OF A FREEWARE DATA-PROCESSING TOOL IMPLEMENTING A SAP-DoA TECHNIQUE

VISITING SCIENTIST: SIMONE MESCHINO, AIRBUS DS, SAR SYSTEMS
ENGINEERING, FRIEDRICHSHAFEN, GERMANY
SIMONE.MESCHINO@GMAIL.COM

HOST SCIENTIST: LARA PAJEWSKI, SAPIENZA UNIVERSITY OF ROME,
DEPARTMENT OF INFORMATION ENGINEERING ELECTRONICS AND
TELECOMMUNICATIONS, ROME, ITALY
LARA.PAJEWSKI@UNIROMA1.IT

STSM DATES: 27TH DECEMBER 2016 – 05TH JANUARY 2017

1. PURPOSE OF THE STSM

This STSM contributed to the achievement of the objectives of Working Group 3 of COST Action TU1208 “Civil Engineering Applications of Ground Penetrating Radar” and was devoted to finalizing the work carried out during two previous STSMs:

- April 3rd – 10th, 2015
- Jan 4th – 10th, 2016

During the third STSM, a MATLAB Graphical User Interface (GUI) was implemented and a Manual was written, for the SAP-DoA codes that we developed during the previous two missions. Let us recall that our SAP-DoA codes allow detecting and localizing metallic and dielectric cylindrical objects of arbitrary shape embedded in a host material. The software (constituted by the GUI and the codes) is called SPOT-GPR and is available for public download on the website of our COST Action, www.GPRadar.eu.



2. WORK CARRIED OUT DURING THE STSM AND MAIN RESULTS

This STSM report was selected for open-access publication on the first issue of the first volume of the new journal *Ground Penetrating Radar* (www.GPRadar.eu/journal). The interested Readers are therefore kindly invited to download the paper [1], which basically describes what we did during this STSM.

3. FUTURE COLLABORATION WITH THE HOST INSTITUTION

Our plans for future work include:

- Testing our SAP-DoA approach on experimental data. We wish to process some radargrams of the TU1208 dataset coming from measurements performed at the IFSTTAR Geophysical Test Site (Nantes, France).
- Comparing the SAP-DoA method with an automatic detection algorithm based on neural networks developed at the Faculty of Technical Sciences of Novi Sad (Serbia).
- Combining the SAP-DoA approach with Support-Vector-Machine (SVM) techniques, in cooperation with the University of Genoa (Italy). These techniques are expected to increase the robustness of our approach with respect to the distance between sought targets, as they are more powerful than standard DoA algorithms in handling electromagnetic interactions between objects.
- Adding to the software further DoA algorithms. Currently the employed DoA algorithm is MUSIC. We also considered the following algorithms: Bartlett, Capon, Linear Prediction, Maximum Entropy, Minimum Norm, PHD. We will soon prepare a new release of the software where also these algorithms will be available.



4. FORESEEN PUBLICATIONS/ARTICLES RESULTING FROM THE STSM

As already mentioned, based on this STSM the paper [1] was prepared. Moreover, in the recent paper [2] we described the approach that we developed and implemented during the previous two STSMs, and presented some results.

We are currently working on the comparison between SPOT-GPR and the automated detection algorithm developed in Serbia. With our colleagues Željko Bugarinović, Miro Govedarica, Aleksandar Ristić, Milan Vrtunski and Xavier Derobert we will publish the results of such comparison in an invited paper that will be entitled “Automated Data Extraction from Synthetic and Real Radargrams of Complex Structures” and will be submitted to the Journal of Environmental & Engineering Geophysics.

5. ACKNOWLEDGEMENT

We are grateful to COST, European Cooperation in Science and Technology, for funding COST Action TU1208 and this STSM.

6. REFERENCES

- [1] S. Meschino and L. Pajewski, “A practical guide on using SPOT-GPR, a freeware tool implementing a SAP-DoA technique,” Ground Penetrating Radar, Vol.1(1), pp. 104-122, January 2018.
- [2] S. Meschino and L. Pajewski, “SPOT-GPR: A Freeware Tool for Target Detection and Localization in GPR Data Developed within the COST Action TU1208,” Journal of Telecommunications and Information Technology, Vol. 2017(3), pp. 43-54, September 2017.



STSM 6

GPR ASSESSMENT OF RAILWAY BALLAST

VISITING SCIENTIST: SALIH SERKAN ARTAGAN, ANADOLU UNIVERSITY,
ESKIŞEHİR, TURKEY
SSARTAGAN@ANADOLU.EDU.TR

HOST SCIENTIST: ANDREA BENEDETTO, DIPARTIMENTO DI INGEGNERIA,
UNIVERSITA' DEGLI STUDI “ROMA TRE,” ROME, ITALY
ANDREA.BENEDETTO@UNIROMA3.IT

STSM DATES: 23RD JANUARY – 02ND FEBRUARY 2017

1. PURPOSE OF THE STSM

As stated in the Memorandum of Understanding of COST Action TU1208, one of the aims of the Action is to enhance more efficient and wider exploitation of the GPR technique in the monitoring of infrastructures, hence facilitating their overall management and minimizing the severe and fatal accidents caused by infrastructure deformations.

Present STSM contributed to the achievement of the objectives of Working Group 2 of COST Action TU1208. The purpose of the STSM was to evaluate the electromagnetic (EM) response of ballast material (coarse crushed stones), which is the key element for the railway infrastructures, under different configurations of laboratory experiments. In particular, the main aim was to understand how and to what extent GPR signal is influenced by the clean and fouled configurations of ballast material with and without the reinforced concrete sleepers and rails by using four different air-coupled antennas. One of the goals was to determine the variation of relative permittivity of ballast material caused by fouling.



2. DESCRIPTION OF THE WORK CARRIED OUT DURING THE STSM

2.1 INTRODUCTION TO GPR APPLICATIONS ON RAILWAYS

Since the STSM topic is focused on ballast material testing, it is noteworthy to introduce the railway ballast and its crucial functions on railways. Railways are regarded as the most environment-friendly, cost effective type of transportation with its more reliable and better organized nature [1]. Moreover, higher capacity, suitability for bulky and heavy goods, high speed over long distances and relative safety compared to other transportation modes are the basic advantages of railway transportation at the first glance [1, 2]. Therefore, maintaining the economic, safe, comfortable and fast transportation conditions on railways is of crucial importance to the railway operator companies. To accomplish this, timely maintenance of track structure with minimum traffic interruptions and slow orders is required. Typical railway structure can be categorized into two main groups as substructure and superstructure, where substructure is composed of ballast, sub ballast and subgrade, while superstructure comprises rails, sleepers (ties) and other fastening accessories [3].

The status of railway substructure has a substantial impact on track performance. Track substructure in poor condition not only may generate an immense rate of track geometry deterioration but also lead to higher degrees of wear or even failures of rails, sleepers, fasteners, etc. [4]. Currently, majority of track inspection processes is carried out by means of traditional methods, which are visual inspection by an experienced railway engineer and/or opening trenches at the locations where potential deterioration is likely to occur [3, 5, 6]. Portable ballast samplers is also a way of inspection [7]. However, none of these methods provide continuous information and there is the possibility to miss out the potential degraded sections in between two selected trench locations. Besides, the whole procedure in traditional methods requires labor



and takes a considerable amount of time [1, 3, 8]. At this point, it has to be noted that high quality ballast has a pivotal role in track structure and overall stability [9] since ballast has the following fundamental functions [3, 6, 9]:

- Resist vertical, longitudinal and lateral stresses applied to sleepers to preserve the track position.
- Decrease stress implemented to weaker interfaces.
- Reduce formation of frost.
- Provide flexibility and ensure energy and noise absorption for the track.
- Enable drainage of water from the track platform.

Therefore, appropriately maintaining ballast is the most essential subject in avoiding the gradual worsening of the track bed and subsequently the deformation of the tracks. An ignorance in minor drainage complications together with an overlook in fouling levels in the ballast body may give rise to severe maintenance troubles and induce lower safe speeds and raise the probability of derailments [9].

In other words, ballast fouling -i.e. contamination of ballast- may disable the ballast body of the track to fulfil the above-mentioned expected functions and risk the overall safety of the track [3]. Ballast fouling takes place when voids in the ballast are filled because of ballast breakdown and infiltration of other materials from the ballast surface or infiltration from the base of the ballast layer [10].

According to Selig and Waters [5], reasons of ballast fouling could be divided into five categories, which are:

- Ballast breakdown (76 %)
- Underlying granular layer infiltration (13 %)



- Ballast surface infiltration (7 %)
- Subgrade infiltration (3 %)
- Sleeper wear (1 %).

Taking into account the destructive work, elapsed time, discontinuity of surveys, traffic obstructions and low speed limitations encountered during the traditional railway maintenance works, rail industry has been seeking for time saving and cost-effective maintenance procedures. In this respect, Ground Penetrating Radar (GPR) has excited great interest of researchers and practitioners in railway ballast evaluation as a noninvasive geophysical detection method overcoming the restrictions of the traditional methods [1, 11].

GPR is a probing technique, which uses discrete pulses of EM (electromagnetic) energy in order to detect variations of electrical properties of the subsurface [12, 13]. GPR has been in use for about 5 decades and it has proven itself as a strong geophysical method in order to diagnose and monitor the subsurface structural and material aspects [14, 15]. Especially with the recent improvements of the hardware and software technology, there has lately been a boost in both applications and researchers getting involved in the method [14].

[16] notes that railway industry has also begun to make use of GPR technology in mid-nineties in Europe (mainly in Switzerland, UK, Finland), and North America and since then many conducted GPR surveys over railways have almost transformed the use of the method into a routine, fast, economic and continuous inspection tool in mainly ballast surveys [16].

Basically, GPR has been used in a wide range of evaluation aspects for railway infrastructure such as determination of layer thicknesses[17], investigation of embankment stability [18], localization of trapped water areas [11]. GPR has also seen use particularly to assess the fouling of ballast [10, 19–25].



However, there seems to be an open and challenging issue for evaluation of GPR signal through railway ballast where it is located between and under sleepers and rails as in the real case. It is also stated by researchers [23,26] that the information beneath the sleepers is more valuable than the ones in the cribs (the regions between the sleepers).

2.2 PREPARATION OF THE LABORATORY TESTS AND CONFIGURATIONS

As explained in [27], ballast aggregate particles were gradually polluted with fine-grained silty soil (within the A4 group as per AASHTO) within a methacrylate tank representing a railway track bed structure. Almost 50 % of the ballast material fall in dimensions between 31.5 mm ÷ 50 mm and categorically falls into Class A identified by the EN 13450:2002/AC:2004 standard [27].

When I arrived at Universita' Degli Studi Roma Tre, the ballast material in the flexi-glass was already in highly fouled condition (24 %) [27]. Figure 1 depicts above-mentioned fouled condition.

RFI 230 type sleeper was selected as per the code in Italy. Then, reinforced concrete sleepers are prepared accordingly and reinforcement bars were tied.



FIG. 1 – Fouled condition of ballast in the tank at the beginning of the laboratory experiments.



However, less number of stirrups was used in the sleepers, in order just to hold the longitudinal bars and to evaluate only their effects on GPR response. Aggregates, sand, water and cement were weighed according to the concrete mix design and sleepers were casted in concrete with required tools and appropriate workability condition of concrete provided. Preparation stage of sleepers and schematic representation of their cross-section can be seen in Figures 2 and 3, respectively.



FIG. 2 - Preparation of sleepers and placing them in the tank.

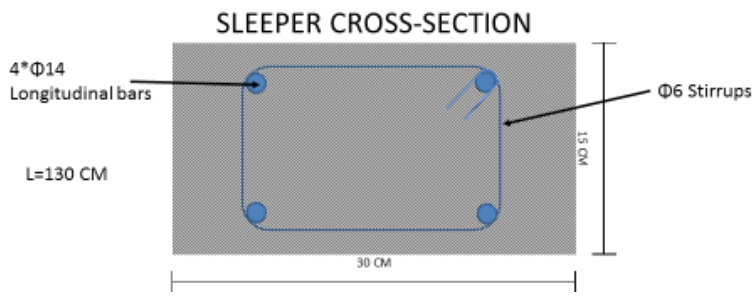


FIG. 3 - Sleeper Cross-Section.



2.3 INSTRUMENT AND EQUIPMENT USED FOR LABORATORY EXPERIMENTS

The experimental tests were conducted using four air-coupled systems (Figure 4), all of which were manufactured by IDS (Ingegneria dei Sistemi S.p.A.), with three different nominal frequencies of 1000 MHz (RIS Hi-Pave HR1 1000), 1500 MHz (RIS Hi-Pave VEE 1500), and 2000 MHz (RIS Hi-Pave HR1 2000 and 2000 NA).

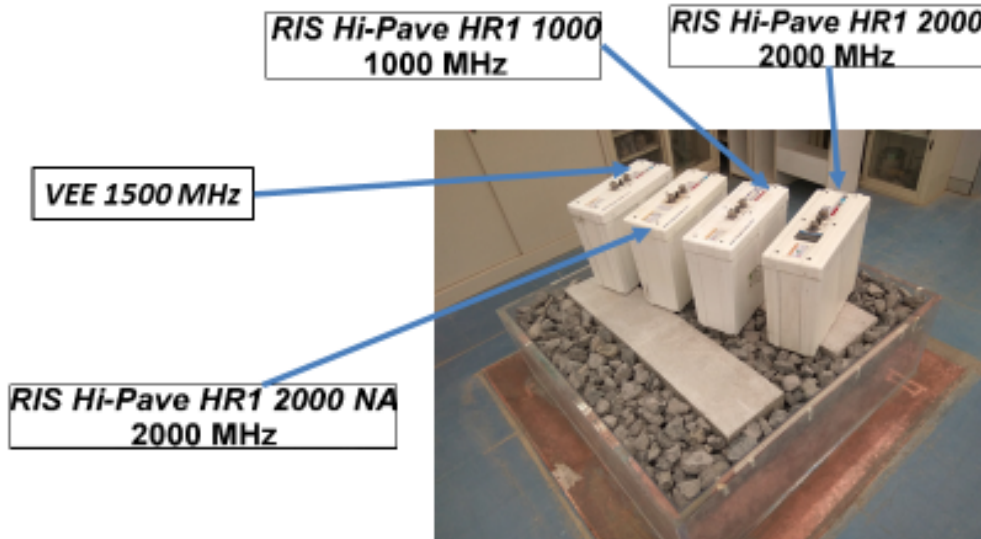


FIG. 4 – Instruments used for laboratory experiments.

Regarding the 2000 MHz radar systems, one normal (i.e., 2000 MHz EU) and one depowered (i.e., 2000 MHz NA) version of the horn antenna for the European (EU) and the North-American (NA) markets, respectively, were used.

Time windows of 25 ns for the 1000 MHz and the 1500 MHz systems were used and 15 ns were set for the 2000 MHz systems. 512 time samples were used for 1000 MHz and 2000 MHz



antennas, whereas 1024 time samples were used for 1500 MHz antenna.

The metallic reflector metallic sheet at the bottom of the tank is 2 x 2 m. The square-based methacrylate tank with outer base sides and height of, respectively, 1.55 m and 0.55 m [27]. The air gap between the bottom of antenna and the surface of ballast is 40 cm, as recommended by the manufacturer of antennas (IDS). Two steel rods in horizontal position were used to imitate the rails and they were placed in such a way that the standard rail gauge of 143.5 cm is ensured between them. The height of fouling material (silty soil) is 30 cm. All mentioned dimensions, equipment and materials can be seen in Figure 5.

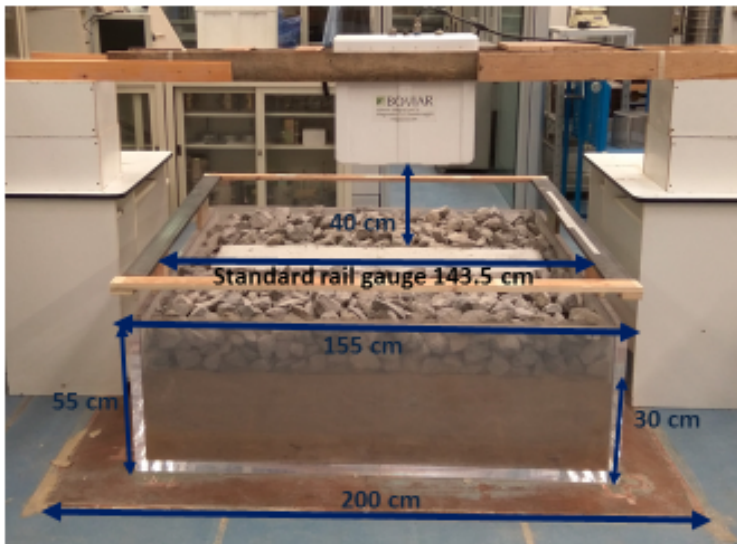


FIG. 5 - Basic dimensions of test set up.

During the STSM in Rome, laboratory characterization of railway ballast with respect to different configurations was performed. 5 levels of parameters were tested. Figure 6 indicates the parameters tested in order of hierarchy during laboratory experiments.





FIG. 6 - Parameters tested in order of hierarchy from left to right.

2.4 TESTED PARAMETERS

The tested parameters were the ballast condition, the number of sleepers in the tank, with or without rail imitating steel rods, antenna orientation, antennas used during the measurements

BALLAST CONDITION

The major parameter tested was fouling condition of ballast. There were two different scenarios. Fouled ballast condition (24 %) was formed in such a way that the fouling material reached a height of 30 cm in the tank [27]. The other scenario was clean ballast condition. As I expressed above, when I arrived at the laboratory of Universita' Degli Studi Roma Tre for STSM, the ballast material in the flexi-glass was already in fouled condition [27]. Then after the tests for fouled ballast was completed, the silty soil was removed from the tank, in order to perform the same tests for the clean ballast configuration. The fouled ballast configuration, removal phase of fouling material from the tank and the clean ballast configuration can be seen in Figure 7, respectively.





FIG. 7- Fouled ballast configuration, arrangement of the tank for clean ballast configuration and finally clean ballast configuration.

NUMBER OF SLEEPERS IN THE TANK

There have been three scenarios in this category; namely "no sleeper" case, "one sleeper" case and "two sleepers" case. These three different sleeper cases were tested under both fouled and clean ballast configurations as can be seen in Figure 8.



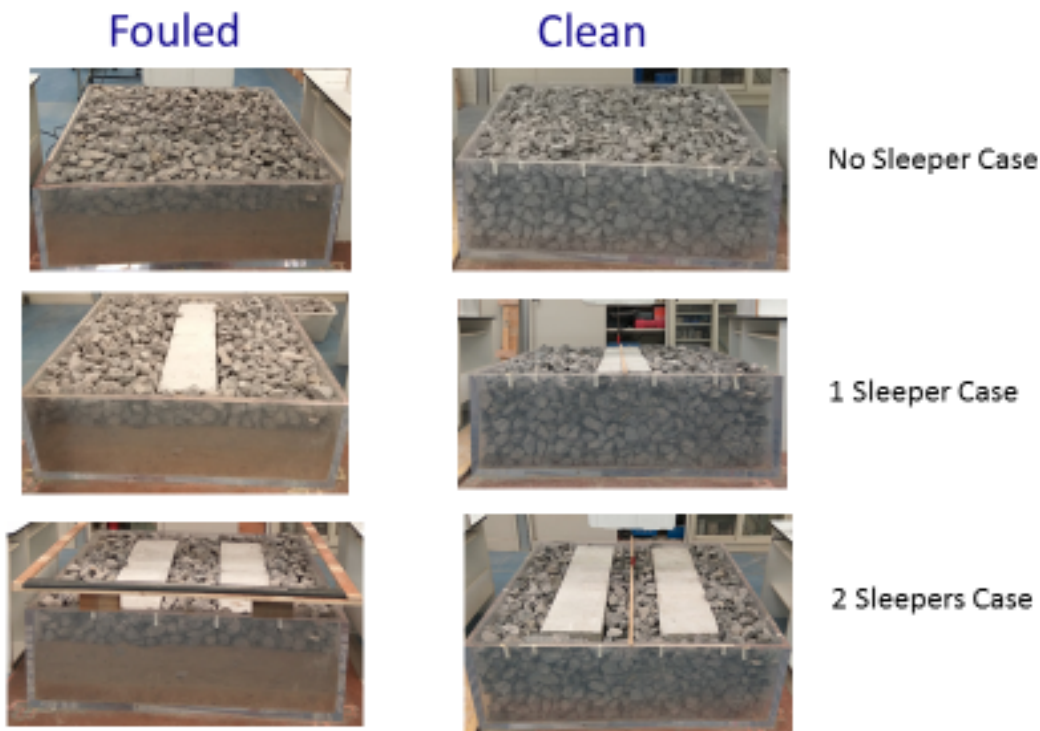


FIG. 8- No sleeper, one sleeper and two sleepers cases.

WITH OR WITHOUT RAIL IMITATING STEEL RODS

Under “ballast condition” main category and “number of sleepers” sub-category, all the cases are tested with and without rails except for “no sleeper” case. In Figure 9, the steel rods which were placed horizontally, are presented. They were used to replicate the real rails together with “with rails” and “without rails” configurations. Also in fouled ballast condition with two sleepers case, we tried an additional steel rod which were placed vertically just under one of the horizontal steel rods to imitate the rail conditions better. However, as it will also be mentioned in the results part of this report, it turned out to have no significant effect compared to the same configuration without this vertical steel rod. Therefore, this vertical rod was not used for the other scenarios.



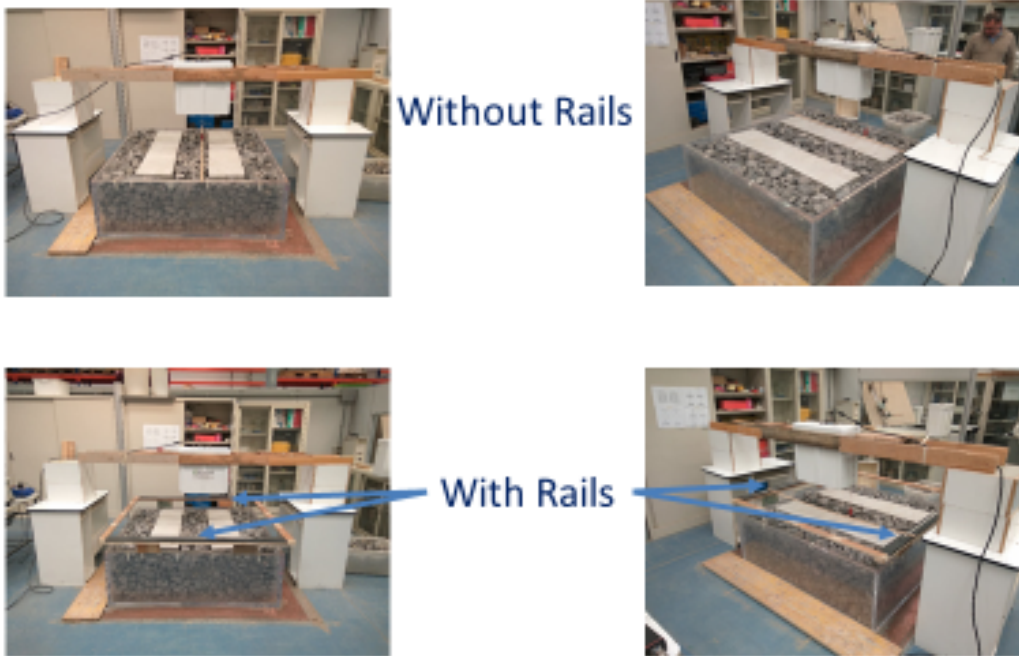


FIG. 9 - “Without rails” and “With rails” cases and steel rods used to replicate the real rails.

ANTENNA ORIENTATION

This sub-category comprises two types of orientation, namely longitudinal and transverse orientations. In longitudinal orientation, the antenna was moved in such a way that the longer size of the antenna in its plan view was perpendicular to the sleepers. In other words, the antenna movement direction was the same direction as a train’s travelling direction through a real track. On the other hand, in transverse orientation, the antenna was moved in such a way that longer size of the antenna is parallel to the sleepers. All tests conducted in “ballast condition” main category and “number of sleepers” sub-category and “with rails” and “without rails” sub-category were also performed in longitudinal and transverse directions.



In Figure 10a, longitudinal orientations of antennas in one sleeper and in Figure 10b two sleeper cases are sketched. In this figure black arrows indicate the movement of antenna from one end to the other end. These ends are dictated by the edge influences of the tank on the GPR signal. Actually, the dimensions of the tank were determined taking into account those edge effects, after evaluation of the antenna's footprints as described in [27].

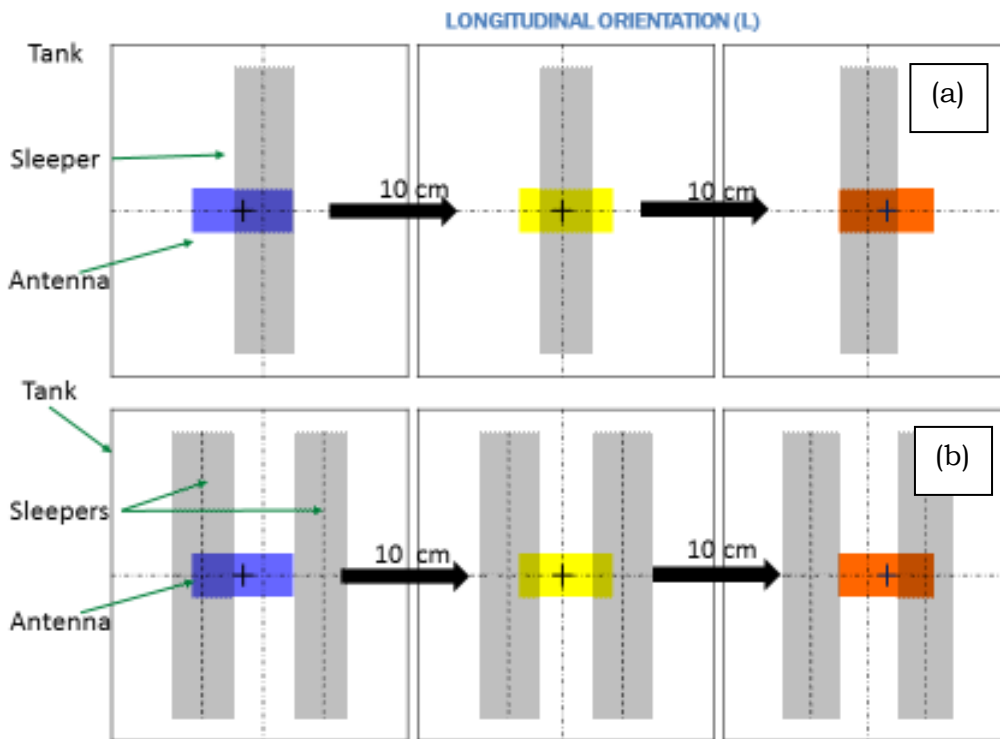


FIG.10- Longitudinal orientation of antenna with respect to sleepers: (a) One sleeper case and (b) Two sleepers case.

In the longitudinal orientation, the antenna was moved from -10 cm to +10 cm, in 2 cm intervals at a total of 20 cm length, to avoid edge effects. For both, one and two sleeper cases, the leftmost part was the starting point of measurement with the GPR antenna (-10

cm). The middle part was the central position of the route of antenna, that it is exactly located over the center of the tank, which was "zero" position. The rightmost part was the ending point of the measurement with GPR antenna (+10 cm).

Figure 11 depicts the photographs taken exactly at the leftmost, middle and rightmost positions of the antenna during the longitudinal orientation measurements in the clean ballast configuration with two sleepers case.

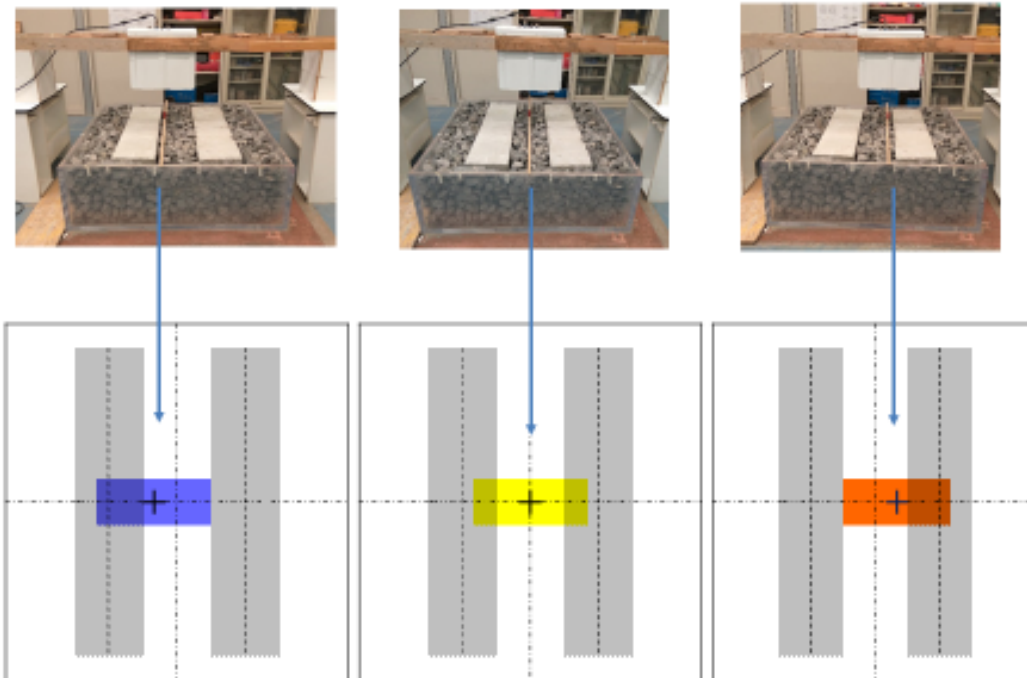


FIG. 11- Photographs taken exactly at the leftmost, middle and rightmost positions of the antenna during the longitudinal orientation measurements in the clean ballast configuration with two sleepers case.

From the beginning point to the ending point of measurements, at each 2 cm a measurement was conducted. In total, 11 acquisitions



were recorded and at each point acquisition, at least 100 traces are collected in auto-stacking mode (static mode).

As for the transverse antenna orientation, measurements were performed considering the edge effects. However, in this case, the orientation of antenna with respect to the tank allowed us to move the antenna a longer distance of 80 cm, which resulted in a quite intense data collected at each 2 cm intervals from -40 cm to +40. In Figure 12a, transverse orientations of antennas in one sleeper and in Figure 12b two sleeper cases are shown. In this figure, black arrows indicate the movement of antenna from one end to the other end. These ends were dictated by the edge effect of the tank on the GPR signal. See also Figure 13.

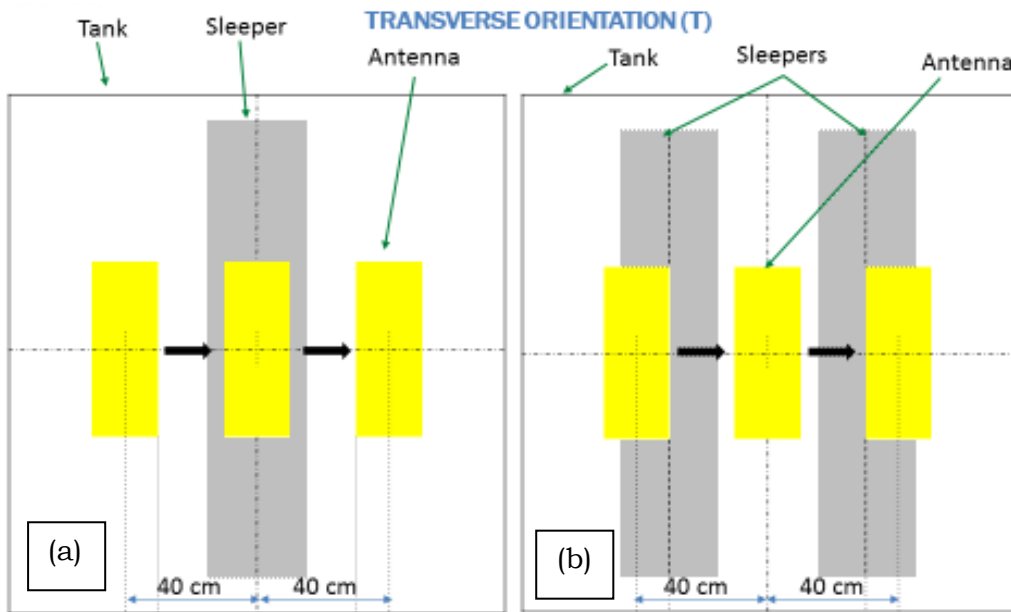


FIG. 12- Transverse orientation of antenna with respect to sleepers: (a) One sleeper case and (b) Two sleepers case.



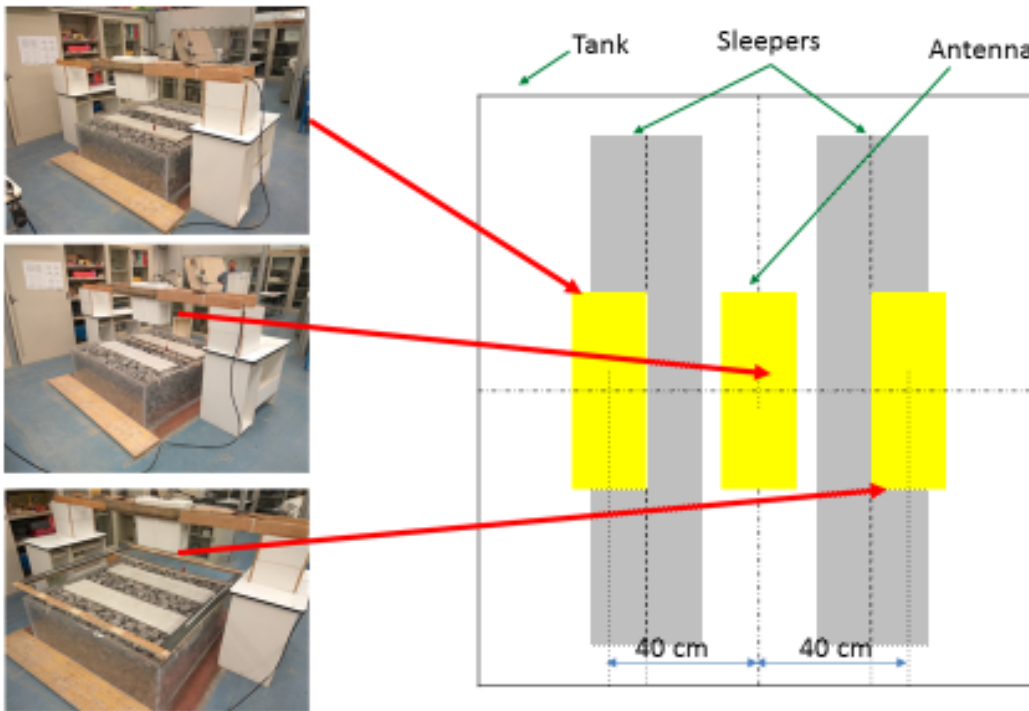


FIG. 13- Photographs taken exactly at the leftmost, middle and rightmost positions of the antenna during the transverse orientation measurements in the clean ballast configuration with two sleepers case.

From the beginning point to the ending point of measurements, at every 2 cm a measurements was conducted. In total, 41 acquisitions were performed and at each measurement point and at least 100 traces were collected in auto-stacking mode.

ANTENNAS USED DURING THE MEASUREMENTS

Four air-coupled antennas (Figure 4) with three different central frequencies (1 GHz, 1.5 GHz and 2 GHz) were used for all of the tests performed. The antennas were employed in every described scenario: “ballast condition” main category, “number of sleepers”



sub-category, “with rails”, “without rails” sub-category and “antenna orientation” (Figure 6).

For data acquisition, K2 Fast Wave software was used, whereas Reflex W was used for data post-processing.

As a result of above-mentioned 5 parameters tested, according to the Figure 6, to summarize the type of acquisitions Table 1 and 2 were created, in which the number of surveys performed is detailed.

As can be observed in Table 1, for fouled ballast condition, 42 surveys were conducted, and as detailed in Table 2, for clean ballast condition, 40 surveys were conducted. The difference in the number of surveys was due to the fact that to imitate the rail conditions more realistically, we performed an additional pair of tests with an extra steel rod which was placed vertically just under one of the horizontal steel rods. However, no significant influence was observed compared to the same configuration without this vertical steel rod. Therefore, vertical steel rod was not used for the other tests.

Some of the sub-categories in Table 1 and 2 are strikethrough, which means that those tests were conducted. For no sleeper case, horizontal steel rods, which imitated rails, were not used, since when we did not use sleepers, it did not make sense to have rails in the surveys. In specific surveys, we did not use the 2000 MHz NA antenna.

If one asks about a summary of experiments performed during this STSM by numbers, the following will be the answer of this question:

- 1 week for preparation of sleepers (concrete casting and curing).



- 3 days for arranging the scenarios of clean and fouled ballast.
- 5 levels of parameters tested.
- 10 days for taking the scans from 4 antennas.
- A total of 11 surveys and 82 acquisition obtained.

3. DESCRIPTION OF THE MAIN RESULTS OBTAINED DURING THE STSM

3.1 RELATIVE PERMITTIVITY CALCULATIONS

The relative permittivity of railway ballast reveals the condition of ballast in terms of its fouling level (i.e. clean, fouled, and highly fouled). The relative permittivity is computed with the so-called known depth method, where the height of the tank full of ballast (either clean or fouled) is known. In this method the temporal differences between the maximum reflection amplitudes of air/ballast interface and the ballast/metal interface are used (Figure 4). This temporal difference is widely known as the two-way travel time (twt) in GPR glossary.

To obtain relative permittivity of ballast, following formulas were used:

$$v = \frac{2h}{twt} \quad (1)$$

$$\varepsilon_r = \left(\frac{c}{v}\right)^2 \quad (2)$$

where, h is the known height of the tank with ballast, twt is the two-way radar travel time to and from the target or stratigraphic interface of interest, v is the propagation velocity in railway ballast, ε_r is the relative permittivity of railway ballast and c is the speed of light.



The velocity of the ballast medium is computed from eq. 1, since height of the tank was known and two-way travel time was obtained from GPR measurements. Then using eq. 2, relative permittivity values were calculated.

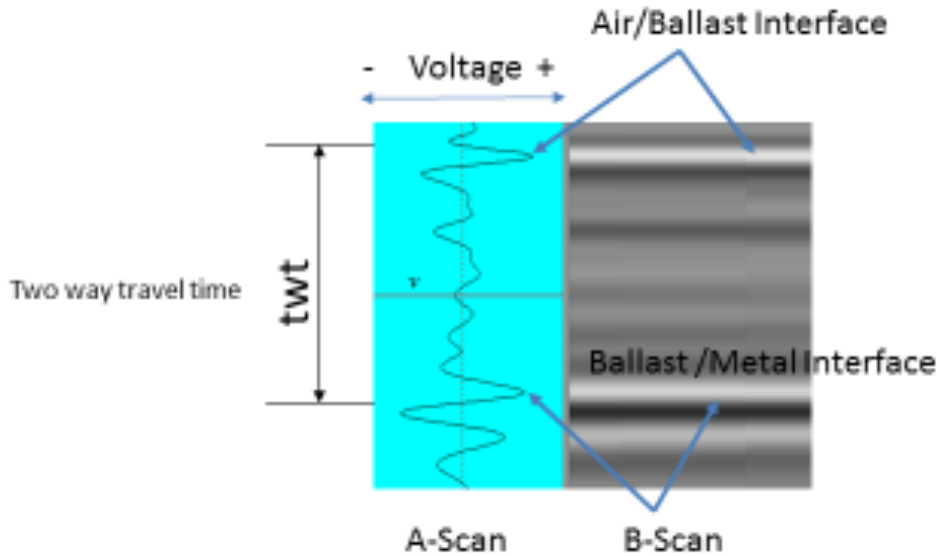


FIG. 14- Representation of air/ballast interface and ballast/metal interface in A-Scan and B-Scan.

Before presenting the relative permittivity values obtained from the experiments during the course of STSM, previously published relative permittivity values will be noted herein for comparison in Table 3.

As stated in the thesis work [28], the correlation between the values in Table 3 is encouraging taking into account the small ballast grading differences between UK and US. All the values in Table 3 were granite ballasts.

However, an average value of 4.8 for granite clean ballast was also published in [30]. But this difference could be derived from different grading curves, as well as the regional climate (the

moisture content in the air could be quite different in Portugal, where this study was realized) and the different quarries, from where crushed granite ballast come.

In Table 4, the relative permittivity values obtained during STSM for clean ballast are detailed, regarding the nominal frequency of antennas, data processing and orientation of antenna (longitudinal or transverse). There are two types of 2 GHz frequency antennas, being the EU type or NA type.

The processing steps conducted in the radargrams to calculate relative permittivity values were:

- Dewow (subtract-mean) function in 1D filter sub menu to remove low frequency content.
- Envelope function in complex trace analysis sub menu to confirm identification and exact position of surface reflection.
- Move start time in static correction/muting sub menu was used to adjust surface reflection to time zero level.
- Extract wavelet function in 1D filter sub menu to average (stack) traces in order to minimize random noises.
- Insert profile function in edit traces/trace ranges sub menu to combine all the statically acquired scans into a B-scan.
- Bandpass butterworth function in 1D filter sub menu to remove very low and very high frequencies from the data.

These post-processing steps were accomplished in Reflex W Software produced by [31].

The relative permittivity average of all 16 surveys ($\epsilon_r = 3.916$) was used as representative value for basalt stones used in the STSM. This result was quite in line with the values in Table 3, especially with the one published by [29]. It is noteworthy to mention that



the origin of the crushed stones where different from the ones used in [6,29].

In this STSM, basalt material was used as also stated in [32]. In the previous work [32] conducted in the same laboratory in University of Rome TRE with the same ballast materials an average relative permittivity for dry clean ballast was found as 3.757. Slightly higher representative value for clean ballast was obtained during this STSM compared to the previous work [32]. This may result from the fact that, the tank was filled with fouled ballast, before arranging the tank for clean configuration.

However, although enough attention was paid to remove the fouling material from the ballast stones during arrangement of clean ballast configuration, some traces of this fouling material (silty sand) could have remained within the stone perimeters. Since fouling material has a higher relative permittivity (5.03 according to [27]), those traces could have made that slight increase in the relative permittivity value.

TABLE 3 – Previously published relative permittivity of ballast under different conditions [16,28].

TYPE	RELATIVE PERMITTIVITY Clart et al. (2001) [6] UK	RELATIVE PERMITTIVITY (Susmann, 1999) [29] US
Dry Clean Ballast	3.0	3.6
Moist Clean Ballast	3.5	4.0
Dry Spent Ballast	4.3	3.7
Moist Spent Ballast	7.8	5.1
Wet Spent Ballast	38.5	7.2



TABLE 4 – Relative permittivity values obtained for clean ballast as a function of frequency of antennas, antennas being EU type or NA type, data processing and orientation of antenna (long. or trans.).

	1 GHz	1.5 GHz (VEE)	2 GHz (EU)	2 GHz (NA)	Average ϵ_r
Raw-Long.	3.853	3.969	3.911	3.911	3.911
Raw-Trans	3.853	3.969	3.807	3.911	3.885
Proc.-Long	3.911	4.027	3.911	3.911	3.940
Proc.-Trans.	3.911	4.057	3.807	3.945	3.930
Average Long. ϵ_r	3.882	3.998	3.911	3.911	3.925
Average Trans. ϵ_r	3.882	4.013	3.807	3.928	3.907
Average Raw. ϵ_r	3.853	3.969	3.859	3.911	3.898
Average Proc. ϵ_r	3.911	4.042	3.859	3.928	3.935
Average ϵ_r	3.882	4.005	3.859	3.919	3.916

The relative permittivity values obtained from 1.5 GHz (VEE type) antenna were slightly higher than those values obtained with other antennas (Table 4). This could be caused by the different nature of this antenna (as we were told by IDS), compared to other three horn antennas.

No significant changes were observed in the values regarding the orientation of antenna, whether it was longitudinal or transverse. Values acquired from processed data tend to have slightly higher values than the ones obtained from raw materials.

To better monitoring the variations of relative permittivity values (Table 4), the following graphs are depicted (Figure 15 and 16).



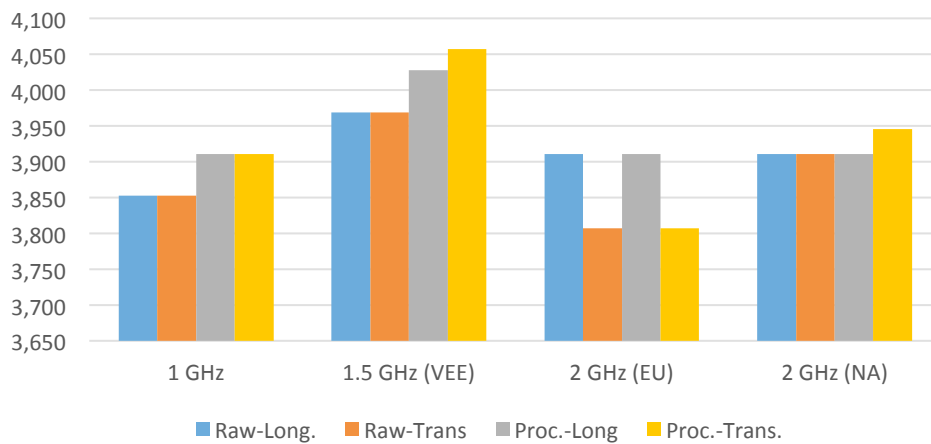


FIG. 15 - Change in dielectric value of clean ballast with respect to frequency versus processing and orientation.

From Figure 15, it can be clearly seen that 2 GHz NA antenna had better consistency, in terms of the permittivity values under different scenarios compared to the other antennas.

And as for fouled ballast condition, similar calculations were performed, which results are presented in Table 5.

The average representative value for all 16 surveys was 5.279 for basalt stones used in the STSM. This result was quite in line with the value of 5.1 in Table 3, which was the value for moist spent ballast published by [29].

Similar to the clean ballast case, the relative permittivity values obtained from 1.5 GHz (VEE type) antenna, were slightly different than those values obtained with other antennas. Contrary to the clean ballast case, this time those values were lower than the ones obtained by other frequency antennas. As in the clean ballast case, this slight difference was attributed to the different structure of the mentioned antenna.



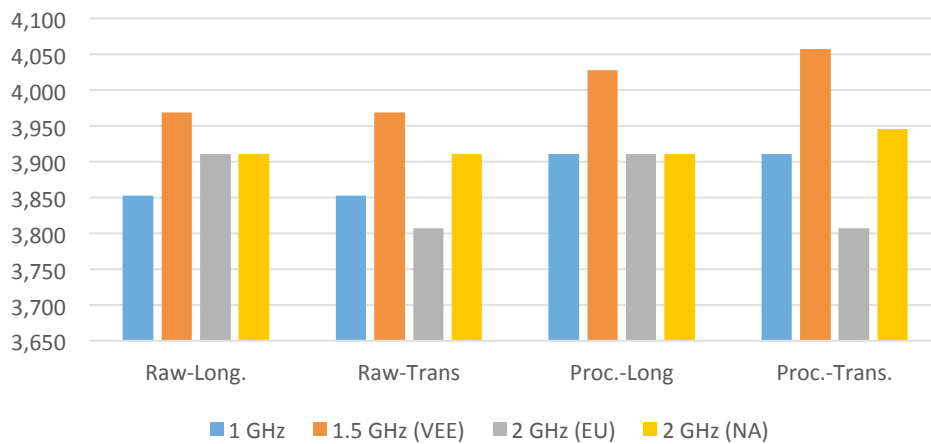


FIG. 16 - Change in dielectric value of clean ballast with respect to processing and orientation versus frequency.

To better visualizing the variations of the relative permittivity values, Figure 17 and 18 were created from the data of Table 5.

It can be observed in Figure 17, that slightly higher relative permittivity values were acquired from raw data, compared to ones acquired from processed data.

There exists also an alternative method in estimation of relative permittivity values: Reflection Coefficient Method. However, it was observed in [27,32] that this method yielded rather lower values, which could be caused by the scattering of the basalt stones in the surface. Therefore, this particular method was not exploited in this STSM.

Likewise, the clean ballast case, it was observed that 2 GHz NA antenna had better consistency, in terms of the permittivity values (Figure 18).

TABLE 5 – Relative permittivity values obtained for fouled ballast as a function of frequency of antennas, antennas being EU type or NA type, data processing and orientation of antenna (long. or trans.)

TYPE	1 GHz	1.5 GHz (VEE)	2 GHz (EU)	2 GHz (NA)	Average ϵ_r
Raw-Long.	5.425	4.990	5.466	5.343	5.306
Raw-Trans	5.357	4.893	5.343	5.343	5.234
Proc.-Long	5.425	5.023	5.466	5.262	5.294
Proc.-Trans.	5.289	5.189	5.303	5.343	5.281
Average Long. ϵ_r	5.425	5.007	5.466	5.303	5.300
Average Trans. ϵ_r	5.323	5.041	5.323	5.343	5.257
Average Raw. ϵ_r	5.391	4.941	5.404	5.343	5.270
Average Proc. ϵ_r	5.357	5.106	5.384	5.303	5.287
Average ϵ_r	5.374	5.024	5.394	5.323	5.279

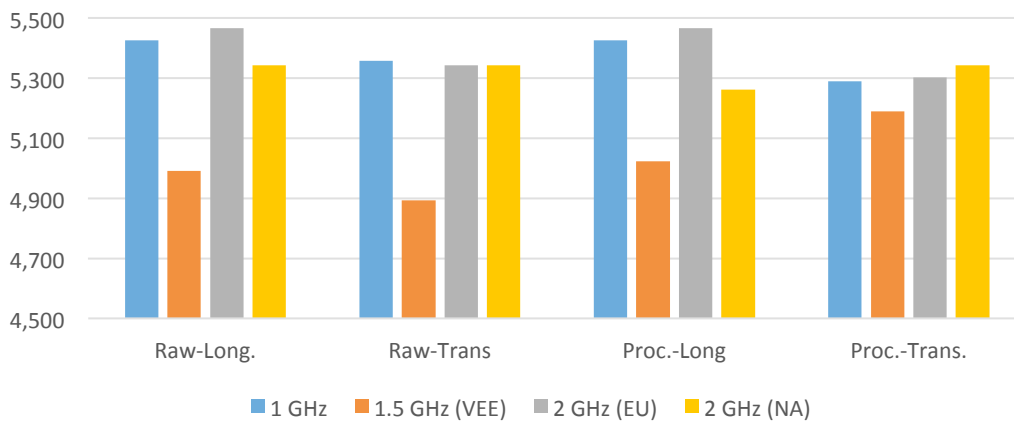


FIG. 17- Change in dielectric value of fouled ballast, with respect to frequency versus processing and orientation.



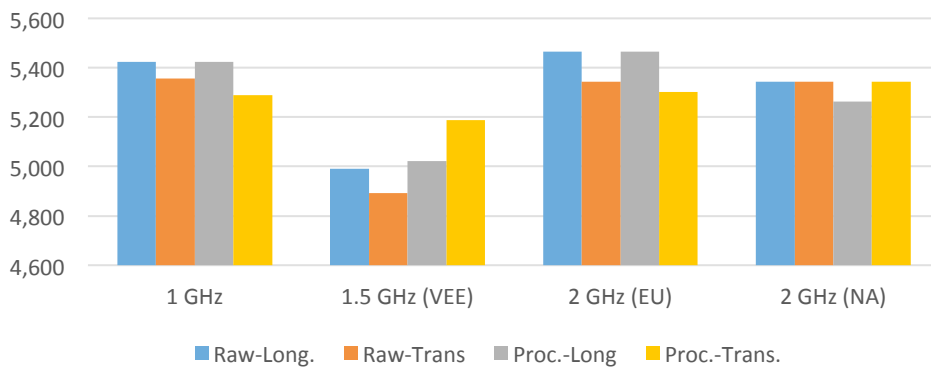


FIG. 18- Change in dielectric value of fouled ballast, with respect to frequency versus processing and orientation.

3.2 COMPARISON & INTERPRETATION OF RADARGRAMS FROM DIFFERENT SCENARIOS

In this section, by means of comparing the radargrams under different scenarios, interpretations were figured out in order to evaluate the influence of tested parameters. For example, in Figure 19, a radargram is presented from fouled ballast condition, in 1 sleeper case, with rails. 2 GHz EU antenna was used in transverse orientation. In this figure, from top to bottom, firstly antenna direct wave can be observed. Then the surface reflection is visible. The effect of sleeper is visible just under the surface reflection. Interface between fouled and clean ballast is seen and at the bottom the total metal reflector can be observed. One of the most obvious outcome, in this radargram, is that the total metal reflector is masked, when the antenna is over the sleeper which is actually expected due to longitudinal rebars existing in the sleepers.

The metal plate masking is more obvious in Figure 20, where radargrams from 1 GHz antenna in longitudinal direction were compared in terms of no sleeper and 1 sleeper cases in clean ballast.

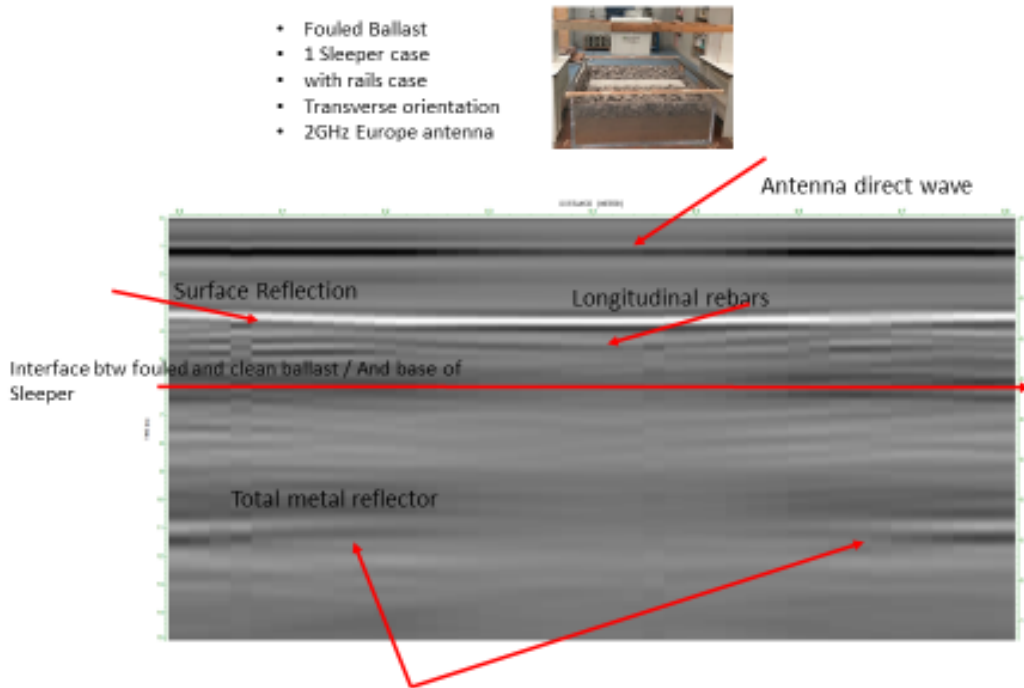


FIG. 19- Radargram interpretation from fouled ballast, 1 sleeper case, with rails and with a 2 GHz EU antenna in transverse orientation.

In Figure 20, left panel, which is the no sleeper case, the metal plate reflection was quite high and visible, while in Figure 20, right panel, with 1 sleeper case, metal plate reflection was quite masked and barely visible.

In Figure 21, two antennas (1 GHz and 2 GHz EU in transverse orientation) are compared with each other, to see the influence of fouling. In case of fouled material, the relative permittivity was higher than the clean ballast. Then, the wave propagation velocity decreased, which in turn resulted in a higher two-way travel time. In this case, the metal plate reflection appeared in a deeper location.



Clean – No Sleeper-w/o rails -1000MHz- Longitudinal Clean – 1 Sleeper-w rails-1000MHz- Longitudinal

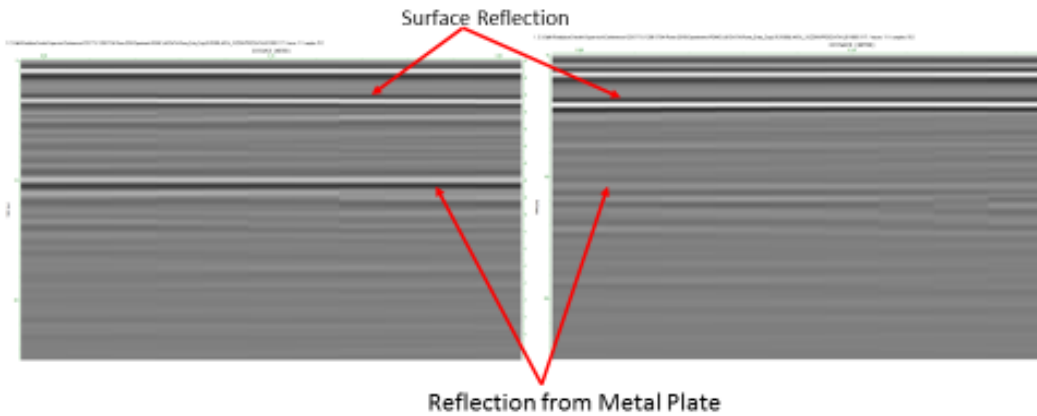


FIG. 20- Comparison of radargrams with 1 GHz antenna in longitudinal direction, in terms of no sleeper and 1 sleeper cases in clean ballast.

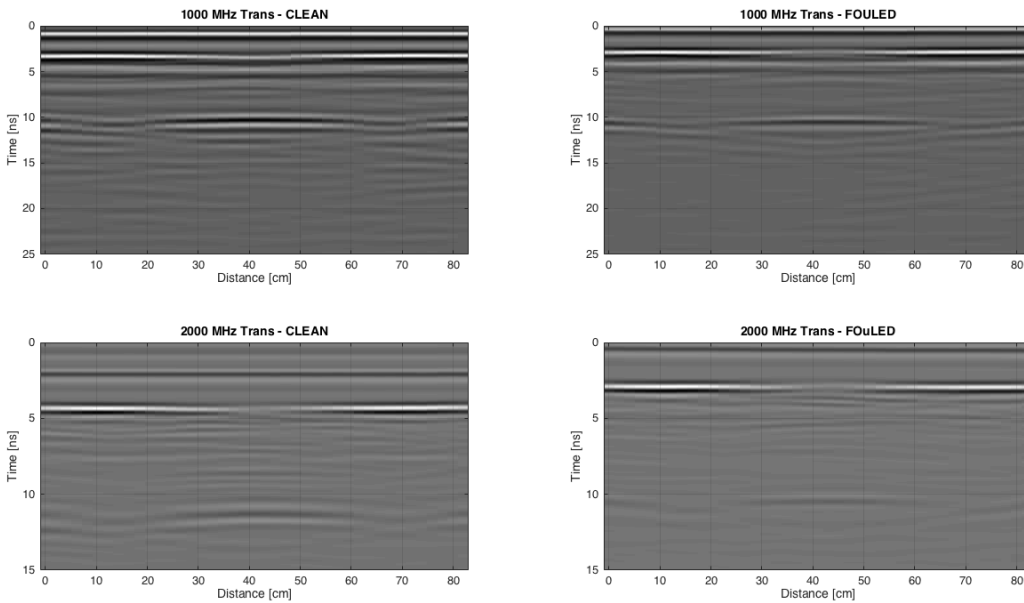


FIG. 21- Comparison of radargrams from measurements with 1 GHz and 2 GHz antenna in transverse direction, in terms of clean and fouled ballast conditions.

The 2 GHz NA antenna was used in fouled ballast condition with 1 sleeper case with rails. Comparison was made between the orientation of antennas. Figure 22a represents the longitudinal orientation whereas, Figure 22b exhibits the transverse orientation. The sleeper masking effect was obvious in both of the radargrams, since the metal plate reflection was almost invisible. Figure 22b (transverse orientation) gave better imaging and better tracking of the surface reflection variation due to the fact that the antenna was moved along a longer distance (80 cm) compared to the case with longitudinal orientation (20 cm).

Figure 23a is the obtained radargrams with 2 horizontal steel rods, Figure 23b with 2 horizontal plus 1 vertical steel rod and Figure 23c without any steel rods to imitate rail effects. 1 GHz antenna was used in transverse orientation in fouled ballast condition with two sleepers case. As can be seen in Figure 23, steel rods used to replicate the rails did not pose a discernible, significant difference in the radargrams.

Figure 24 presents the radargrams from 4 antennas in transverse orientation with the same configurations, namely fouled ballast condition with no sleeper and rails. Among all 1.5 GHz VEE type had different character repeating its direct wave in every 20 nanoseconds. Use of 4 antennas proved very beneficial in both calculations of relative permittivity and interpretations of radargrams.

4. FUTURE COLLABORATION WITH THE HOST INSTITUTION

For future works and collaboration, different processing steps could be evaluated, in order to have better and clearer images especially under the sleepers. And more comparison combinations could be performed in order to have a better understanding of the parameters tested.



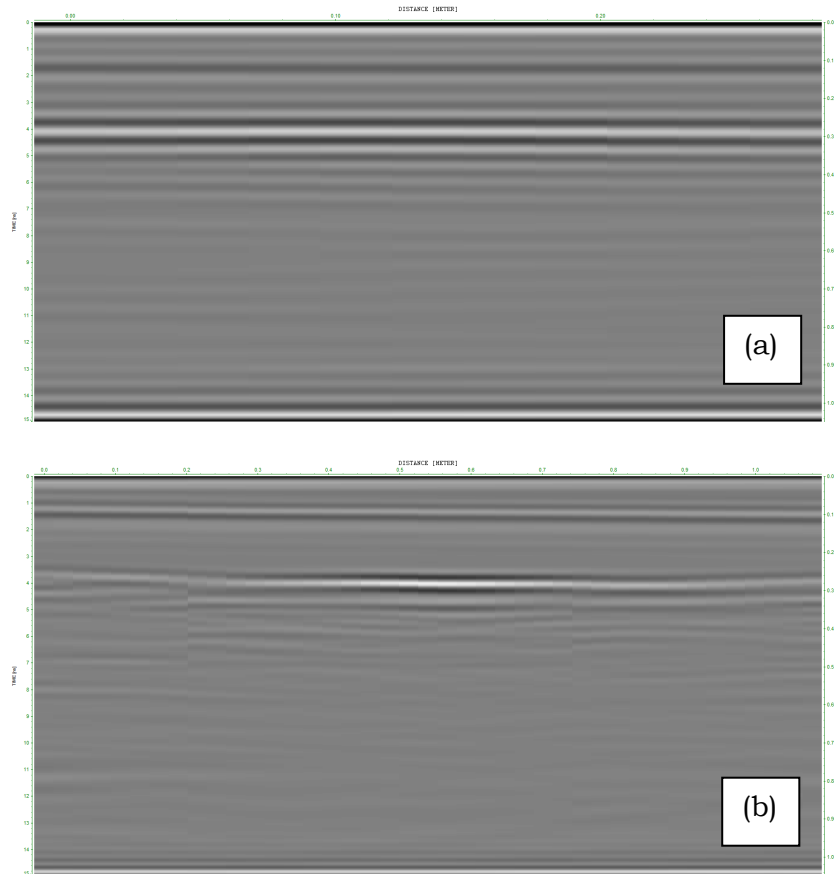


FIG. 22 - Comparison of radargrams from measurements with 2 GHz NA antenna with 1 sleeper case, in terms of longitudinal and transverse orientations in fouled ballast.

The STSM has been very productive and rewarding. This was a great opportunity to learn more about GPR signals over railway ballast. Future collaborations are foreseen, regarding real track measurements.

A scientific collaboration between Roma Tre and University of Pardubice (Czech Republic), where there are different types of GPR antennas, could produce very fruitful results.



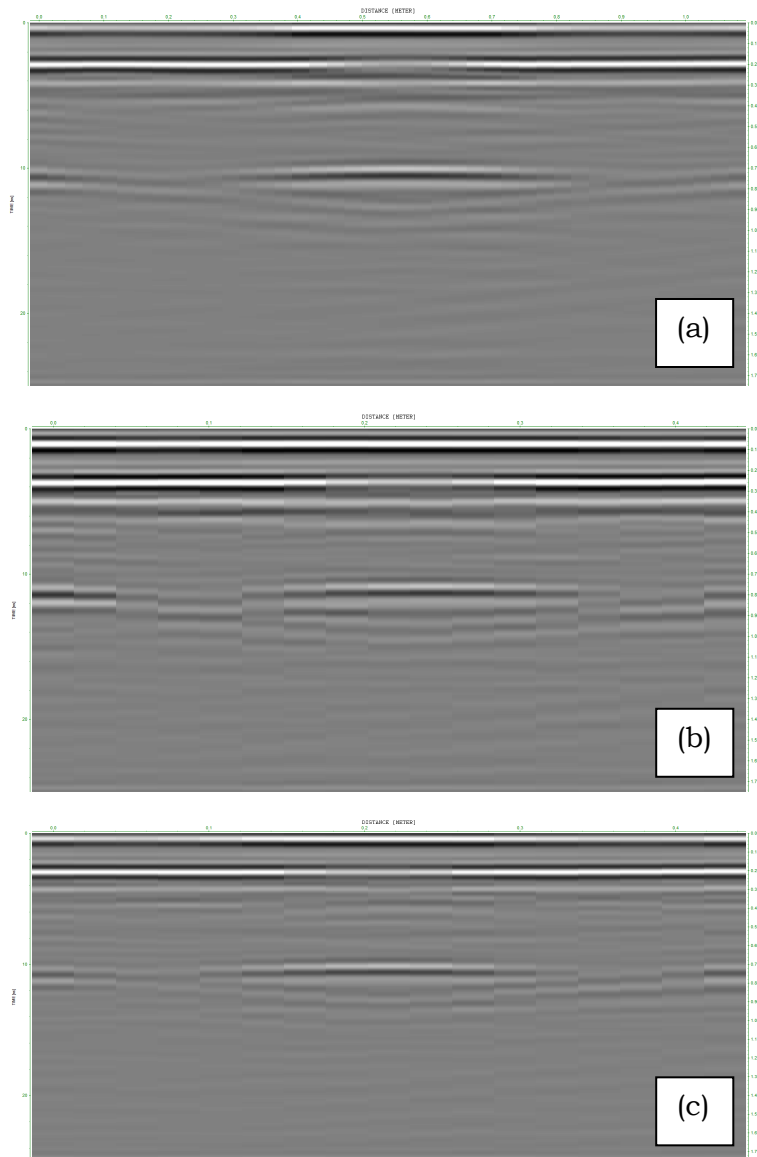


FIG. 23- 1 GHz antenna was used in transverse orientation in fouled ballast condition with two sleepers case: (a) with 2 horizontal steel rods imitating rail effects, (b) with 2 horizontal and 1 vertical steel rods imitating rail effect and (c) with no steel rods imitating rail effects.



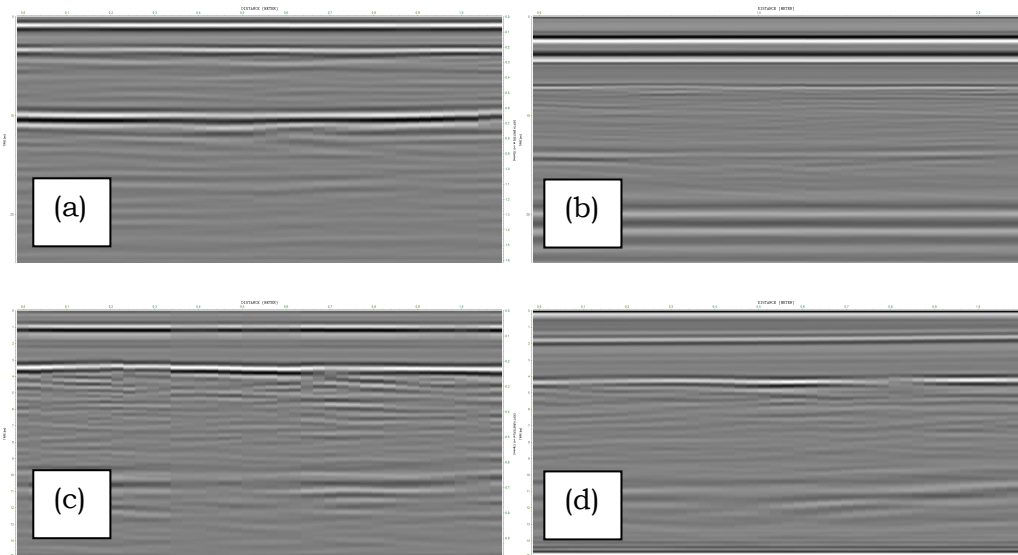


FIG. 24- Radargrams from 4 antennas in transverse orientation with the same configurations, namely fouled ballast condition with no sleeper and rails: (a) 1 GHz antenna, (b) 1.5 GHz VEE antenna, (c) 2 GHz EU antenna and (d) 2 GHz NA antenna.

Also the collaboration between University of Rome Tre and University of Anadolu (Turkey) could be constructed and it probably may serve beneficial outcomes.

Co-operation constructed between institutions from less research intensive countries (like Czech Republic and Turkey) with the universities from research intensive countries is a unique opportunity and represents a very promising and strong outcome of the STSM tool of the COST Actions.

5. FORESEEN PUBLICATIONS/ARTICLES RESULTING FROM THE STSM

From this STSM, I believe that good quality paper(s), conference proceedings and posters will be produced.



6. ACKNOWLEDGEMENTS

I would like to sincerely thank Prof. Benedetto, Mr. Luca Bianchini Ciampoli, Miss Maria Giulia Brancadoro, Mr. Spartaco Cera and University of Rome Tre for hosting me for this STSM, for their warm welcoming and nice co-operation during the STSM. To say the least, I am really glad to have priority to cooperate with Prof. Benedetto and his research team. I would like to express my gratitude to COST for funding COST Action TU1208, supporting this STSM.

7. REFERENCES

- [1] W. Shao, A. Bouzerdoum, S.L. Phung, L. Su, B. Indraratna, C. Rujikiatkamjorn, Automatic Classification of Ground-Penetrating-Radar Signals for Railway-Ballast Assessment, *IEEE Trans. Geosci. Remote Sens.* 49 (2011) 3961–3972. doi:10.1109/TGRS.2011.2128328.
- [2] R.C. Agarwal, Advantages and Disadvantages of Railway Transport, *YourArticleLibrary.com Gener. Libr.* (n.d.). <http://www.yourarticlelibrary.com/geography/transportation/advantages-and-disadvantages-of-railway-transport/42134/> (accessed September 13, 2015).
- [3] I.L. Al-Qadi, W. Xie, R. Roberts, Z. Leng, Data analysis techniques for GPR used for assessing railroad ballast in high radio-frequency environment, *J. Transp. Eng.* 136 (2010) 392–399.
- [4] D. Li, D. Read, H. Thompson, T. Sussmann, R. McDaniel, N.S. Railway, V.A. Roanoke, Evaluation of Ground Penetrating Radar Technologies for Assessing Track Substructure Conditions, (n.d.). https://www.arena.org/files/library/2010_conference_proceedings/evaluation_of_ground_penetrating_radar_technologies_for_assessing_track_substructure_conditions.pdf (accessed August 4, 2015).
- [5] E.T. Selig, J.M. Waters, *Track Geotechnology and Substructure Management*, Thomas Telford, 1994.



- [6] M.R. Clark, R. Gillespie, T. Kemp, D.M. McCann, M.C. Forde, Electromagnetic properties of railway ballast, *NDT E Int.* 34 (2001) 305–311.
- [7] R. Jack, P. Jackson, Imaging attributes of railway track formation and ballast using ground probing radar, *NDT E Int.* 32 (1999) 457–462.
- [8] J. Hugenschmidt, Railway track inspection using GPR, *J. Appl. Geophys.* 43 (2000) 147–155.
- [9] B. Solomon, *Railway Maintenance Equipment*, Voyageur Press, n.d.
- [10] P. Anbazhagan, P.S.N. Dixit, T.P. Bharatha, Identification of type and degree of railway ballast fouling using ground coupled GPR antennas, *J. Appl. Geophys.* 126 (2016) 183–190. doi:10.1016/j.jappgeo.2016.01.018.
- [11] J.P. Hyslip, S.S. Smith, G.R. Olhoeft, E.T. Selig, Assessment of railway track substructure condition using ground penetrating radar, in: 2003 Annu. Conf. AREMA, 2003. https://www.arena.org/files/library/2003_Conference_Proceedings/0010.pdf (accessed August 4, 2015).
- [12] M. Robinson, C. Bristow, J. McKinley and A. Ruffell “Ground Penetrating Radar” *Geomorphological Techniques*, Part 1, Sec. 5.5 British Society for Geomorphology, ISSN 2047-0371, 2013
- [13] A. Neal, Ground-penetrating radar and its use in sedimentology: principles, problems and progress, *Earth-Sci. Rev.* 66 (2004) 261–330. doi:10.1016/j.earscirev.2004.01.004.
- [14] A.P. Annan, J.L. Davis, Ground penetrating radar—coming of age at last, in: *Proc. Explor.*, 1997: pp. 515–522. http://dmec.ca/ex07-dvd/Decennial%20Proceedings/Expl97/06_05__.pdf (accessed August 11, 2015).
- [15] H. B. Thompson II, G. Carr, “Ground Penetrating Radar Evaluation and Implementation” *Research Results Report*, Federal Railroad Administration, 2014.
- [16] T. Saarenketo, *Electrical properties of road materials and subgrade soils and the use of Ground Penetrating Radar in traffic infrastructure surveys*, University of Oulu, 2006.



- [17] Fernandes, F., Pereira, M., Gomes Correia, A., Lourenço, P. Caldeira, L., Assessment of layer thickness and uniformity in railway embankments with ground penetrating radar, in: E. Ellis, N. Thom, H.-S. Yu, A. Dawson, G. McDowell (Eds.), *Adv. Transp. Geotech.*, CRC Press, 2008: pp. 571–575. <http://www.crcnetbase.com/doi/abs/10.1201/9780203885949.pt8> (accessed October 20, 2015).
- [18] T.R. Sussmann, E.T. Selig, J.P. Hyslip, Railway track condition indicators from ground penetrating radar, *NDT E Int.* 36 (2003) 157–167.
- [19] A. Benedetto, L. Pajewski, eds., *Civil Engineering Applications of Ground Penetrating Radar*, Springer International Publishing, Cham, 2015. <http://link.springer.com/10.1007/978-3-319-04813-0> (accessed July 23, 2016).
- [20] P. Anbazhagan, S. Lijun, I. Buddhima, R. Cholachat, Model track studies on fouled ballast using ground penetrating radar and multichannel analysis of surface wave, *J. Appl. Geophys.* 74 (2011) 175–184. doi:10.1016/j.jappgeo.2011.05.002.
- [21] P. Anbazhagan, Characterization of Rail Track Ballast Fouling Using Ground Penetration Radar and Field Sampling, (2013). <http://cistup.iisc.ernet.in/Demo/cistup/presentations/Research%20project/CIST024.pdf> (accessed October 20, 2015).
- [22] R. Roberts, I.L. Al-Qadi, E. Tutumluer, A. Kathage, Ballast fouling assessment using 2 GHz horn antennas-GPR and ground truth comparison from 238 km of track, in: 9th Int. Railw. Eng. Conf., 2007. http://alphageofisica.com.br/gssi/gpr_2008/RailEng%202007_br.pdf (accessed October 26, 2015).
- [23] R. Roberts, J. Rudy, S. GSSI, Railroad ballast fouling detection using ground penetrating radar. A new approach based on scattering from voids, *ECNDT 2006–Th 45. 1* (2006). <http://citeseerx.ist.psu.edu/viewdoc/download?doi=10.1.1.159.4471&rep=rep1&type=pdf> (accessed October 26, 2015).
- [24] L.D. Suits, T.C. Sheahan, L.-J. Su, C. Rujikiatkamjorn, B. Indraratna, An Evaluation of Fouled Ballast in a Laboratory Model



- Track Using Ground Penetrating Radar, *Geotech. Test. J.* 33 (2010) 103045. doi:10.1520/GTJ103045.
- [25] R.M. Maturana, B.D. Bautista, Á.A. Aguacil, M.R. Plaza, S.S. Castaño, Preventive Maintenance of Railway Infrastructures using GPR–Ground Penetrating Radar, (n.d.). http://www.railway-research.org/IMG/pdf/g7_minguez_maturana_raul.pdf (accessed August 4, 2015).
- [26] A. Eriksen, B. Venables, J. Gascoyne, S. Bandyopadhyay, Benefits of high speed GPR to manage trackbed assets and renewal strategies, in: *PWI Conf.* June, 2006. http://www.researchgate.net/profile/Asger_Eriksen/publication/239586033_Benefits_of_high_speed_GPR_to_manage_trackbed_assets_and_renewal_strategies/links/54c664b80cf256ed5a9e5f54.pdf (accessed September 21, 2015).
- [27] A.Benedetto, F.Tosti, L.Bianchini Ciampoli, A.Calvi, M.G. Brancadoro, A.M. Alani, “ Railway Ballast Condition Assessment Using Ground-Penetrating Radar-An Experimental, Numerical Simulation and Modelling Development” *Construction and Building Materials*, Feb. 2017, Doi: 10.1016/j.conbuildmat.2017.02.110
- [28] R.P. De Bold, Non-destructive evaluation of railway trackbed ballast, (2011). <http://www.era.lib.ed.ac.uk/handle/1842/5027> (accessed September 16, 2015).
- [29] T.R., Sussmann, Application of Ground Penetrating Radar to Railway Track Substructure Maintenance Management. PhD thesis. University of Massachusetts., 1999.
- [30] F. De Chiara, S. Fontul, E. Fortunato, GPR Laboratory Tests For Railways Materials Dielectric Properties Assessment, *Remote Sens.* 6 (2014) 9712–9728. doi:10.3390/rs6109712.
- [31] K.J. Sandmeier, Windows™ 9x/NT/2000/XP/7-program for the processing of seismic, acoustic or electromagnetic reflection, refraction and transmission data, (1998).
- [32] F.Tosti, A.Benedetto, A.Calvi, L.Bianchini Ciampoli, “Laboratory investigations for the electromagnetic characterization of railway ballast through GPR” 16th International Conference on Ground Penetrating Radar (GPR), Hong Kong, Jun. 2016.



STSM 7

INTEGRATED GEOPHYSICAL INVESTIGATIONS OF SITES OF CULTURAL INTEREST IN MALTA

VISITING SCIENTIST: RAFFAELE PERSICO, INSTITUTE FOR
ARCHAEOLOGICAL AND MONUMENTAL HERITAGE IBAM-CNR, ITALY
R.PERSICO@IBAM.CNR.IT

HOST SCIENTIST: SEBASTIANO D’AMICO, UNIVERSITY OF MALTA, MALTA
SEBASTIANO.DAMICO@UM.EDU.MT

STSM DATES: 5TH MARCH – 18TH MARCH 2017

1. PURPOSE OF THE STSM

The STSM “Integrated Geophysical Investigations of Sites of Cultural Interest in Malta” was performed in the period 5-18 March 2017. It aimed at investigating sites of cultural interest by means of GPR and other geophysical techniques. Also a site of environmental (more than cultural) interest was investigated.

The sites of interest proposed in the STSM application were: the Agrotti Garden in Floriana, the co-cathedral of St. John in Valletta, the site of Mgarr (Gnejna Bay and L-Iskorovit), the Nympeum within the Agrotti Garden and the Palace de la Salle in Valletta. In this last site the degradation of the frescoes did not allow to perform the scheduled investigations, but the other sites were investigated. On the other hand, we achieved rather obscure results in the co-cathedral of St John, where we prospected a few walls. Therefore, for comparison purposes, we performed similar tests on some walls of the University of Malta. The walls of the co-cathedral and those of the University were both nominally made of globigerina; and so we added this further case study, which was not initially scheduled.



2. DESCRIPTION OF THE WORK CARRIED OUT DURING THE STSM AND MAIN RESULTS

This STSM report was selected for open-access publication on the first issue of the first volume of the new journal *Ground Penetrating Radar* (www.GPRadar.eu/journal). The interested Readers are therefore kindly invited to download the papers [1] and [2], which describe what we did during this STSM.

3. FUTURE COLLABORATION WITH THE HOST INSTITUTION

The University of Malta and IBAM-CNR opened their collaborations in July 2015, when another STSM was performed in the framework of COST Action TU1208. This time, moreover, some colleagues of another Institute of the Italian National Research Council have been involved in the activities: Dr Enzo Rizzo and Dr Luigi Capozzoli. They mainly, but not only, contributed to the investigations with their competences and equipment with regard to electrical resistivity tomography (ERT).

In the last two years, several ideas came out for continuing the cooperation between The University of Malta and the IBAM-CNR, and in particular we have presented an Italy-Malta INTERREG project, together with further institutions in Malta and in Sicily. This proposal is currently being evaluated. Moreover, some budget for consultancies has been reserved, in other projects, in order to exploit virtuously and reciprocally the expertise present in both institutions. In particular, IBAM-CNR has reserved a budget in a proposed Italy-Greece INTERREG project, which is intended to carry out some joint work in the area of Salento and in the Ionian areas of Greece (in particular in the island of Zachyntos) within this project - if it will be approved.

Further ideas are being debated, in particular with regard to time domain reflectometry (TDR) probes, also together with the group of Electromagnetics of the University of Malta.



Independently from the financing of the above-mentioned proposed projects, IBAM-CNR and University of Malta believe in the validity of the results achieved together and are intentioned to go on in their collaboration.

Last but not least, the University of Malta and IBAM-CNR have collaborated within a school organized by COST Action TU1208 in Malta in January 2016 and subsequently in another school, organized by the University of Messina, in September 2016. Possibly and hopefully, we plan to collaborate also in future schools, and some ideas are being discussed in this sense, too.

4. FORESEEN PUBLICATIONS/ARTICLES RESULTING FROM THE STSM

In addition to the journal papers [1] and [2], the collaboration between the University of Malta and IBAM-CNR carried out in the framework of TU1208 has produced some papers presented to international and national conferences, part of which peer reviewed. In particular:

- R. Persico, D. Dei, F. Parrini, L. Matera, S. D’Amico, A. Micallef, P. Galea, Application of the Reconfigurability of the Integration Time in Stepped Frequency GPR Systems: First examples in the field, Proc. GNGTS Conference, Trieste, Italy, November 2015.
- R. Persico, S. D’Amico, L. Matera, Use of GPR and standard geophysical methods to explore the subsurface: Example from the Maltese Archipelago, Proc. EGU Meeting, Vienna, April 17-22, 2016.
- R. Persico, L. Matera, S. D’Amico, R. P. Borg, P. Galea, Integrated GPR and passive seismic investigations in cultural heritage sites: case studies in Malta, Proc. 16th International Conference on Ground Penetrating Radar GPR2016, Honk-Kong, June 13-16, 2016.



- R. Persico, S. D’Amico, L. Pajewski, V. P. Garcia, L., Ground-Penetrating Radar prospection at the Jesuits’ Church in Valletta, Malta, Proc. of NSG conference, Barcellona, Spain, September 4-8, 2016.
- V. Crupi, S. D’Amico, F. Longo, D. Maiolino, R. Persico, M. Saccone, G. V. Spagnolo, V. Venuti, Indagini multidisciplinari e rilievo 3D fotogrammetrico presso il sito archeologico di Scifi’, Proc. GNGTS Conference, Lecce, Italy, November 2016.
- V. Crupi, S. D’Amico, D. Majolino, G. Paladini, R. Persico, M. Saccone, G. Spagnolo and V. Venuti, Multidisciplinary Investigations embedded in a photogrammetric three dimensional survey in an archaeological site and St Peter and Paul Church in Agro Valley (Messina, Italy), Proc. EGU Meeting, Vienna, April 23-28, 2017.
- V. Crupi, S. D’Amico, D. Majolino, G. Paladini, R. Persico, M. Saccone, G. Spagnolo and V. Venuti, Multidisciplinary Investigations and 3D virtual model at the Archeological Site of Scifi’ (Messina, Italy), accepted for the 9th International Workshop on Advanced Ground Penetrating Radar IWAGPR, Edinburgh, UK, June 2017.

We plan further papers to be published on international journals, such as Near Surface Geophysics or Archaeological Prospection, as well as paper to be presented in further international conferences. Regarding this, meetings of particular interest are the International Conference on Metrology for Archaeology and the International Conference on Ground Penetrating Radar to be held in Switzerland in March 2018.

5. ACKNOWLEDGEMENTS

We thank COST, European Cooperation in Science and Technology, for funding COST Action TU1208 and this STSM.



6. REFERENCES

- [1] R. Persico, S. D'Amico, E. Rizzo, L. Capozzoli, and A. Micallef, "Ground Penetrating Radar investigations in sites of cultural interest in Malta," *Ground Penetrating Radar*, Vol.1(1), pp. 38-61, January 2018.
- [2] R. Persico, S. D'Amico, E. Rizzo, L. Capozzoli, and A. Micallef, "Electrical Resistivity Tomography investigations in Mgarr (Malta)," *Ground Penetrating Radar*, Vol.1(1), pp. 62-74, January 2018.



STSM 8

DESIGN AND REALIZATION OF A FREQUENCY-MODULATED CONTINUOUS WAVE (FMCW) GROUND PENETRATING RADAR (GPR) DEDICATED TO EDUCATIONAL PURPOSES. EXTENSION OF INTERACTIVE SETUP FUNCTIONALITIES.

VISITING SCIENTIST: MARGARITA CHIZH, BAUMAN MOSCOW STATE
TECHNICAL UNIVERSITY, MOSCOW, RUSSIAN FEDERATION
MCHIZH@RSLAB.RU

HOST SCIENTIST: VINCENZO FERRARA, SAPIENZA UNIVERSITY OF ROME,
DEPARTMENT OF INFORMATION ENGINEERING ELECTRONICS AND
TELECOMMUNICATIONS, ROME, ITALY
VINCENZO.FERRARA@UNIROMA1.IT

STSM DATES: 06TH MARCH – 02ND APRIL 2017

1. PURPOSE OF THE STSM

This STSM aimed at contributing to a project carried out in the framework of COST Action TU1208, devoted to the development of an affordable frequency-modulated continuous-wave (FMCW) Ground-Penetrating Radar (GPR) [1] for training purposes. GPR allows obtaining images of objects concealed in dielectrically contrast media and has various technical and scientific applications. Creating a cheap GPR and introducing it into the educational process will promote a wider use of this effective non-invasive and non-destructive technique. Therefore, a FMCW radar is being developed by TU1208 [2] and the work is mainly carried out at Sapienza University of Rome. The system under development combines cheapness with fine operating characteristics and a possibility of switching toward a large number of modulation patterns.



During the STSM, the following tasks were set and achieved: developing a software program for the FMCW GPR prototype in the form of graphical user interface (GUI), allowing simpler and more convenient user interaction with the system, and developing corresponding firmware program providing new control functionalities.

2. DESCRIPTION OF THE WORK CARRIED OUT DURING THE STSM

2.1 INTRODUCTION TO THE INITIAL STATE OF THE PROJECT

On the previous stages of the project, a radar system composed of a modulator, radio frequency (RF) chain and video amplifier was designed and implemented [1]. To pilot the tuning voltage of the voltage-controlled oscillator (VCO) and to create the synchronization pulse, the mbed NXP LPC1768 microcontroller board, with high performance ARM Cortex-M3 core, was used. A photo of the radar system is shown in Figure 1 and a block diagram of a FMCW radar is presented in Figure 2.

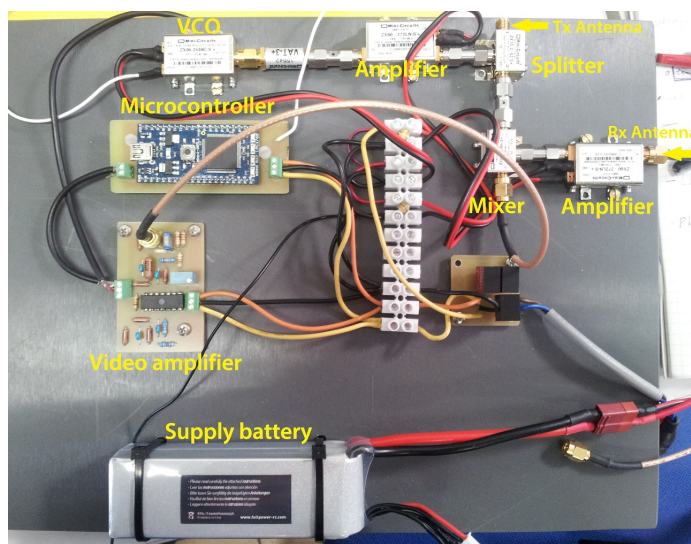


FIG. 1 – Photo of the radar system.



The initial project for controlling the mbed NXP LPC1768 prototyping board was written in C language, with the help of integrated development environment (IDE) CooCox. In this project drivers to use several interfaces for data transmission to a personal computer (PC) and generation of a triangular wave were implemented. Thus, the existing project did not allow interactive control of the MCU and changing the signal parameters implied altering the firmware code each time. The project was based on Cortex Microcontroller Software Interface Standard (CMSIS) package, and as CMSIS included only basic functions, the project had complex structure and was badly documented, which seriously complicated the task of its modification.

Considering all this, it was decided to rewrite the project with the help of ARM mbed OS [3], which is an open source embedded operating system that includes CMSIS. This is a low level component and provides C/C++ software development kit (SDK) with libraries to build various applications.

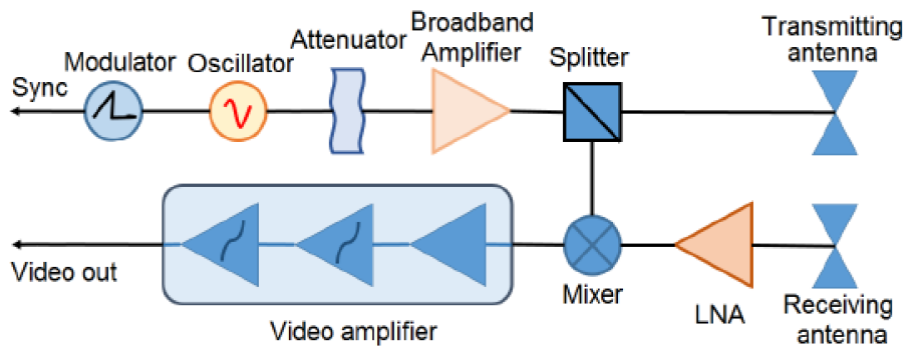


FIG. 2 – Block diagram of a FMCW radar.

2.2 FIRMWARE MODIFICATIONS

For communication between the user’s host PC and the peripheral radar system USB (Universal Serial Bus) was selected. The Serial



Interface defaults to a 9600 baud standard serial connection (8 bits, 1 stop bit, no parity), therefore the host program was set to the same settings. To establish the serial connection mbed MCU was configured as a USB Virtual Serial Port.

To ensure correct connection between LPC1768 mbed-board and the PC, a test project was created. LPC1768 mbed-board driver for Windows was installed onto the workspace PC. The test project was created in language C++ and compiled in on-line compiler on the official mbed website [4]. The mbed MCU was then flashed with the obtained firmware binary file. The listing of the simple test program is given below:

```
#include "mbed.h"

Serial pc (USBTX, USBRX); // tx, rx
int main () {
    pc.printf ("Hello GPR!\n");
}
```

At first, an open-source terminal program for engineering and debugging RealTerm [5] was used to test connection between the PC and mbed MCU. The main window of RealTerm is showed in Figure 3.

Several similar examples from SerialPC Handbook [6] were implemented and modified, so that the terminal was replaced by a program in Python language anticipating the development of the radar software.

The next step was to obtain a signal with triangular waveform, which means that the VCO frequency should change with a desired period T in the selected range $f_{\min} \div f_{\max}$, corresponding to the Digital-to-Analog Converter (DAC) tuning voltage of $V_{\min} \div V_{\max}$. It can be seen from VCO ZX95-2700A+ documentation that dependence of the VCO output frequency on the tuning voltage is nonlinear (Figure 4).



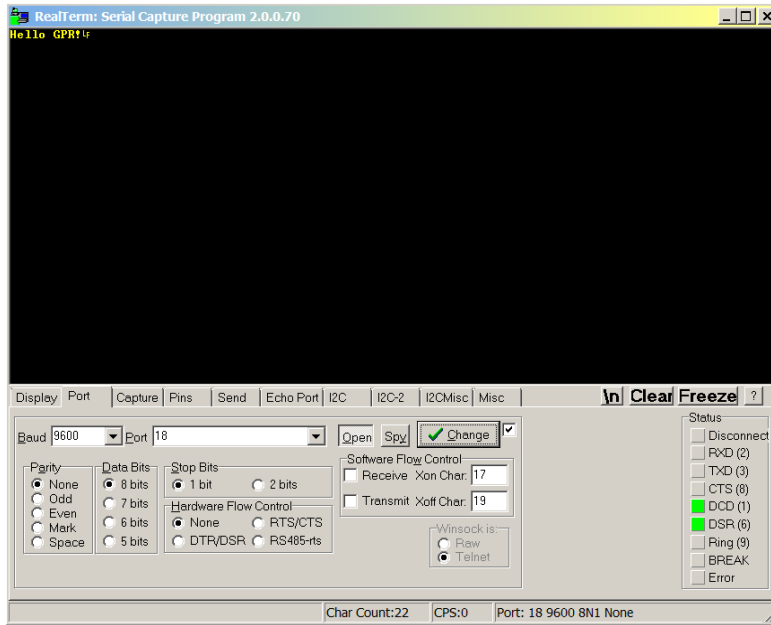


FIG. 3 – RealTerm terminal program communicating with the mbed. MCU.

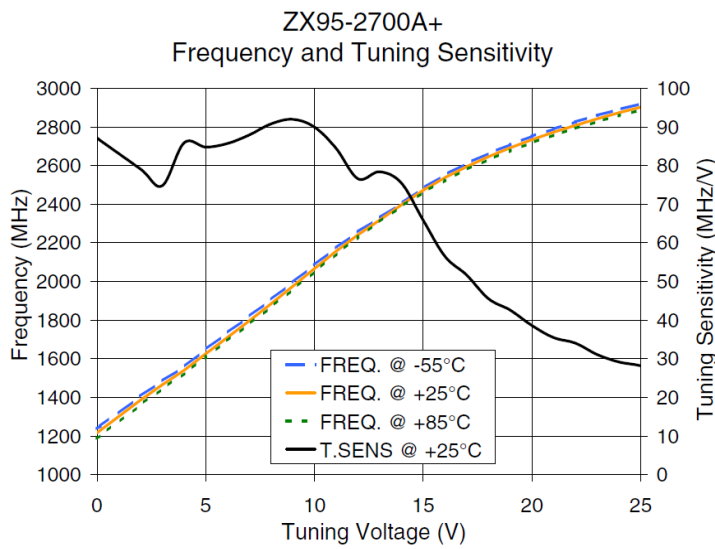


FIG. 4 – Dependence of the VCO output frequency on the tuning voltage.



For simplicity, at first a linear dependency was considered. From VCO ZX95-2700A+ documentation the coefficient of linear dependency of the voltage on the output signal frequency was calculated as follows:

$$\frac{V_{ctrl_min} - V_{ctrl_max}}{f_{min} - f_{max}} \quad (1)$$

At the normal temperature of 25°C for $V_{ctrl_min} = 0V$, the output is:

$$\begin{aligned} f_{min} &= 1216.7\text{MHz}, \\ V_{ctrl_max} = 25V - f_{max} &= 2902.5\text{MHz} \end{aligned}$$

Using these parameters the required control voltage V_{ctrl} for each selected frequency f_{sel} can be calculated:

$$V_{ctrl}(f_{sel}) = \frac{V_{ctrl_min} - V_{ctrl_max}}{f_{min} - f_{max}} (f_{sel} - f_{min}) + V_{ctrl_min}. \quad (2)$$

The mbed's LPC1768 chip has a 10-bit DAC. For each digital value input to the DAC, there is a corresponding analog output value given by:

$$V = \frac{D}{2^n} (V_{max} - V_{min}) \quad (3)$$

where V_{max}, V_{min} are maximum and minimum output voltages, D is the digital input and $n = 10$ for the 10-bit DAC, $2^{10} = 1024$.

The step size, or resolution, is therefore $3.3/1024$, i.e. 3.2 mV per bit [7]. By default, as the analog object the AnalogOut function takes a floating point number between 0.0 and 1.0 and outputs this to pin 18. The actual output voltage on pin 18 is between 0 V and 3.3 V. So the floating point number that is output as a voltage is scaled by a factor of 3.3.



On the PC-side in Python language, a function `DAC_Value_for_F()` was created for calculating the tuning voltage values for the selected frequencies f_{\min} , f_{\max} :

```
# Function to CALCULATE DAC VOLTAGE for F_min, F_max -  
linear law:  
  
# from VCO ZX95-2700A+ documentation -  
  
FREQ_MIN = 1216.7  
FREQ_MAX = 2902.5  
VCNTR_MIN = 0.0  
VCNTR_MAX = 25.0  
  
dv_df_coef = (VCNTR_MAX - VCNTR_MIN)/(FREQ_MAX -  
FREQ_MIN)  
  
def DAC_Value_for_F(F):  
    V_DAC = dv_df_coef*(F - FREQ_MIN) + VCNTR_MIN  
    return V_DAC      # DAC output voltage
```

These boundary tuning voltage values and the selected signal period value were packed into a string in ascii format and transferred to the mbed MCU through the Serial connection.

On the mbed-side the actual voltage values were calculated:

```
#include "mbed.h"  
Serial pc(USBTX, USBRX);    // mbed communicates  
with a host PC through a USB Virtual Serial Port  
  
DigitalOut mypin(p25);      // GPIO, P2_1  
AnalogOut Aout(p18);        // DAC, P0_26  
  
// Calculate buffer[num_values] of DAC voltage:  
for (int i = 0; i < num_values; i++) {  
    double t;  
    t = i*dt;                // current time value  
  
    if (0 <= t && t < T/2) {  
        // the straight line equation, normalized by 3.3 V
```



```
for
Analog output:
    DAC_buff[i] = (coeff*t + V_min)/3.3;
}

else if (T/2 <= t && t < T) {
    // the straight line equation, normalized by 3.3 V
for
    Analog output:
        DAC_buff[i] = (-coeff*t + 2*V_max - V_min)/3.3;
}
}
```

Thus, for interactive control of the VCO output signal three parameters should be defined: $1216.7 \text{ MHz} \leq f_{\min}, f_{\max} \leq 2902.5 \text{ MHz}$ and $10 \leq T \leq 100 \text{ ms}$.

It was decided to use one of the 26 available on the Mbed board general-purpose input/output (GPIO) pins for generating a square wave with which the measured radar signal would be synchronized. Mbed OS provides functions for various pins and interfaces configurations.

For implementing the synchronizing signal the DigitalOut Interface was used, which sets the state of the output pin (pin 25 in this case), and also reads back the current output state.

To form a regular signal, the DAC values should be updated at regular time intervals, which is usually accomplished by using the MCU clock and interrupt routines.

In this project, two functions for triggering a signal were tested: Wait() and Ticker(). The latter is used to setup a recurring interrupt to repeatedly call a function at a specified rate. Programs for creating the synchronizing square signal with 10 microsecond period are listed in Table 1.



Testing these two functions at different period values of the signal with the help of an oscilloscope showed that Ticker() provides time resolution of tens of microseconds, while Wait() only of a hundred microseconds.

TABLE 1 – Package organization.

Wait():	Ticker():
<pre>#include "mbed.h" DigitalOut mypin (p25); int main () { mypin = 0; while (1){ mypin = !mypin; wait(0.00001); //seconds } }</pre>	<pre>#include "mbed.h" Ticker T; DigitalOut mypin (p25); void flip () { mypin = !mypin; } int main () { mypin = 1; T.attach_us (&flip, 10); } //microseconds</pre>

For Ticker() at 10 us period the signal is stable, the measured period standard deviation is less than 200 picosecond. Therefore, the obtained square wave on the GPIO has a high time resolution of 10 us, fully meeting the specified requirement of 100 us, and can be applied for synchronization in the radar system.

In Figure 5, oscillograms of the DAC output (yellow) and the synchronizing square wave on GPIO pin 25 (blue) with the period of 200us are given.

These oscillograms show that the achieved accuracy of the signals synchronization is very high and the error is about one microsecond.



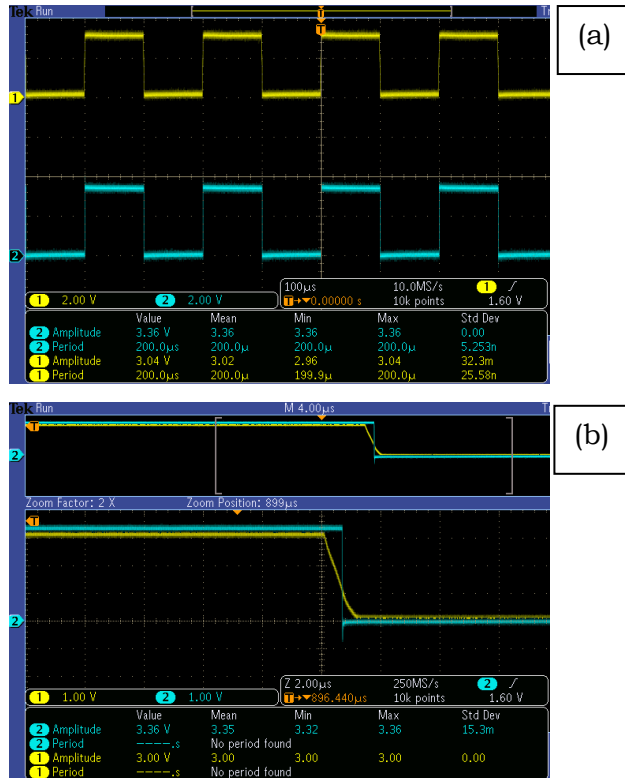


FIG. 5 – Oscillograms of the generated signals – DAC output and the synchronizing square wave. (a) Channel 1 (yellow): Analog output of the DAC, Channel 2 (blue): Synchronizing square wave on GPIO pin 25; (b) Same signals superimposed and zoomed.

2.3 SOFTWARE IMPLEMENTATION

For developing a graphical user interface (GUI), Python programming language was chosen, because it allows using various open-source libraries and provides simple, powerful and flexible functions.

For the GUI creation several popular libraries were examined, such as PyQt 5 (with IDE Qt Creator), wxPython, Tkinter. Finally,



Tkinter [8] package was selected for its simplicity, providing detailed tutorials and ready layouts.

The developed GUI was aimed at providing interactive control of the radar system. In particular, it was aimed to choose the frequency range of the transmitted signal, to select its period and to change the waveform. These control options were realized in the form of four sliders, moving the handlers of which the user can choose the desired parameters values. The main window of the designed GUI and the Help window containing instructions for the user are shown in Figure 6 and 7.

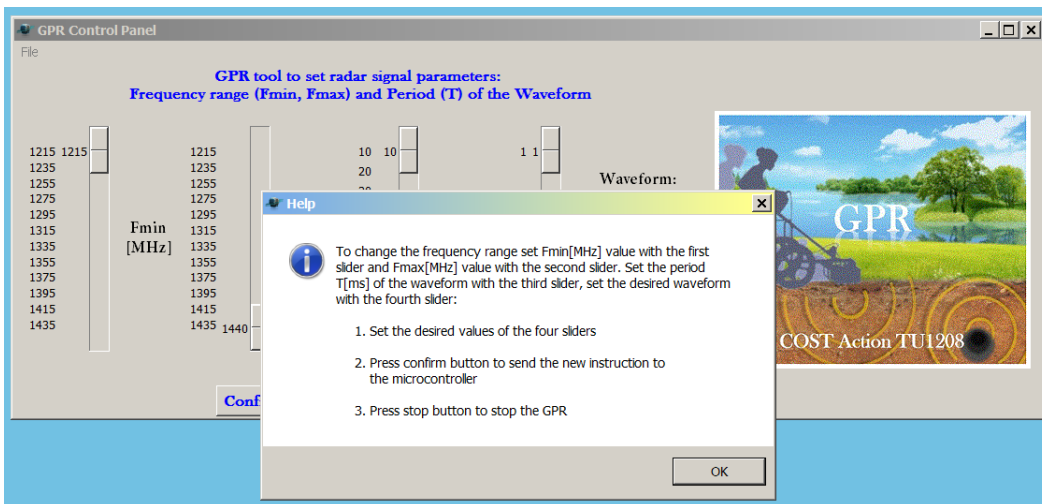


FIG. 6 – The main and Help windows of the developed GUI.

After the user specifies the values, he or she should press the Confirmation button. In the developed GUI program the change of the button's state is the event calling the slot (– a method that reacts to the signal), which reads the sliders values, packs them into a string and sends to the mbed MCU.

Communication with the mbed MCU was implemented on the basis of the designed test projects.



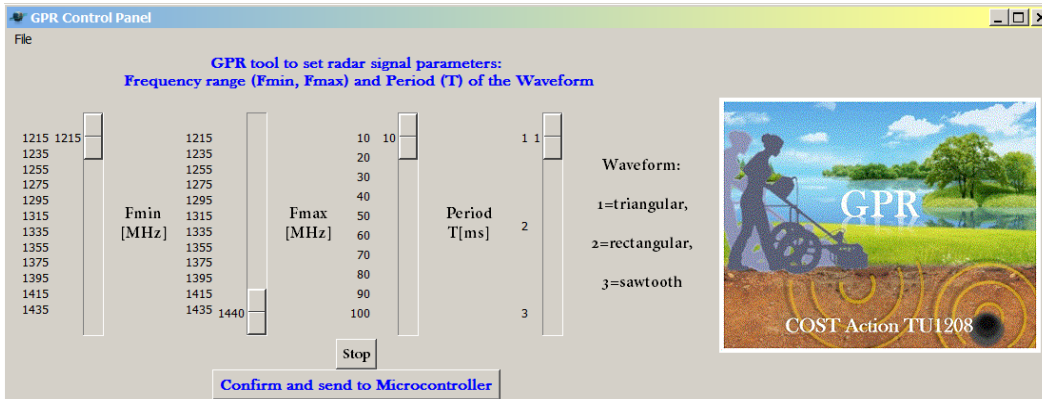


FIG. 7 – The main window of the developed GUI with the default sliders positions.

A part of the GUI program responsible for the Serial port configuration and data transmission is given below.

```
import serial

# Configure the Serial port:
# change COM number according to your PC connection!

ser = serial.Serial("COM20", baudrate=9600, bytesize=8,
    parity='N',
    stopbits=1, timeout=None, rtscts=1)

# Create SLIDER slot:

def getSlider():
    if (sldFmin.get()<sldFmax.get()):

        # Get values from sliders:

        F_min = sldFmin.get()
        F_max = sldFmax.get()
        T = sldT.get()
        W_form = sldW.get()
```



```
# Calculate DAC voltage for F_min, F_max:
V_DAC_min = DAC_Value_for_F(F_min)
V_DAC_max = DAC_Value_for_F(F_max)

# Transmit data to Mbed:
s = "{} {} {} \n".format(V_DAC_min, V_DAC_max, T,
W_form) # Forming a string
bs = bytes(s, 'ascii')# Only bytes encoded string can
be send to Serial
num_bytes = ser.write(bs)# Sending data to Mbed
through Serial

# Warning if F_min < F_max:
else:
    messagebox.showinfo(title= "Warning",
    message="Minimum frequency value (Fmin) cannot
    be higher than maximum frequency "
    "value (Fmax), please adjust the frequency border")
```

As can be seen from the code, it contains a check that the initial frequency of the signal is lower than the final one. In case of violating this condition, a warning appears. The Stop button at the GUI panel sets the default parameters values.

All new control functionalities for the GPR prototype were tested with the help of oscilloscope. The results of these measurements are shown in Figure 8.

These oscillograms show that three types of the signal waveform were successfully realized: triangular, rectangular and sawtooth. The synchronizing square signal matches the DAC output signal with high precision, as was previously proved. It is also shown that the period of the signal T can be interactively changed with the help of the developed GUI.



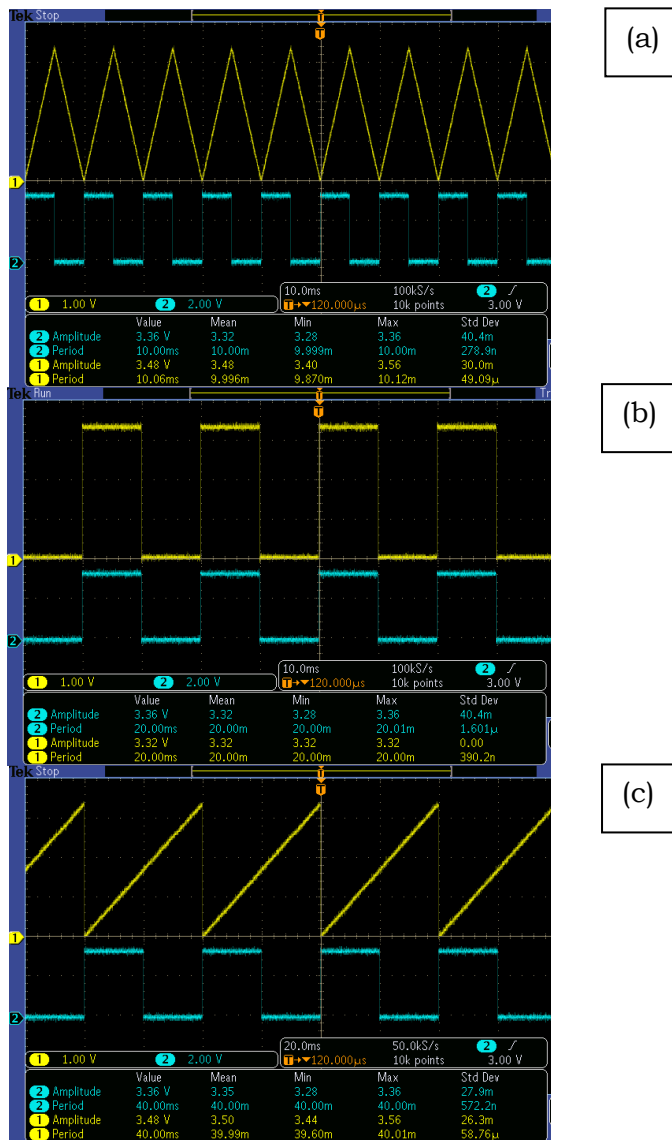


FIG. 8 – Test results of the new GPR control functionalities. Channel 1 (yellow): Analog output of the DAC. Channel 2(blue): Synchronizing square wave on GPIO pin 25. (a) Triangular waveform $T = 10$ ns; (b) Rectangular wave form $T = 20$ ns; (c) Sawtooth waveform $T = 40$ ns.

2.4 IMPLEMENTATION OF VOLTAGE PREDISTORTION. TESTING THE DEVELOPED PROGRAMS

Another software program was developed in Python programming language for performing all calculations on the user's computer side, which increases the speed of radar data generation in comparison to the calculations on the side of mbed MCU.

This program provides functions to calculate the buffer of the DAC voltage values required for obtaining the desired waveform at the VCO output and to pack the buffer into binary format and transmit it to mbed MCU through the serial connection. As an example, the function `W_form_sawtooth (f_min_s, f_max_s, T, N = NO)` for calculating the frequency values for the sawtooth waveform is given below, functions for the triangular and rectangular waveforms are similar.

The function `Predistort (f_desired)` for mapping the desired frequencies to the tuning voltage values accepts as an argument the precalculated array of frequencies and is universal for all waveforms.

The `Predistort (f_desired)` function considers the nonlinear dependence by using linearly interpolated actual coefficients specified in the VCO documentation. It should also be mentioned that DAC voltage values are scaled by a factor of $3.3/25.0$ to consider the effect of the voltage amplifier that will be placed between the DAC and VCO, to enable generating the full range of VCO frequencies.

After performing all required calculations the data are normalized by a factor of 3.3, as it is required by the `AnalogOut ()` function described earlier, packed into a binary array and transmitted to the mbed MCU through the Serial connection.



```
# SAWTOOTH WAVE:

def W_form_sawtooth(f_min_s, f_max_s, T, N=N0):
    f_sawtooth = np.empty(N)
    dt = T/N # ms
    coeff_s = (f_max_s - f_min_s)/((N - 1)*dt) # Sawtooth
    wave tangent

    # Calculate VCO output frequency values [N] for a
    sawtooth wave:

    for i in range(0, N):
        t = i*dt # Current time value
        f_sawtooth[i] = (coeff_s*t + f_min_s) # The straight
        line equation
    return f_sawtooth

# Calculates DAC voltages required for the VCO producing
f_desired,

# in accordance with the documented non-linear dependence
f(V):

def Predistort(f_desired):
    N = len(f_desired)
    f_dac = np.empty(N)
    DAC_values = np.empty(N)

    # Correlate desired freq values with the documented
    ("actual_interpolated") values:

    for i in range(0, N):
        f_dac[i], idx = find_nearest(f_act_intr, f_desired[i])
        # find actual freq value nearest to the desired freq
        DAC_values[i] = V_act_intr[idx]
    return DAC_values
```



```
# TRANSMIT DATA TO MBED:
```

```
dt = T*1000/num_values # *1000 - ms-->us, dt is time between  
DAC's updates  
DAC_values /= 3.3 # normalize by 3.3 V for mbed Analog  
Output (- accepts 0...1)  
values_to_pack = append(DAC_values, dt) # uniting two arrays  
str_packed = pack('%sf' % len(values_to_pack),  
*values_to_pack) # pack each value into a float - 4 bytes  
num_bytes = ser.write(str_packed) # Sending data to Mbed  
through Serial
```

In Figure 9 the computer-calculated values of the VCO frequencies and the corresponding predistorted DAC voltage are shown, for all three waveforms and the period of 20 ms. In Figure 10 the measured oscillograms are given, showing the real DAC output voltage for the user-specified frequency ranges, waveforms and the period of 20 ms.

Comparison of the DAC voltages in Figure 9 and 10 shows that they are in a good agreement. After adding this software program to the project the mbed LPC1768-side firmware was respectively modified. The firmware was redesigned to be independent from the radar signal parameters chosen by the user.

A universal function was created to receive and parse data from the PC. It follows the same instructions and receives data in universal format for each radar signal range and waveform defined on the software side. Such design of the project encourages its further development, allowing further software enhancement, while keeping the firmware program unchanged.



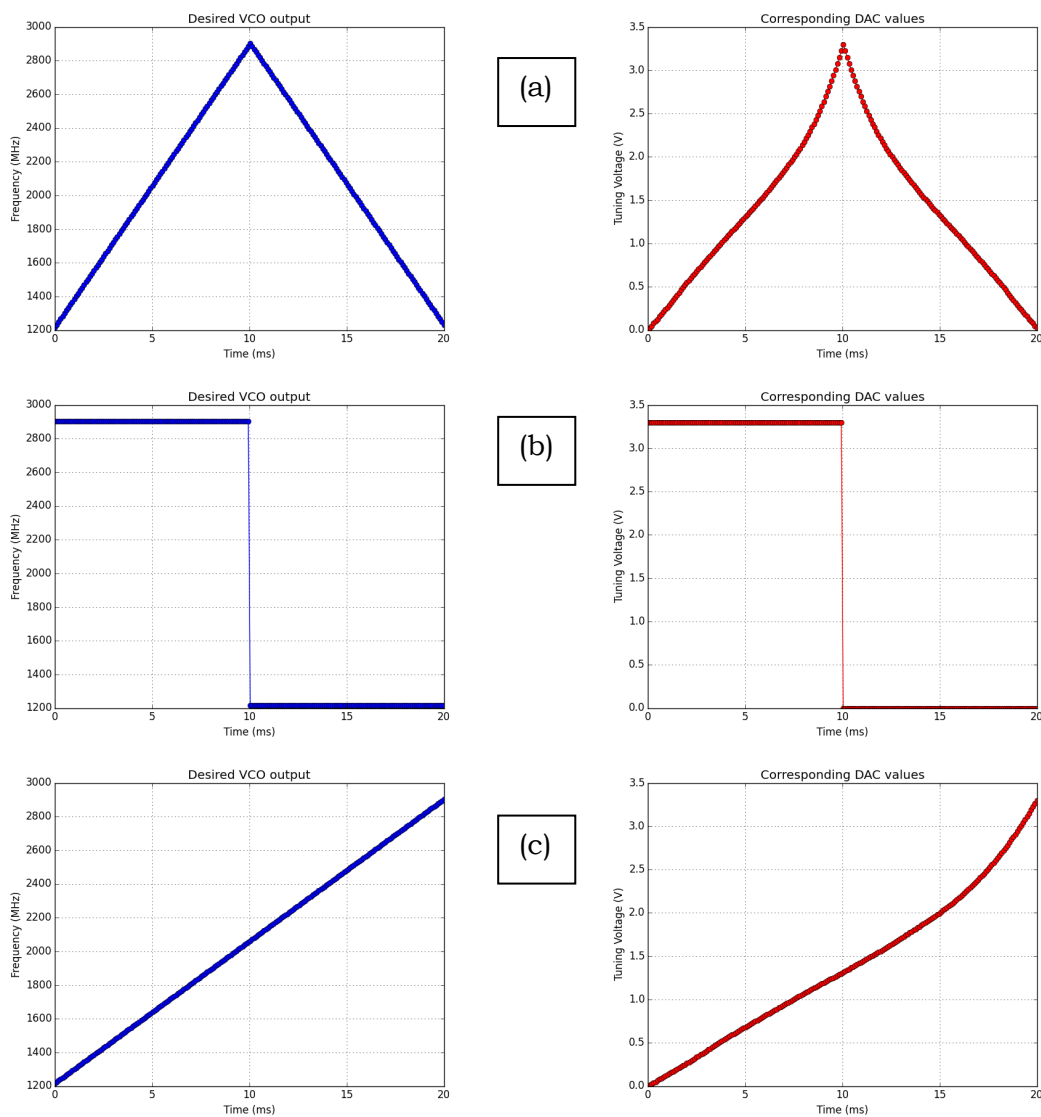


FIG. 9 – Computer-calculated predistorted values of the DAC voltages corresponding to the desired VCO frequency values. (a) Triangular waveform $T = 10$ ns; (b) Rectangular wave form $T = 20$ ns; (c) Sawtooth waveform $T = 20$ ns.



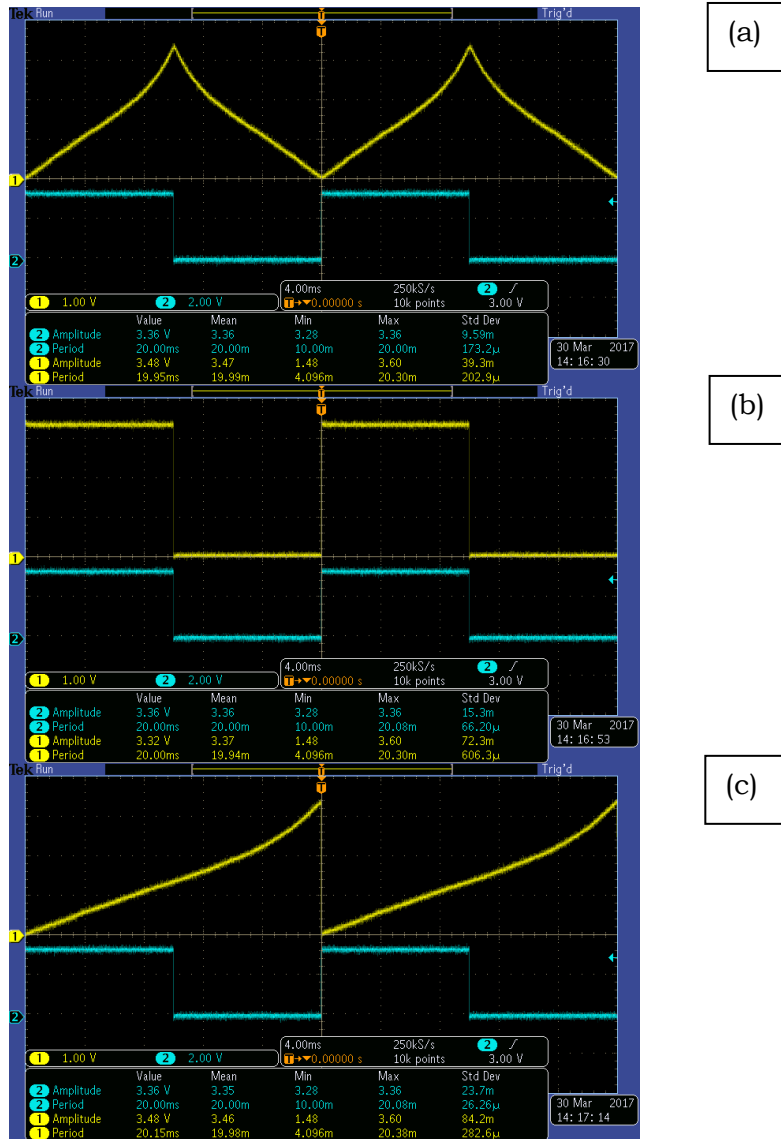


FIG. 10 – Oscillograms of the predistorted values of the DAC voltages corresponding to the desired VCO frequency values. (a) Triangular waveform $T = 10$ ns; (b) Rectangular wave form $T = 20$ ns; (c) Sawtooth waveform $T = 40$ ns.



3. DESCRIPTION OF THE MAIN RESULTS OBTAINED DURING THE STSM

In the course of this mission, the following main results were obtained:

1. **Graphical user interface** was developed in Python programming language, which allows using various open-source libraries and provides simple, powerful and flexible functions. All new control functionalities for the GPR prototype were tested with the help of oscilloscope. The results of these measurements are in good agreement with the computer simulation. The developed GUI program is user-friendly and will facilitate students interaction with the radar system in the framework of the education-oriented project carried out by COST Action TU1208.
2. Another **software program** was developed in Python programming language for performing all calculations on the user's computer side, which increases the speed of radar data generation in comparison to the calculations on the side of mbed MCU. This program provides functions to calculate the buffer of the DAC voltage values required for obtaining the desired waveform at the VCO output and to pack the buffer into binary format and transmit it to mbed MCU through the serial connection. A strong feature of the developed program is the consideration of nonlinear dependence of the VCO output frequency on the tuning voltage. This was achieved by implementing the voltage predistortion based on the actual coefficients stated in the VCO documentation.
3. **Firmware for mbed LPC1768** was developed that corresponds to the advanced GPR functionality implied by the software. With the help of APIs provided by mbed OS, the mbed MCU was represented as a virtual COM port, which enabled serial data transmission. A universal



function was created to receive and parse data from the PC. The project was designed in the way that the firmware program does no longer depend on the radar signal parameters chosen by the user. It follows the same instructions and receives data in universal format for each radar signal range and waveform defined on the software side. Such design of the project encourages its further development, for example, a modification of the RF-chain part of the system will require making changes only in the software, implemented in Python, while keeping the firmware program unchanged.

4. FUTURE COLLABORATION WITH THE HOST INSTITUTION

During this STSM a fruitful cooperation between the visiting and host scientists has started. We plan to continue the collaboration on the stated project devoted to the affordable FMCW GPR development carried out by COST Action TU1208.

5. FORESEEN PUBLICATIONS/ARTICLES RESULTING FROM THE STSM

During the STSM some important results summarized in this report were obtained. A paper covering these results will be prepared and submitted to an international journal.

6. ACKNOWLEDGEMENT

The visiting and host scientists would like to thank COST for funding COST Action TU1208 and this STSM.

7. REFERENCES

- [1] V. Ferrara, F. Troiani, F. Frezza, F. Mangini, L. Pajewski, P. Simeoni, N. Tedeschi, Design and Realization of a cheap Ground Penetrating Radar prototype @ 2.45 GHz, Proceedings of the 10th European Conference on Antennas and Propagation



(EuCAP 2016), Davos, Switzerland, 10-15 April 2016, pp. 1-4, doi: 10.1109/EuCAP.2016.7482008.

- [2] Lara Pajewski, Raffaele Persico, Vincenzo Ferrara, Simone Chicarella, Fabrizio Frezza, Filippo Troiani, Ground Penetrating Radar prototypes developed in COST Action TU1208, 24th International Conference on Software, Telecommunications and Computer Networks (SoftCOM 2016), 2016, Split, Croatia September 22-24, 2016.
- [3] Mbed OS: <https://www.mbed.com/en/development/mbed-os/>
- [4] Mbed online compiler:
<https://developer.mbed.org/compiler/#nav:/>
- [5] RealTerm serial terminal program for engineering:
<https://sourceforge.net/projects/realterm/>
- [6] Mbed Serial Communication with a PC handbook:
<https://developer.mbed.org/handbook/SerialPC>
- [7] Mbed DAC course-notes:
https://developer.mbed.org/media/uploads/robt/mbed_course_notes_-_analog_input_and_output.pdf
- [8] Tkinter package: <https://docs.python.org/2/library/tkinter.html>



STSM 9

ORGANIZATION OF THE FINAL CONFERENCE AND EDITORIAL ACTIVITIES.

VISITING SCIENTIST: LARA PAJEWSKI, SAPIENZA UNIVERSITY OF ROME,
DEPARTMENT OF INFORMATION ENGINEERING ELECTRONICS AND
TELECOMMUNICATIONS, ROME, ITALY
LARA.PAJEWSKI@UNIROMA1.IT

HOST SCIENTIST: MARIAN MARCINIAK, NATIONAL INSTITUTE OF
TELECOMMUNICATIONS OF POLAND, WARSAW, POLAND
M.MARCINIAK@ITL.WAW.PL

STSM DATES: 6TH JUNE – 24TH JUNE 2017

1. PURPOSE OF THE STSM

The main purposes of the STSM were:

(I) To work at the organization of the Final Conference of COST Action TU1208. The final event of our Action was held in the National Institute of Telecommunications of Poland, in Warsaw, on September 25-27, 2017.

(II) To work at an open-access Special Issue entitled "Recent Progress in Electromagnetic Theory and its Applications" – Journal of Telecommunications and Information Technology (JTIT). This is a bimonthly journal published by the National Institute of Telecommunications of Poland.

For what concerns activity (I), our goals were to book the necessary areas and buy/order materials, organize technical support and complementary activities, and define the general structure of the scientific programme of the event.



As far as activity (II) is regarded, the special issue was proposed in the framework of COST Action TU1208 to support the internalization of the journal whilst offering to Members the valuable opportunity to publish open-access papers free of charge. Guest Editors of the Special Issue are the Visiting Scientist, the Host Scientist and Prof. Hovik Baghdasaryan (TU1208 MC Observer from Armenia).

2. DESCRIPTION OF WORK CARRIED OUT DURING THE STSM

We shared three intense and fruitful weeks of work.

Half of the time was devoted to organizing the Final Conference of the Action. We booked the necessary areas and facilities in the National Institute of Telecommunications of Poland. We organized the secretarial support for the management of delegate registrations. We organized the IT support for the technical management of oral sessions, the remote connection with an invited speaker who cannot attend the conference, and the video recording of the whole event. We organized the catering (tea & coffee breaks; lunches), two common dinners, and a concert and guided tour of Warsaw for the Sunday preceding the event. Conference materials were designed and ordered/printed (badges, personalized bags and gadgets for conference delegates; posters for decorating the conference areas). We prepared the scientific programme of the event (to be finalized and printed in September).

Half of the time was dedicated to the JTIT Special Issue “Recent Progress in Electromagnetic Theory and its Applications.” We brought forward and finalized the review process of the submitted papers, our objective was to have the Special Issue ready for the Final Conference. We had the opportunity to discuss and finalize some papers co-authored by us, which are included in the Special Issue. We wrote the Preface to the Special Issue, comprising an introduction to the Ground Penetrating Radar method, basic information on COST programme and Action TU1208, and the customary presentation of all papers included in the issue. This



work was carried out in remote cooperation with Prof. Hovik Baghdasaryan.

During the STSM, we also had useful discussions about follow-up activities of the Action and our future collaboration.

3. DESCRIPTION OF THE MAIN RESULTS OBTAINED

As far as the organization of the Final Conference is concerned, the STSM turned out to be crucial for the success of the event. Without this STSM, the event would not be the same.

The webpage of the Final Conference is the best and most complete reference, for evaluating the outcomes of our joint efforts:

<http://gpradar.eu/events-dissemination/conferences/finalconference.html>

For what concerns the JTIT Special Issue, we are very satisfied about the feedback received by TU1208 Members and the results of our work. The issue is a collection of fourteen papers and it is structured in two parts. Part I includes eight papers on Ground Penetrating Radar (GPR) technology, methodology and applications; Part II contains six papers dealing with other applications of electromagnetic fields. Overall, the papers are authored by scientists from nineteen institutes in nine countries (Armenia, France, Germany, India, Ireland, Italy, Poland, Russia, and United Kingdom). The effective collaboration with the editorial office of the journal allowed us to conclude the work on time, so that the Special Issue was published as the September issue and presented during the final event.

The webpage of the Special Issue, where all papers are available for free download as of September 2017, is the best reference for appreciating the outcomes of our joint work:

<http://www.nit.eu/archive?view=kwartalrok&rok=2017&kwartal=3>



4. FUTURE COLLABORATIONS

The collaboration between the Host Scientist and the Visiting Scientist started in the COST framework and has always been fruitful and pleasant. Therefore, we are looking forward to continuing it. Some plans for the near future (to be realized after the end of the Action) are listed in the following.

1. Preparation of a joint comprehensive paper about the Short-Term Scientific Missions carried out in COST Action TU1208.
2. Editing of books where we will publish all reports of STSMs carried out during TU1208 Grant Periods 3, 4 and 5. A selection of reports will be published in the first issue of the new journal Ground Penetrating Radar, initiated by the Members of COST Action TU1208.
3. Organization of a new Session within the European Geosciences Union General Assembly (EGU GA), entitled “COST Actions in Geosciences: breakthrough ideas, research activities and results” (Convener: Lara Pajewski; co-Conveners: Simona Fontul, Marian Marciniak, Aleksandar Ristic). The EGU GA is held every April in Vienna, Austria. The new proposed session aims at creating a common space for multidisciplinary scientific discussion, where EGU-GA delegates involved in running or recently ended COST Actions can meet, share ideas, present the research activities carried out in their Actions, and disseminate the scientific results of their efforts. This is the webpage of the 2018 edition of the session <http://meetingorganizer.copernicus.org/EGU2018/session/27232>
4. Organization of a Training School on Science Management, to be held in Warsaw, in the framework of TU1208 GPR Association activities. We will probably be able to organize this school in 2020.



5. ACKNOWLEDGEMENTS

The visiting and host scientists are grateful to COST for funding and supporting COST Action TU1208 “Civil engineering applications of Ground Penetrating Radar.”



STSM 10

JOINT REVIEW AND FINALIZATION OF SOME EDUCATION PACK MODULES

VISITING SCIENTIST: SANTO PRONTERA, SAPIENZA UNIVERSITY OF ROME,
DEPARTMENT OF INFORMATION ENGINEERING ELECTRONICS AND
TELECOMMUNICATIONS, ROME, ITALY
SANTO.PRONTERA@UNIROMA1.IT

HOST SCIENTIST: MARIAN MARCINIAK, NATIONAL INSTITUTE OF
TELECOMMUNICATIONS OF POLAND, WARSAW, POLAND
M.MARCINIAK@ITL.WAW.PL

STSM DATES: 12TH SEPTEMBER – 1ST OCTOBER 2017

1. PURPOSE OF THE STSM

The main purposes of the STSM were:

(I) To review and finalize some modules of the GPR Education Pack that we decided to develop within COST Action TU1208.

(II) To help with the organization of the Final Conference of COST Action TU1208. The final event of our Action was held in the National Institute of Telecommunications of Poland, in Warsaw, on September 25-27, 2017.

As far as activity (I) is regarded, a lot of didactical material was been prepared by Members of COST Action TU1208, to be made available in open access on the website of the Action. This didactical material will help professors and researchers in all countries to initiate new courses in their Universities, on the GPR technique. However, almost every module needed refinement and integration. During the STSM, we reviewed jointly some modules and improve their content and format.



For what concerns activity (II), our goal was to support the organization of the final event. For example, we prepared the version of the conference programme to be printed, including the description of the research activities carried out in the Host Institution; we prepared the final list of participants and printed individual badges; and we decorated the areas of the conference.

For most of the time, my colleague Alessio Ventura was carrying out a simultaneous STSM in Warsaw.

2. DESCRIPTION OF WORK CARRIED OUT DURING THE STSM

About half of the time was dedicated to the TU1208 Education Pack. We discussed some of the modules and improved them.

Another half of the time was devoted to the organization of the Final Conference. The programme of the event was already written on the Action’s website, but we prepared the programme book, to be printed – which is something that takes a lot of time, longer than one could expect. In the programme book we included a long description of the Host Institute (available laboratories and research activities carried out by researchers working in the institute); the preparation of this description required interaction with local colleagues, to retrieve information and photos.

We edited and printed the individual badges of the participants – which is also something that takes longer time than we imagined.

During the weekend before the conference, we prepared and decorated the conference areas.

This whole experience was useful to understand what does it mean to organize a scientific event, which are the main difficulties and challenges, and the steps to be done.

3. DESCRIPTION OF THE MAIN RESULTS OBTAINED

As far as the organization of the Final Conference is concerned, it



was very important for the success of the event that we arrived in Warsaw two weeks before.

More information about the conference is found here: <http://gpradar.eu/events-dissemination/conferences/finalconference.html>

For what concerns the Education Pack, the following modules were finalized:

Lectures Authored by Carl Van Geem

- GPR applied to roads and bridges.
- Combined use of GPR and deflection measurement devices on roads.
- Structural evaluation of existing pavements, based on deflection measurements and GPR data.
- Pavement management.
- Practical session: GPR data processing – Roads.

Lecture authored by Dušan Kocur, Mária Švecová, Daniel Novák, Mária Gamcová

- Person localization based on detection of vital signs.

Lecture authored by Raffaele Persico

- Evaluation of wave propagation velocity.

Lecture authored by Andrej Gosar, Marjana Zajc, Teja Čeru

- Application of GPR in karsts.

Lecture authored by Jana Ježová, Sébastien Lambot

- Environmental applications of GPR.

At the link: <http://gpradar.eu/resources/educationpack.html> it is possible to download the modules.



4. FUTURE COLLABORATIONS

The collaboration with Host Scientist was very pleasant and I hope that there will be the opportunity to continue it. I am contributing at the preparation of a book where we will present all reports of STSMs carried out during TU1208 Year 3.

5. ACKNOWLEDGEMENTS

The visiting and host scientists are grateful to COST for funding and supporting COST Action TU1208 “Civil engineering applications of Ground Penetrating Radar.”



STSM 11

REVIEW AND FINALIZATION OF SOME EDUCATION PACK MODULES AND WEBSITE IMPROVEMENT

VISITING SCIENTIST: ALESSIO VENTURA, SAPIENZA UNIVERSITY OF ROME,
DEPARTMENT OF INFORMATION ENGINEERING ELECTRONICS AND
TELECOMMUNICATIONS, ROME, ITALY
ALESSIOVENTURA@HOTMAIL.COM

HOST SCIENTIST: MARIAN MARCINIAK, NATIONAL INSTITUTE OF
TELECOMMUNICATIONS OF POLAND, WARSAW, POLAND
M.MARCINIAK@ITL.WAW.PL

STSM DATES: 18TH SEPTEMBER – 1ST OCTOBER 2017

1. PURPOSE OF THE STSM

The main purposes of the STSM were:

(I) To finalize the organization of the Final Conference of COST Action TU1208. The event was held in the National Institute of Telecommunications of Poland, in Warsaw, on September 25-27, 2017.

(II) To jointly review and finalize some Education Pack modules.

My colleague Santo Prontera was in Warsaw, too, carrying out a simultaneous STSM.

For what concerns activity (I), our goal was to support the organization of the final event during the days immediately preceding it. For example, we worked at the version of the conference programme to be printed, prepared the final list of participants, printed individual badges, and decorated the areas of the conference.



As far as activity (II) is regarded, I mainly focused on the following three Education Pack modules:

- Radar Systems
- Antennas for GPR Systems
- History of GPR (to be still completed).

2. DESCRIPTION OF WORK CARRIED OUT DURING THE STSM

Based on last minute declinations and registrations, we finalized the programme of the event. Moreover, while the programme was already written on the Action’s website, we had to prepare the programme book, to be printed. We also edited and printed the individual badges of the participants. I worked at disseminating information about the conference locally, encouraging Polish researchers and professionals based in the Warsaw area to participate in the event. During the weekend before the conference, we prepared and decorated the conference areas.

This experience was useful to understand what does it mean to organize a scientific event, which are the main difficulties and challenges, and the steps to be done.

Half of the time was dedicated to the Education Pack modules. We brought forward the modules “Introduction to Radar Systems” and “Antennas for Ground Penetrating Radar”; we also worked at a module entitled “History of GPR” but further work is needed to complete it. The aim of our work was to increase the contents of the Education Pack, which will be useful to foster a wider dissemination of the GPR techniques in the universities and to share knowledge and experience in the different countries.

3. DESCRIPTION OF THE MAIN RESULTS OBTAINED

As far as the organization of the Final Conference is concerned, the STSM turned out to be very important for the success of the event. The webpage of the Final Conference is the best and most



complete reference, for evaluating the outcomes of our joint efforts:
<http://gpradar.eu/events-dissemination/conferences/finalconference.html>

For what concerns the Education Pack at the page:

<http://gpradar.eu/resources/educationpack.html>

is possible to see the modules and also the University courses, PhD Schools and other initiatives that are already making use of the TU1208 Education Pack as didactic material.

As mentioned in Section 1, I contributed to the review and further development of the modules about radar systems (1), about GPR antennas (2), and about the history of GPR (3). Such modules were realized: (1) by exploiting training material developed for three TU1208 Training Schools held in Karlsruhe, coordinated by Prof. Werner Wiesbeck (Germany); (2) by exploiting the chapter about antennas published in the TU1208 Springer book, and in cooperation with Sébastien Lambot (Belgium); (3) by exploiting documents available in the literature and some initial work done by Patrizio Simeoni (Ireland) and Fabrizio Frezza (Italy).

4. FUTURE COLLABORATIONS

The collaboration with the Host Scientist was very pleasant and I hope that there will be the opportunity to continue it, although I am starting to work in an Italian company soon, and therefore I will have less time for academic research and teaching.

5. ACKNOWLEDGEMENTS

The visiting and host scientists are grateful to COST for funding and supporting COST Action TU1208 “Civil engineering applications of Ground Penetrating Radar.”



TABLE OF CONTENTS

PREFACE

Lara Pajewski (Italy), Isabel Rodriguez-Abad (Spain) & Marian Marciniak (Poland) 1

STSM 1: Enhancement of GPR-Ground matching by chirped multilayer structure: Numerical modelling by the method of single expression 4

Visiting Scientist: Tamara Knyazyan (Armenia)
Host Scientist: Marian Marciniak (Poland)

1. Purpose of the STSM 4
2. Description of the work carried out during the STSM and main results 4
3. Future collaboration with the host institution 13
4. Foreseen publications/articles resulting from the STSM 15
5. Acknowledgements 15
6. References 15

STSM 2: Testing of a new lightweight radar system for tomographical reconstruction of circular structures 18

Visiting Scientist: Alessandro Fedeli (Italy)
Host Scientists: Jana Jezova & Sébastien Lambot (Belgium)

1. Purpose of the STSM 18
2. Description of the work carried out during the STSM 19
 - 2.1. Test of the radar prototype with different antennas 20
 - 2.2. Antenna coupling with sand of different volumetric water content 21



2.3 Measurements in sand box with buried objects	22
2.4 Measurements around circular cylinder with void inclusion	26
2.5 Reconstruction methods applied to GPR data	28
3. Description of the main results obtained during the STSM	29
3.1 Experiments with sand of different volumetric moisture content	29
3.2 Sand box with buried objects	31
3.3 Circular cylinder with void inclusion	39
4. Future collaboration with the host institution	42
5. Foreseen publications/articles resulting from the STSM	43
6. Acknowledgements	43
7. References	43

STSM 3 & STSM 4: Development of guidelines for flexible pavement evaluation and for the detection of buried utilities and voids in urban areas, by using ground-penetrating radar	45
--	----

Visiting Scientists: Xavier Dérobert (France) & Simona Fontul (Portugal)

Host Scientist: Lara Pajewski (Italy)

1. Purpose of the STSM	45
2. Description of the work carried out during the STSM	46
3. Future collaboration with the host institution	47
4. Acknowledgement	47
5. References	47



STSM 5: Finalization of a freeware data-processing tool implementing SAP-DoA technique 48

Visiting Scientist: Simone Meschino (Germany)

Host Scientist: Lara Pajewski (Italy)

1. Purpose of the STSM	48
2. Work carried out during the STSM and main results	49
3. Future collaboration with the host institution	49
4. Foreseen publications/articles resulting from the STSM	50
5. Acknowledgement	50
6. References	50

STSM 6: GPR assessment of railway ballast 51

Visiting Scientist: Salih Serkan Artagan (Turkey)

Host Scientist: Andrea Benedetto (Italy)

1. Purpose of the STSM	51
2. Description of the work carried out during the STSM	52
2.1 Introduction to GPR applications on railways	52
2.2 Preparation of the laboratory tests and Configurations	55
2.3 Instruments and equipment used for the laboratory experiments	57
2.4 Tested parameters	59
3. Description of the main results obtained during the STSM	70
3.1 Relative permittivity calculations	70
3.2 Comparison & interpretation of radargrams from different scenarios	78
4. Future collaboration with the host institution	81



5. Foreseen publications/articles resulting from the STSM	84
6. Acknowledgements	85
7. References	85

STSM 7: Integrated Geophysical Investigations of Sites of Cultural Interest in Malta 89

Visiting Scientist: Raffaele Persico (Italy)
Host Scientist: Sebastiano D’Amico (Malta)

1. Purpose of the STSM	89
2. Description of the work carried out during the STSM and main results	90
4. Future collaboration with the host institution	90
5. Foreseen publications/articles resulting from the STSM	91
6. Acknowledgements	92
7. References	93

STSM 8: Design and realization of a Frequency-Modulated Continuous Wave (FMCW) Ground Penetrating Radar (GPR) dedicated to educational purposes. Extension of interactive setup functionalities 94

Visiting Scientist: Margarita Chizh (Russia)
Host Scientist: Vincenzo Ferrara (Italy)

1. Purpose of the STSM	94
2. Description of the work carried out during the STSM	95
2.1 Introduction to the initial state of the project	95
2.2 Firmware modifications	96



2.3 Software implementation	103
2.4 Implementation of voltage predistortion. Testing the developed programs	108
3. Description of the main results obtained during the STSM	113
4. Future collaboration with the host institution	114
5. Foreseen publications/articles resulting from the STSM	114
6.Acknowledgement	114
7.References	114

STSM 9: Organization of the Final Conference and editorial activities 116

Visiting Scientist: Lara Pajewski (Italy)
Host Scientist: Marian Marciniak (Poland)

1. Purpose of the STSM	116
2. Description of the work carried out during the STSM	117
3. Description of the main results obtained	118
4. Future collaboration with the host institution	119
5. Acknowledgements	120

STSM 10: Joint review and finalization of some education pack modules 121

Visiting Scientist: Santo Prontera (Italy)
Host Scientist: Marian Marciniak (Poland)

1. Purpose of the STSM	121
2. Description of the work carried out during the STSM	122
3. Description of the main results obtained	122



4. Future collaboration with the host institution	124
5. Acknowledgements	124

STSM 11: Review and finalization of some education pack modules and website improvement 125

Visiting Scientist: Alessio Ventura (Italy)
Host Scientist: Marian Marciniak (Poland)

1. Purpose of the STSM	125
2. Description of the work carried out during the STSM	126
3. Description of the main results obtained	126
4. Future collaboration with the host institution	127
5. Acknowledgements	127



COST Action TU1208 - STSMs Years 4 and 5
www.GPRadar.eu, info@GPRadar.eu

Published by TU1208 GPR Association, Rome, Italy